

A PANEL METHOD STUDY OF VORTEX SHEETS WITH SPECIAL EMPHASIS
ON SHEETS OF AXISYMMETRIC GEOMETRY

Ichiro Sugioka and Sheila E. Widnall

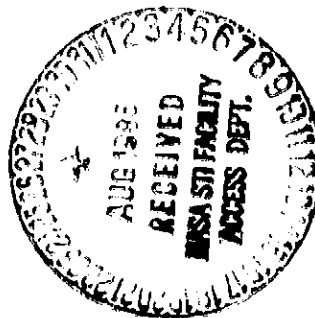
(NASA-CR-177365) A PANEL METHOD STUDY OF
VORTEX SHEETS WITH SPECIAL EMPHASIS ON
SHEETS OF AXISYMMETRIC GEOMETRY N.S. Thesis
(Massachusetts Inst. of Tech.) 115 p
HC A06/ME A01

N85-32095

Unclas
25485

CSCL 01A G3/02

CONTRACT NAG2-251
August 1985



NASA

A PANEL METHOD STUDY OF VORTEX SHEETS WITH SPECIAL EMPHASIS
ON SHEETS OF AXISYMMETRIC GEOMETRY

Ichiro Sugioka and Sheila E. Widnall
Fluid Dynamics Research Laboratory
Department of Aeronautics and Astronautics
Massachusetts Institute of Technology
Cambridge, Massachusetts

Prepared for
Ames Research Center
under Contract NAG2--251



National Aeronautics and
Space Administration

Ames Research Center
Moffett Field, California 94035

Table of Contents

Nomenclature	2
1. Introduction	4
1.1. Foundation of Vortex Sheet Studies	4
1.2. Instabilities in Numerical Vortex Sheet Models	6
1.3. Application to wake of a lifting surface	7
1.4. The Motivation for this Study	9
2. Mathematical Formulation of Vortex Elements	11
2.1. A Review of Concepts Regarding Vorticity	11
2.2. Two-Dimensional Vortex Elements	12
2.2.1. The Point Vortex	12
2.2.2. The Vortex Panel	13
2.3. Extension to Axisymmetric Geometries	15
2.3.1. The Axisymmetric Problem	15
2.3.2. The Method of Matched Asymptotic Expansion	16
2.3.2.1. The Outer-Solution	17
2.3.2.2. The Inner-Solution	17
2.3.2.3. The Inner/Outer Matching Solution	19
2.3.2.4. The Composite, Uniformly-Valid Solution	21
2.3.3. The Self-Induced Velocity	23
3. Numerical Behavior of Vortex Elements	27
3.1. The Velocity Profiles of Two-Dimensional Elements	27
3.2. The Velocity Profiles of Axisymmetric Elements	27
3.3. Integration of Vortices in the Form of a Vortex Panel	28
4. Discrete Numerical Approximation of a Vortex Sheet	35
4.1. The Uniform Downwash Solution for Discretized Vortex Sheets	35
4.1.1. Point Vortex Representations of the Vortex Sheet	36
4.1.2. Vortex Panel Representation of the Vortex Sheet	38
4.1.3. Vortex Band Representation of the Vortex Sheet	39
4.2. Summary	40
5. Numerical Simulation of Vortex Sheet Dynamics	48
5.1. The Numerical Roll-Up of Vortex Sheets	48
5.1.1. The Time-Integration Scheme	48
5.1.2. The Reconstruction and Rediscretization of the Vortex Sheet	49
5.1.3. The Treatment of the Inner Roll-Up Region	50
5.2. Results of the Roll-Up Calculations	51
5.2.1. Two-Dimensional Roll-Up	51
5.2.2. Roll-Up Produced by an Impulsive Movement by a Disk	53

5.2.3. Roll-Up of a Helicopter Wake	55
5.2.4. Kelvin-Helmholtz Instability	56
6. Conclusions	76
References	78
Appendix	80
Appendix A. The Vortex-Velocity Routines	81
Appendix B. The Initial Conditions for Roll-Up Simulations	87
Appendix C. The Vortex Sheet Dynamics Program	92
Appendix D. Inputs Used to Generate the Figures in the Text	107

List of Figures

Figure 2-1:	Velocity Vectors Associated with a Vortex Panel	25
Figure 2-2:	The Coordinate System	25
Figure 2-3:	Plot of the Axial Velocity and its Constituent Parts	26
Figure 3-1:	The velocity profile on axis tangential to the vortex panel	29
Figure 3-2:	The velocity profile on axis normal to the vortex panel	29
Figure 3-3:	The radial velocity profile of a 0 deg vortex band	30
Figure 3-4:	The axial velocity profile of a 0 deg vortex band	30
Figure 3-5:	The radial velocity profile of a 90 deg vortex band	31
Figure 3-6:	The axial velocity profile of a 90 deg vortex band	31
Figure 3-7:	Baseline Flow: a single vortex panel spanning $x = \pm 1$	32
Figure 3-8:	Point Vortex Flow: 4 vortices	32
Figure 3-9:	Point Vortex Flow: 10 vortices	33
Figure 3-10:	Vortex Panel Flow: 2 panels	33
Figure 3-11:	Vortex Panel Flow: 10 panels	34
Figure 4-1:	Vertical velocity profile for elliptic loading	41
Figure 4-2:	The downwash profile for Westwater's initial distribution	41
Figure 4-3:	Downwash Profile: Integration of equal strength vortices	42
Figure 4-4:	Downwash Profile: Integration of equally spaced vortices	42
Figure 4-5:	Velocities half-way between equally spaced vortices	43
Figure 4-6:	Downwash Profile: Integration of equal strength vortex panels	43
Figure 4-7:	Downwash Profile: Integration of equal width vortex panels	44
Figure 4-8:	Downwash Profile: Equal width panels with roll-up model	44
Figure 4-9:	Downwash Profile: The effect of virtual core	45
Figure 4-10:	Virtual-Core Location: Normalized w.r.t. the tip panel	45
Figure 4-11:	Virtual-Core Strength: Normalized w.r.t. the tip panel	46
Figure 4-12:	Moving Disk: Circular line vortex representation	46
Figure 4-13:	Moving Disk: Vortex band representation	47
Figure 4-14:	Moving Disk: Vortex bands with tip core	47
Figure 5-1:	Flow Chart of the Vortex Dynamics Program	58
Figure 5-2:	The First-Order Runge-Kutta Scheme	59
Figure 5-3:	The Reconstruction of the Vortex Sheet	60
Figure 5-4:	The Rediscretization of the Vortex Sheet	60
Figure 5-5:	Initial Configuration of the Vortex Sheet and Roll-Up	61
Figure 5-6:	The Core Dumping Approach	61
Figure 5-7:	Roll-Up of Elliptically Loaded Wing Wake	62
Figure 5-8:	The Corresponding Circulation Distribution	62
Figure 5-9:	Distribution of Circulation Surrounding the Roll-Up Core	63
Figure 5-10:	Blow-up of Fig. 5-9	63
Figure 5-11:	Roll-Up of Wing Wake at $T = 1.00$	64
Figure 5-12:	Detail of Figure 5-11	64

Figure 5-13:	Roll-Up Produced by a Moving Disk	65
Figure 5-14:	The Corresponding Circulation Distribution	65
Figure 5-15:	Distributions of Circulation Surrounding the Roll-Up Core	66
Figure 5-16:	Detail of Fig. 5-15	66
Figure 5-17:	The Sheet Geometry: $T = 0.55$	67
Figure 5-18:	The Blow-Up of the Spiral	67
Figure 5-19:	Helicopter-type Loading Distribution	68
Figure 5-20:	Downwash Profile: Vortex Bands with the Above Loading	68
Figure 5-21:	Roll-Up for a Helicopter Type Loading	69
Figure 5-22:	The Corresponding Circulation Distribution	69
Figure 5-23:	Distribution of Circulation Surrounding the Roll-Up Core	70
Figure 5-24:	Detail of Fig. 5-23	70
Figure 5-25:	Helicopter Roll-Up: $T = 0.500$	71
Figure 5-26:	Blow-Up of the Tip Spiral in Fig. 5-25	71
Figure 5-27:	Geometry of the Wake Vortex Sheet	72
Figure 5-28:	Repeated Magnification of a Section of Vortex Sheet	73
Figure 5-29:	Repeat of Fig. 5-13 with Finer Paneling: $T = 0.350$	74
Figure 5-30:	The Corresponding Circulation Distribution	74
Figure 5-31:	Circulation Distribution Around the Main Roll-Up	75
Figure 5-32:	Detail of Fig. 5-31	75
Figure B-1:	Kaden's Similarity Solution and its Numerical Model	89
Figure B-2:	Initial Roll-Up Model for Axisymmetric Vortex Sheet	89

A PANEL METHOD STUDY OF VORTEX SHEETS
WITH SPECIAL EMPHASIS ON SHEETS
OF AXISYMMETRIC GEOMETRY¹

by
Ichiro Sugioka and Sheila E. Widnall

FDRL Report No. 85-3 August, 1985

NASA/Ames Research Center contract NAG2-251

Fluid Dynamics Research Laboratory
Department of Aeronautics and Astronautics
Massachusetts Institute of Technology
Cambridge, MA 02139

The self-induced evolution of a vortex sheet was simulated by modelling the sheet using an integration of discrete elements of vorticity. Replacing small sections of a vortex sheet by flat panels of constant vorticity is found to reproduce more accurately the initial conditions for the Lagrangian simulation technique than replacement by point vortices. The flat panel method for the vortex sheet was then extended to model axisymmetric vortex sheets. The local and far field velocities induced by the axisymmetric panels were obtained using matched asymptotic analysis, and some of the uncertainties involved in other models of the axisymmetric vortex sheet have been eliminated. One important result of this analysis is the determination of the proper choice of core size for a circular vortex filament which may replace a section of an axisymmetric vortex sheet. Roll-up of both two-dimensional and axisymmetric vortex sheets was computed using the panel methods developed in the report.

¹Adapted from the S.M. Thesis by Ichiro Sugioka, "The Study of Vortex Sheets Using a Panel Method", M.I.T., August, 1985.

Nomenclature

Roman Letters

a	Half-Width of a Panel ($a = 1/2w$)
b	Semi-Span of the Wing or Radius of the Rotor
(a_o, b_o)	Position of Two-Dimensional Roll-up Core
E_1	Elliptic Integral of the Second Kind
F_1	Elliptic Integral of the First Kind
Q_n	Panel-Position Polynomials; see Equations (2.14) - (2.18)
R	Radius of the Axisymmetric Vortex Element
(R_o, c_o)	Position of Axisymmetric Roll-Up Core
r	Distance Between Points or to the Symmetry Axis
r_o	Radius of Circular Vorticity Distribution
r_1	Shortest Distance to the Vortex
r_2	Longest Distance to the Vortex
(r, z)	Coordinates for an Axisymmetric Cylindrical System
\vec{s}	Line Integral Path Vector
s	Distance Along the Vortex Sheet or Panel
T	Elapsed Time
(u, v)	Velocity Components for a Cartesian System
\vec{v}	Velocity Vector
w	Width of the Panel
X_o	Distance from the Edge of the Sheet
\vec{x}	Position Vector
(x, y)	Coordinates for a Cartesian System on the Vortex

Greek Letters

Γ	Circulation
Γ_o	Reference Circulation; Total Circulation
e	Curvature; Small Quantity Parameter
θ	Inclination of a Panel
κ	"Gradient of Circulation"; Local Strength of the Vortex Sheet
λ	Elliptic Integral Parameter; see Equation (2.24)
$\vec{\omega}$	Vorticity Vector
ψ	Stream Function

ψ_0 $O(1)$ Stream Function Solution
 ψ_1 $O(\epsilon)$ Stream Function Solution

Superscripts

$()^i$ The Inner-Limit
 $()^o$ The Outer-Limit

Subscripts

$()_i$ Pertaining to the i^{th} Panel
 $()_{i \pm 1/2}$ Pertaining to the Point Half-Way Between the Panels
 $()_{\text{homo}}$ The Solution to the Homogeneous Equation
 $()_{\text{in}}$ The Inner-Solution
 $()_{\text{io}}$ The Intermediate-Solution
 $()_o$ Pertaining to the Mid-Point of a Panel
 $()_{\text{out}}$ The Outer-Solution
 $()_p$ The Solution to the Particular Equation
 $()_{2D}$ The Two-Dimensional Solution

Chapter 1

Introduction

1.1. Foundation of Vortex Sheet Studies

A common feature of flows at high Reynolds number is the formation of thin regions of sharp changes in velocity known as shear layers. In the limit of infinite Reynolds Number, the diffusive effect of viscosity is eliminated, and the regions of velocity gradients are reduced to surfaces of step changes in velocity. Such surfaces are known as vortex sheets. Although the formation of shear layer is a viscous process, shear layers are commonly approximated by vortex sheets in the study of inviscid, irrotational "potential" flow.

A vortex sheet can be represented as an integration over infinitesimal vortex lines. The dynamics of vortex lines, and thus the dynamics of the sheet, are given by Helmholtz's vortex theorem. The theorem shows that vortex lines are material lines of the fluid and are convected by the local flow. In flows without sources or sinks, the distribution of vorticity determines the flow. If the flow is irrotational, the vorticity is concentrated in small regions of the fluid. Thus, an unsteady potential flow can be determined by tracking the vortex sheet as it is moved and deformed by the flow field.

A rigorous approach to tracking a vortex sheet will involve solving singular integro-differential equations. The time integration can be simplified by using a numerical scheme involving finite increments in time. However even with this simplification, a rigorous representation of the vortex sheet will make the contour integral intractable. Thus, a further numerical approximation must be used to represent the continuous vortex sheet using finite, discrete elements of circulation.

The linear instability of a vortex sheet can be shown analytically, but its subsequent

development is difficult to describe. Laboratory experiments with thin shear layers, which are expected to be similar to vortex sheets, show spontaneous generation and growth of spatially periodic rollup. This instability of the shear layer, known as the Kelvin-Helmholtz Instability, was the subject of the first numerical study of vortex sheets by Rosenhead [1]. In this study, a continuous two dimensional vortex sheet was replaced by a collection of discrete points of finite circulation, or point vortices. The initial flat geometry of the vortex sheet was represented by a straight row of point vortices. Rosenhead then adopted a Lagrangian approach of following each point vortex over time. The motions of the vortices are the result of the flow induced by the particular arrangement of vortices for each step in time. Rosenhead's calculations showed that the vortices form loose spirals within a small number of time steps if the initial arrangement of vortices were given a small periodic displacement. Because of the tedious manual computations involved, Rosenhead proceeded no further than the early stages of rollup. As a result, the problems associated with this Lagrangian method were not known until many years later.

The Lagrangian approach to the initial value problem involving vortex sheets is not a universally accepted concept. A pioneering effort by Birkhoff and Fisher [2] questioned the foundation of vortex sheet studies for invicid fluids. They were skeptical of the well posedness of applying invicid analysis to the dynamics of a viscously generated phenomenon. A recent review of the work in this area can be found in the article by Saffman and Baker [3].

Undaunted by questions regarding the well-posedness of the method, for the last fifteen years there has been an increasing interest in refining Rosenhead's technique. There are two reasons for the revival of interest in this area of study. First, the increase in availability of powerful computers encouraged the development of computational fluid dynamics. Second, the desire to extend the invicid analysis for high-speed aerodynamics to free vortex wakes has encouraged the development of the numerical approaches.

1.2. Instabilities in Numerical Vortex Sheet Models

The Lagrangian approach to simulating a vortex sheet is often plagued by instabilities caused by the numerical approach, the manner in which vortex sheets are modelled, and the inherent instability of an actual vortex sheet. The first is usually due to the inaccuracies inherent in numerical time integration techniques and in approximating the varying geometry of the vortex sheet. The second cause of instability is due to loss of accuracy dictated by the amount of computation available for the problem. In order to satisfy the practical limitations in computing, the number and the complexity of vortex elements must be reduced. Since the Lagrangian technique uses the result of each time step as the input for the next time step, inaccuracies in the technique compound over time. However, indiscriminate elimination of instability is undesirable since the physical instability of a vortex sheet is indistinguishable from the artificial instability. The inherent instability of the vortex sheet is the most important source of difficulty in the calculation of vortex sheet behavior.

Vortex sheets can be modelled in many ways but whether these models can realistically represent an infinitesimally thin shear layer is often not clear. Moore [4] has demonstrated that point-vortex methods will always be unstable. He found that the numerical instability mimics the Kelvin-Helmholtz instability in which the smallest wavelength resolvable, using points equal to twice the spacing, was found to be the most unstable. However, this instability causes the vortex sheet being represented by the point-vortices to cross itself, which is inconsistent with the allowed behavior of material surfaces. In the most successful point-vortex methods, the vortices are repeatedly redistributed along the sheet which unintentionally acts as a low pass filter, damping out the instability to delay the onset of chaos.

Baker [5] and Murman [6] have tackled the vortex sheet problems using a mixed Lagrangian-Eulerian approach, commonly referred to as the "cloud-in-cell" approach. In this scheme, the Euler Equation for the flow is solved for each cell formed by a spatial grid network. The use of the Euler Equation allows the use of a Fast Poisson Solver to significantly increase the efficiency of the numerical method. Murman confines the circulation to vortices which are convected independently. Otherwise vorticity diffuses numerically, and structures with grid related length scales appear. Whether these structures represent physically realistic features which are too small to

be resolved by the grid is not clear. On the other hand, although the small scale structures found by Moore are suppressed, Murman's method can not reproduce the smooth spiralling roll-up expected in a vortex sheet.

Spectral methods have been applied to a small number of cases with simple geometries to study vortex sheet stability. The problem addressed by Rosenhead has been studied using the spectral method by Moore [7] and by Melton, Baker, and Huzag [8]. The former addressed infinitesimal perturbations, while the latter addressed finite amplitude disturbances. They both arrived at consistent results. Singularities in the form of infinite curvature of the vortex sheet were detected within a finite amount of evolution time. Although the method results appear to be extremely reliable, they are too limited to be useful for practical problems such as the one discussed below. They do however illustrate the futility of rigorously following the evolution of a vortex sheet at infinitesimal spatial scales.

1.3. Application to wake of a lifting surface

Any lifting surface of a finite span trails a shear layer in its wake, commonly referred to as the wake vortex sheet. This shear layer can be produced by separation at the leading edge of a highly swept delta wing at high angles of attack or by the loss of vorticity from the vortex "bound" by the aerofoil. In the early 1920's, Prandtl hypothesized that the edges of wake vortex sheets roll-up into exponential spirals. Kaden [9], using dimensional arguments, derived the behavior near the edges of the vortex sheet trailed by a wing with an elliptic lift distribution. This distribution is important in efficient airplane design since it induces a constant downwash which minimizes the induced drag for a given aspect ratio. Using dimensional arguments, Kaden found that the rollup produced a spiral of $2/3$ power and from this the center of the spiral can be approximated. Betz [10] attempted to calculate the distribution of vorticity in the spiral by conserving circulation and impulse. However, Betz's constant which determines the exact shape and the distribution of vorticity with the spiral was later shown to be incorrect by Pullin [11].

Rosenhead's method was first applied to "Kaden's Problem" by Westwater [12]. In order to study the three-dimensional geometry of the trailing vortex sheet, Westwater replaced the streamwise coordinate by a time-like coordinate to form an unsteady, two-

dimensional process. This is equivalent to having the sheet cross-section being swept away from the wing which generated it. This procedure, known as the Trefftz plane method, is now universally used to study wake vortex sheets where the deformation in the streamwise direction is assumed to be small. Westwater discretized the trailing vortex sheet by replacing 20 segments of the sheet with point vortices of the same circulation. The vortices are convected for each timestep by velocities they induce on each other. Although the vortices rolled up more or less smoothly, the spiral did not quite match Kaden's result. The inaccuracy of Westwater's result was initially attributed to the insufficient number of vortices dictated by lack of computational devices.

Attempts to improve Westwater's results by using more point vortices have not been successful. Increasing the number of point-vortices was found to hasten the tendency toward chaotic displacement of vortices. Such failures in achieving higher resolution by increasing the number of point vortices are attributed to the singular nature of point vortices. The velocity singularity at the location of the point vortex can be removed by replacing an individual or a group of vortices with a nonsingular distribution of vorticity. However this method has been found to only delay the onset of numerical instability while introducing an ad hoc length parameter for the size of the distribution. The failure of the discrete vortex approach may be due to the impossibility of reproducing the sheet-like nature by a finite number of positions. On a sheet, each position possesses its own unique orientation, which is the result of the sheet's continuous nature.

The method of equal-spaced rediscrretization introduced by Fink and Soh [13, 14] is notable for its simplicity and for its success in delaying or eliminating instability. Fink and Soh found that replacing a vortex sheet segment with a point vortex at the middle of the segment will significantly reduce the discretization error. This in fact truncates the formula for the velocity associated with a vortex panel, a small segment of the vortex sheet. By placing point vortices at equal distances along the sheet, it is possible to replace equal length segments of vortex sheet by point vortices at the centers of the segments. Since this procedure is repeated after each time step, Fink and Soh can decrease the distances between points as desired to resolve the rollup of a finite vortex sheet. In addition to maintaining the spatial resolution, the method reduces the singular behavior induced by a vortex on neighboring points along the

sheet. However, singular behavior will appear when two parts of the vortex sheet approach each other closely as in the turns of a spiral.

Baker [15] questioned Fink and Soh's practice of amalgamating the inner region of the rollup into a single "core vortex". "Core dumping" is a simple approximation of the singularity at the edge of a finite vortex sheet. In order to analyze its effects, Baker used Fink and Soh's method for describing the wake trailed by a ring wing, a circular vortex sheet with sinusoidal vorticity distribution. Upon observing the failure of Fink and Soh's method in dealing with the double-branched rollup associated with the ring wing, Baker concluded that the strong core vortex must be responsible for the smooth rollup observed.

Hoeijmakers and Vaatstra [16] improved Fink and Soh's technique in several ways. First, they introduced the use of a sophisticated splining technique for dividing the sheet into panels with small curvature and polynomial vorticity distribution, characterized as a second-order panel method. Second, Pullin's generalized similarity solution for rollup [11] is invoked to make core dumping acceptable. Since Pullin's analysis also applies to the double-branched rollup, the vortex sheet trailed by a ring wing can be made to rollup just as smoothly as that for a finite wing.

Higdon and Pozrikidis [17] introduced two-dimensional panels which are circular arcs with a polynomial circulation distribution. Since vortex dumping was not used, only closed and infinite vortex sheets were analyzed. Because the panels provide a continuous representation of the sheet, there is no restriction in width of the panels. By using smaller panels to increase local resolution, double-branched rollup can be described without the use of core dumping. The existence of a panel size dependent instability was mentioned, but the nature of the instability was not described.

1.4. The Motivation for this Study

The aim of this thesis is to provide a foundation for a vortex sheet technique which offers a more accurate simulation of a thin, axisymmetric shear layer. The numerical techniques similar to those developed for point-vortex methods will be adopted for flat sections of axisymmetric vortex sheet, giving us a simple panel method for axisymmetric geometries. A careful, systematic study of vortex sheets represented by flat panels has been performed to explore the strengths and weaknesses of this

approach. Unlike some studies of vortex sheet models, the accuracy of the model will be stressed more than the efficiency of the computational technique. It is hoped that much of the artificial behavior, such as that introduced by a rigid wake analysis, can be removed from the simulation of vortex sheet.

The axisymmetric panel method is obtained through the extension of the two-dimensional panel method to axisymmetric geometries. The axisymmetric geometry is unique for being the only three-dimensional geometry with only two-coordinates. Thus, unlike the general three-dimensional flow, an axisymmetric flow can be described by a stream function. Fortunately, many interesting fluid dynamics phenomena exhibit axisymmetry. The circular jet and the buoyant plume are two examples of axisymmetric flows which can be studied easily in the laboratory. A problem of special engineering interest is the axisymmetric equivalent of Westwater's work, the roll-up of the wake-sheets generated by a helicopter in hover. The roll-up of rotor wake is extremely important to helicopter performance because, unlike the wake trailed by airplane wing, the wake remains close to the rotor, significantly affecting the rotor performance and acoustics.

Chapter 2

Mathematical Formulation of Vortex Elements

2.1. A Review of Concepts Regarding Vorticity

Vorticity, $\vec{\omega}$, is a local property of the fluid, defined as the curl of the local velocity, \vec{v} ,

$$\vec{\omega}(\vec{x}) = \nabla \times \vec{v}(\vec{x}) \quad (2.1)$$

This vector quantity describes the rotation of an infinitesimal element of fluid. A vortex line is a curve which is everywhere tangent to the local vorticity vector. To be consistent with the rotational aspect of vorticity, a vortex line must end at the boundaries of the fluid or form a closed curve and may never intersect itself or another vortex line.

In real flows, vorticity is produced as a sheet of parallel vortex lines known as a vortex sheet. In invicid flow, the vortex sheet remains infinitesimally thin and defines a stepwise jump in velocity tangent to the sheet. The difference in velocity across the sheet defines the "strength" at a point on the sheet. The vortex sheet usually rolls-up to form what can be described as a vortex filament. In a real fluid, the vorticity within the vortex filament will become smoothly distributed by viscous diffusion within a finite time span. The structure of an evolved vortex filament is similar to the asymptotic limit for an invicid vortex filament with an infinite number of layers of vortex sheet rolled up into a region of finite cross-section. In invicid analyses, a vortex filament with a smooth distribution of vorticity is commonly used as a model for a tightly wound section of a vortex sheet.

In potential flows, the circulation

$$\Gamma = \oint \vec{v} \cdot d\vec{s} \quad (2.2)$$

is a conserved quantity. This allows the flow associated with a complex vortex system to be determined by summing the contributions from a finite number of vortex elements which make up the system. The amount of circulation in each element must equal the circulation in the section of the vortex system the element replaces. By replacing a vortex system with a set of known vortex elements with a similar distribution of vorticity, the flow of material points in a complex vortex system can be deduced.

2.2. Two-Dimensional Vortex Elements

2.2.1. The Point Vortex

The two-dimensional form of the line vortex is the point vortex. The velocity induced by a point vortex can be derived from the conservation of circulation, (2.2), around a point:

(2.3)

$$\begin{aligned} V_{\text{azimuthal}} &= \frac{-\Gamma}{2\pi r} \\ V_{\text{radial}} &= 0 \end{aligned}$$

(2.4)

where r is the distance from the point vortex. The velocity induced by a point vortex is singular when the distance from the vortex, r , equals zero. From the velocity expression, the stream function of a point vortex is

$$\psi(r) = \frac{-\Gamma}{2\pi} \ln r \quad (2.5)$$

or in Cartesian coordinates centered on the vortex,

$$\psi(x,y) = \frac{-\Gamma}{4\pi} \ln(x^2+y^2) \quad (2.6)$$

The two-dimensional form of a vortex filament is a vortex with finite core. If the cross-section of the core is circular, the flow outside the core is equivalent to the flow induced by a point vortex of equal strength at the core's center. However, unlike the point vortex, the velocity induced by a vortex core is non-singular since the vorticity is distributed over a finite area. A Rankine vortex, an example of a vortex core, consists of a cylinder of fluid in solid body rotation surrounded by an irrotational flow.

2.2.2. The Vortex Panel

A vortex panel is a segment of a two-dimensional vortex sheet. It is equivalent in three-dimensions to a strip of vortex sheet composed of parallel, straight vortex lines. Since inviscid vortex systems would be made up of vortex sheets, accurate modelling of inviscid vortical flow should be possible using vortex panels.

The strength of a vortex panel will depend on the amount and distribution of circulation in the panel. For this study, a panel with uniform distribution of circulation is considered. Then the gross translation of the panel can be defined at its mid-point, its centroid of vorticity. The strength of the panel can be determined by its width and the "gradient of circulation", κ , defined mathematically as

$$\kappa = \frac{\partial \Gamma}{\partial S} .$$

The discrete form of κ is obtained by the central difference scheme

$$\kappa_i \approx \frac{\Gamma_{i+1/2} - \Gamma_{i-1/2}}{S_{i+1/2} - S_{i-1/2}}$$

where Γ_i is the circulation of the i^{th} position on the vortex sheet and S is the arc length taken along the vortex sheet. Then the strength of the i^{th} panel of width w is given by

$$\kappa_i \approx \frac{\Gamma_{i+1/2} - \Gamma_{i-1/2}}{w} . \quad (2.7)$$

Thus, a panel is equivalent to a point vortex with the same circulation "smeared" into the shape of a panel.

The flow induced by the vortex panel can be obtained by representing the vortex lines making up the panel as point vortices of infinitesimal strengths. The velocity induced by the panel can then be obtained by integrating the contributions by the point vortices. This is can be accomplished by integrating along the panel, the effects of point vortices with the strength

$$d\Gamma = \kappa ds \quad (2.8)$$

where κ is given by (2.7).

In order to simplify the mathematics involved, we shall limit ourselves to flat vortex panels. In a two-dimensional representation, the panel will be represented by a line segment having the Cartesian coordinates

$$x(s) = x_0 + s \cos \theta \quad (2.9)$$

$$y(s) = y_0 + s \sin \theta \quad (2.10)$$

where the panel at (x_0, y_0) is inclined at an angle θ .

In a previous work on panel methods Morky [18], using flat panels, carried out the direct integration of infinitesimal velocities to obtain the velocity field induced by a panel. Since the velocity integrand is singular, this involves evaluating a Cauchy principal value integral. However, the logarithmically singular stream function of a point vortex is integrable. Using Equations (2.6)(2.8)(2.9) and (2.10), the stream function is given by integrating along the vortex panel:

$$\psi(x, y) = \frac{-\kappa}{4\pi} \int_{-a}^a \ln[(x - s \cos \theta)^2 + (y - s \sin \theta)^2] ds \quad (2.11)$$

$$= \frac{-\kappa}{4\pi} \int_{-a}^a \ln [Q_5 - 2s Q_3 + s^2] ds \quad (2.12)$$

$$= \frac{-\kappa}{4\pi} [(a - Q_3) \ln Q_2 + (a + Q_3) \ln Q_1 + 2Q_4 \operatorname{arctg} \frac{a - Q_3}{Q_4} + 2Q_4 \operatorname{arctg} \frac{a + Q_3}{Q_4} - 4a] \quad (2.13)$$

$$Q_5 = x^2 + y^2 \quad (2.14)$$

$$Q_4 = y \cos \theta - x \sin \theta \quad (2.15)$$

$$Q_3 = x \cos \theta + y \sin \theta \quad (2.16)$$

$$Q_2 = Q_5 - 2aQ_3 + a^2 \quad (2.17)$$

$$Q_1 = Q_5 + 2aQ_3 + a^2 \quad (2.18)$$

where a is the half-width of the panel ($a \equiv \frac{1}{2}w$).

There are two methods for evaluating the velocities from the stream functions. One method, most suitable for Eulerian analyses with its coordinate-mesh, is to take finite differences over the control-volumes. The alternate method is to evaluate the velocities, which are derivatives of the stream functions, explicitly at the points of interest.

$$u(x,y) = \frac{-\partial\psi}{\partial y} \quad (2.19)$$

$$= \frac{-\kappa}{4\pi} \left[-\sin\theta \ln \frac{Q_2}{Q_1} + 2\cos\theta \left(\operatorname{arctg} \frac{a-Q_3}{Q_4} + \operatorname{arctg} \frac{a+Q_3}{Q_4} \right) \right] \quad (2.20)$$

$$v(x,y) = \frac{\partial\psi}{\partial x} \quad (2.21)$$

$$= \frac{\kappa}{4\pi} \left[-\cos\theta \ln \frac{Q_2}{Q_1} - 2\sin\theta \left(\operatorname{arctg} \frac{a-Q_3}{Q_4} + \operatorname{arctg} \frac{a+Q_3}{Q_4} \right) \right] \quad (2.22)$$

The velocity field produced by the equations are shown in Figure 2-1. In these formulas, the arc-tangent, being multiple valued on the panel, models the jump in tangential velocity as the panel is crossed. Mathematically, the panel is a branch cut in the coordinate space connecting the two logarithmic singularities at the edges of the panels.

2.3. Extension to Axisymmetric Geometries

2.3.1. The Axisymmetric Problem

An axisymmetric vortex sheet is composed of coaxial, circular vortex lines. Thus, a simple-minded extension of the Rosenhead approach to sheet discretization is to replace point vortices by circular line vortices. However this straight-forward approach is unworkable because a curved line vortex is influenced by its own velocity singularity. As a result, a circular line vortex will translate through the fluid at infinite velocities [19]. One way of avoiding the infinite translation velocity involves using circular vortex filaments, or vortex rings, in place of the singular line vortices. This introduces a finite vorticity distribution which induces a finite translation velocity. Another approach is to use polygons made of straight segments of line vortices in place of the vortex rings. A network formed by vortex polygons is known as a vortex lattice. Unlike the strictly axisymmetric models, the vortex polygons should be able to display non-axisymmetric deformations of the vortex sheet. Azimuthal deformations are known to hasten the decay of vortex rings [20], and should have an important consequences for the behavior of three-dimensional vortex sheets.

However, both of the above models of axisymmetric vortex sheet require the selection of a length parameter: the radius of the vortex core or the length of a polygon

element. Thus before any of these models can be used accurately, it is necessary to gain a better understanding of the behavior of vortex sheet these models are designed to reproduce.

The axisymmetric equivalent of the vortex panel is a "vortex band", a section of an axisymmetric vortex sheet. It represents a finite piece of the vortex sheet which, in some models of the axisymmetric vortex sheet, is replaced by vortex rings and vortex polygons. Although a band does not possess any volume, by defining the band's position at the mid-point of the band as was done for the two-dimensional panels, the self-induced velocity of the band is shown to be finite.

The stream function for circular line vortices, expressed using complete elliptic integrals $E_1(\lambda)$ and $F_1(\lambda)$, is given by Lamb [21].

(2.23)

$$\psi(x,y) = \frac{-\Gamma}{2\pi} (r_1 + r_2) \{ F_1(\lambda) - E_1(\lambda) \}$$

$$\lambda = \frac{r_2 - r_1}{r_2 + r_1} \quad (2.24)$$

$r_1 \equiv$ Least distance between (x,y) and the vortex

$r_2 \equiv$ Greatest distance between (x,y) and the vortex

To obtain the flow for a vortex panel, this stream function must be integrated across the panel, resulting in a difficult double-integration of singular elliptic functions.

2.3.2. The Method of Matched Asymptotic Expansion

If the width of the vortex band is small relative to its radius, an asymptotic expansion for the stream function can be obtained. The approach used here for the vortex panel, known as the method of matched asymptotic expansion, was also used in a study of curved vortex filaments [22]. This method derives an uniformly valid solution which asymptotically approaches known behavior of the actual stream function. Thus, it is important to heuristically deduce what is expected from the stream function. We can expect the character of the stream function away from the band to approach that of the stream function for a circular line vortex. Thus, the circular line vortex stream function will be used as the outer-solution. Near the band, the stream function should resemble the two-dimensional solution for a vortex panel. However, the inner-solution must include effects due to curvature in the axisymmetric geometry.

The coordinate systems used in the following analysis are shown in Figure 2-2.

2.3.2.1. The Outer-Solution

The velocity away from the band is derived from (2.23) which gives

$$u_{out} = \frac{\kappa a}{\pi(R+x)} \frac{\partial}{\partial y} \{ (r_1 + r_2) [E_1(\lambda) - E_1(\lambda)] \} \quad (2.25)$$

$$v_{out} = \frac{-\kappa a}{\pi(R+x)} \frac{\partial}{\partial x} \{ (r_1 + r_2) [E_1(\lambda) - E_1(\lambda)] \} \quad (2.26)$$

where R is the radius of the vortex band.

2.3.2.2. The Inner-Solution

The axisymmetric velocity field, for a given axisymmetric stream function ψ , is defined to be

$$u(r,z) = \frac{-1}{r} \frac{\partial \psi}{\partial z} \quad (2.27)$$

$$v(r,z) = \frac{1}{r} \frac{\partial \psi}{\partial r} \quad (2.28)$$

The irrotationality of the potential flow gives

$$\frac{\partial u}{\partial z} - \frac{\partial v}{\partial r} = 0 \quad (2.29)$$

Which is the same as that for two-dimensional flow, $\bar{\omega} = 0$. Combining Equations (2.27)(2.28) and (2.29) gives the governing equation for the axisymmetric stream functions:

$$\frac{\partial^2 \psi}{\partial r^2} + \frac{\partial^2 \psi}{\partial z^2} - \frac{1}{r} \frac{\partial \psi}{\partial r} = 0. \quad (2.30)$$

This equation is the axisymmetric equivalent of the two-dimensional stream function equation

$$\frac{\partial^2 \psi_{2D}}{\partial x^2} + \frac{\partial^2 \psi_{2D}}{\partial y^2} = 0. \quad (2.31)$$

It is now necessary to switch to a panel-centered coordinate system (x,y) , originating at the center of the vortex band of radius R.

$$\frac{\partial^2 \psi}{\partial x^2} + \frac{\partial^2 \psi}{\partial y^2} - \frac{1}{R+x} \frac{\partial \psi}{\partial x} = 0. \quad (2.32)$$

Non-dimensionalizing with respect to the outer length-scale, radius R , gives

$$\frac{\partial^2 \psi}{\partial x^2} + \frac{\partial^2 \psi}{\partial y^2} - \frac{1}{1+x} \frac{\partial \psi}{\partial x} = 0. \quad (2.33)$$

The coordinates can now be rescaled by a small parameter, the curvature, which is $\epsilon = \frac{a}{R}$ where a is the half-width of the band. Rescaling (2.33) by ϵ gives

$$\frac{\partial^2 \psi}{\partial x^2} + \frac{\partial^2 \psi}{\partial y^2} - \frac{\epsilon}{1+\epsilon x} \frac{\partial \psi}{\partial x} = 0. \quad (2.34)$$

with the understanding that (x,y) are non-dimensional, stretched coordinates.

The expanded inner stream function,

$$\psi = \psi_0 + \epsilon \psi_1 + \epsilon^2 \psi_2 \dots \quad (2.35)$$

is used to express the effects of curvature, ϵ , due to the perturbation of the two-dimensional stream function, ψ_0 . In the above series, terms $O(\epsilon^n \ln \epsilon)$ have been included with terms $O(\epsilon^{n-1} \ln \epsilon)$. Using this expansion, the governing equation (2.34) can be broken up into equations for each order in the expansion:

$$O(1) \cdot \frac{\partial^2 \psi_0}{\partial x^2} + \frac{\partial^2 \psi_0}{\partial y^2} = 0 \quad (2.36)$$

$$O(\epsilon) \cdot \frac{\partial^2 \psi_1}{\partial x^2} + \frac{\partial^2 \psi_1}{\partial y^2} = \frac{\partial \psi_0}{\partial x} \quad (2.37)$$

The zeroth-order equation is the governing equation for the two-dimensional stream function (2.31). The subsequent equations for the higher-order terms of the inner stream function are all Poisson's Equations, with the non-homogeneous terms involving the solutions of lower-order equations. Thus, repetitive evaluation of the Poisson's Equation can be used to obtain the desired degree of accuracy.

By assuming the effect of curvature to be small, we will only need to evaluate the first term in the expansion. The particular solution for the first-order Poisson's Equation is

$$\psi_{1p} = \frac{1}{2} x \psi_0. \quad (2.38)$$

Then, using (2.13) for the zeroth-order term of the expansion, the inner stream function is

$$\psi_{in} = (1 + \frac{1}{2}\epsilon x) \psi_0 + \psi_{homo}. \quad (2.39)$$

where ψ_{homo} is some stream function satisfying the homogeneous equation, which is determined by matching the inner and outer solutions as shown in the following section.

Using notations defined by (2.14)(2.15)(2.16)(2.17) and (2.18), The inner solution for the velocity field is

$$u_{in} = \frac{-\kappa}{4\pi} (1 + \frac{1}{2}\epsilon x) [-\sin\theta \ln \frac{Q_2}{Q_1} + 2\cos\theta (\arctg \frac{a-Q_3}{Q_4} + \arctg \frac{a+Q_3}{Q_4})] \quad (2.40)$$

$$v_{in} = \frac{\kappa}{4\pi} (1 + \frac{1}{2}\epsilon x) [-\cos\theta \ln \frac{Q_2}{Q_1} + 2\sin\theta (\arctg \frac{a-Q_3}{Q_4} + \arctg \frac{a+Q_3}{Q_4})] \quad (2.41)$$

$$+ \frac{1}{2}\epsilon [(a-Q_3) \ln Q_2 + (a+Q_3) \ln Q_1 - 4a + 2Q_4 (\arctg \frac{a-Q_3}{Q_4} + \arctg \frac{a+Q_3}{Q_4})]$$

2.3.2.3. The Inner/Outer Matching Solution

The vortex band inner stream function solution (2.39) must be matched to the outer-solution, which is approximated by the circular line vortex solution (2.23). First, the circulations of the perturbed vortex panel and the circular line must be equal. Then it is necessary to equate the outer-limit of the inner-solution to the inner-limit of the outer-solution using a matching criteria. The "matching solution", the intermediate limit solution obtained using the matching criteria, will subsequently be subtracted from the sum of the inner and outer solutions to produce the uniformly valid asymptotic solution. A discussion of the method of matched asymptotic analysis can be found in Reference [23].

The inner-limit of the outer solution is found by expanding the elliptic integrals in (2.23) for small complementary modulus, $1 - \lambda^2$ (2.24), as shown by Jahnke and Emde [24]

$$\psi_{out}^i = \frac{-\Gamma}{2\pi} \{2 + \frac{x}{2R} + \ln \frac{r_1}{8R} (1 + \frac{x}{2R})\} + O(\epsilon^2 \ln \epsilon) \quad (2.42)$$

This result was also obtained by Tung and Ting [25].

The outer-limit of the inner-solution is found at the limit, $r_1 \gg a$, where the panel width and inclination become unimportant. Therefore, using the approximations

$$\begin{aligned} Q_1 &\sim x^2 + y^2 = r_1^2 \\ Q_2 &\sim x^2 + y^2 = r_1^2 \\ \ln \frac{Q_2}{Q_1} &\sim 0 \\ \operatorname{arctg} \frac{a-Q_3}{Q_4} + \operatorname{arctg} \frac{a+Q_3}{Q_4} &= \operatorname{arctg} \frac{2aQ_4}{Q_4^2 - a^2} \sim 0 \end{aligned}$$

we can get the outer-limit of the inner-solution,

$$\psi_{\text{in}}^o = \frac{-\kappa a}{\pi} \ln \frac{r_1}{a} \left(1 + \frac{x}{2R}\right) \quad (2.43)$$

neglecting the higher order terms.

Since the panels span the width $2a$, the definition for κ (2.7)

$$\Gamma_{\text{panel}} = 2 \kappa a \quad (2.44)$$

is substituted into (2.42). The complete intermediate stream function for a vortex band is produced the matching criteria, ψ_{homo} , which equates the two intermediate limits (2.42) and (2.43). Neglecting the higher-order terms, the matching criteria is added to the inner-limit of the outer solution (2.42)

$$\psi_{\text{io}} = \frac{-\kappa a}{\pi} \left\{ 2 + \frac{x}{2R} + \ln \frac{r_1}{8R} \left(1 + \frac{x}{2R}\right) \right\} + \psi_{\text{homo}} \quad (2.45)$$

The matching criteria, ψ_{homo} is obtained by equating the inner-limit of the outer solution (2.45) to the outer-limit of the inner solution (2.43)

$$\begin{aligned} \psi_{\text{io}} &= \frac{-\kappa a}{\pi} \left\{ \ln \frac{r_1}{a} \left(1 + \frac{x}{2R}\right) \right\} \\ &= \frac{-\kappa a}{\pi} \left\{ 2 + \frac{x}{2R} + \ln \frac{r_1}{8R} \left(1 + \frac{x}{2R}\right) \right\} + \psi_{\text{homo}} \end{aligned} \quad (2.46)$$

Then the matching criteria is found to be

$$\psi_{\text{homo}} = \frac{\kappa a}{\pi} \left\{ 2 + \frac{x}{2R} + \ln \frac{e}{8} \left(1 + \frac{x}{2R}\right) \right\}, \quad (2.47)$$

and the intermediate stream function is established, as shown by Equation (2.46), to be

$$\psi = \frac{-\kappa a}{\pi} \left(1 + \frac{x}{2R}\right) \ln \frac{r_1}{a}. \quad (2.48)$$

2.3.2.4. The Composite, Uniformly-Valid Solution

The complete, uniformly-valid stream function for the axisymmetric vortex band is a composite of the inner-solution, ψ_{in} , the outer-solution, ψ_{out} , and the intermediate (matching) solution, ψ_{io} . The complete solution can be formulated to be

$$\psi(x,y) = \psi_{in} + \psi_{out} - \psi_{io} \quad (2.49)$$

where,

$$\psi_{in} \equiv \text{Inner Solution (2.39)}$$

$$= R \left(1 + \frac{x}{2R}\right) \psi_{2D}$$

$$\psi_{2D} \equiv \text{Two-Dimensional Panel Solution (2.13)}$$

$$= \frac{-\kappa}{4\pi} (a - Q_3) \ln Q_2 + (a + Q_3) \ln Q_1 \\ + 2Q_4 \operatorname{arctg} \frac{a - Q_3}{Q_4} + 2Q_4 \operatorname{arctg} \frac{a + Q_3}{Q_4} - 4a$$

$$\psi_{out} \equiv \text{Outer Solution (2.23)}$$

$$= \frac{-\kappa a}{\pi} (r_1 + r_2) \{ F_1(\lambda) - E_1(\lambda) \}$$

$$\psi_{io} \equiv \text{Inner/Outer Matching Solution (2.45)}$$

$$= \frac{-\kappa a}{\pi} R \left[\ln \frac{r_1}{a} \left(1 + \frac{x}{2R}\right) \right]$$

using notations introduced earlier. Notice that ψ_{in} and ψ_{io} have been redimensionalized with respect to the outer-dimension, R .

The above stream function is axisymmetric, thus its velocity field is defined to be

$$u(x,y) = \frac{-1}{R+x} \frac{\partial \psi}{\partial y} \\ v(x,y) = \frac{1}{R+x} \frac{\partial \psi}{\partial x}$$

However, the inner-solution, ψ_{in} , and the intermediate-solution, ψ_{io} , are valid only for the inner-region, $x \ll R$. Thus, the inner-region velocity field, using $R+x \approx R$, becomes

$$u_{in} - u_{io} = \frac{-1}{R} \frac{\partial}{\partial y} (\psi_{in} - \psi_{io})$$

$$v_{in} - v_{io} = \frac{1}{R} \frac{\partial}{\partial x} (\psi_{in} - \psi_{io}),$$

while the outer velocity field remains

$$u(x,y) = \frac{-1}{R+x} \frac{\partial \psi_{out}}{\partial y}$$

$$v(x,y) = \frac{1}{R+x} \frac{\partial \psi_{out}}{\partial x}.$$

Thus, the velocity field is given by a composite solution of the form

$$u(x,y) = u_{in} + u_{out} - u_{io} \quad (2.50)$$

$$v(x,y) = v_{in} + v_{out} - v_{io} \quad (2.51)$$

where,

$$u_{in} = \frac{-\kappa}{4\pi} \left(1 + \frac{x}{2R}\right) \left[-\sin\theta \ln \frac{Q_2}{Q_1} + 2\cos\theta \left(\operatorname{arctg} \frac{a-Q_3}{Q_4} + \operatorname{arctg} \frac{a+Q_3}{Q_4}\right)\right]$$

$$v_{in} = \frac{\kappa}{4\pi} \left(1 + \frac{x}{2R}\right) \left[-\cos\theta \ln \frac{Q_2}{Q_1} - 2\sin\theta \left(\operatorname{arctg} \frac{a-Q_3}{Q_4} + \operatorname{arctg} \frac{a+Q_3}{Q_4}\right)\right]$$

$$+ \frac{1}{2R} \left[(a-Q_3) \ln Q_2 + (a+Q_3) \ln Q_1 - 4a \right. \\ \left. + 2Q_4 \operatorname{arctg} \frac{a-Q_3}{Q_4} + 2Q_4 \operatorname{arctg} \frac{a+Q_3}{Q_4} \right]$$

$$u_{out} = \frac{\kappa a}{\pi(R+x)} \left[\left(\frac{y}{r_1} + \frac{y}{r_2}\right)(K-E) + (r_1+r_2) \frac{\partial(K-E)}{\partial y} \right]$$

$$v_{out} = \frac{-\kappa a}{\pi(R+x)} \left[\left(\frac{x}{r_1} + \frac{x+2R}{r_2}\right)(K-E) + (r_1+r_2) \frac{\partial(K-E)}{\partial y} \right]$$

$$u_{io} = \frac{-\kappa a}{\pi} \left(1 + \frac{x}{2R}\right) \frac{y}{r_1^2}$$

$$v_{io} = \frac{\kappa a}{\pi} \left[\left(1 + \frac{x}{2R}\right) \frac{x}{r_1^2} + \frac{1}{2R} \ln \frac{r_1}{8R} \right].$$

The relationship between parts of the complete solution is shown by Figure 2-3, showing the contributions to the velocity profile taken radially from the cylindrical coordinate axis, denoted by the center-line, through a vortex band ($\theta = 0$). The uniformly-valid, composite solution for the velocity induced by the vortex panel, v_{comp} , is denoted by crosses. Prominent features in the plot are,

- 1) the $1/r$ type singularity of the outer-solution at the center of the panel ($x = 0, r_1 = 0$) matched by the intermediate-solution,
- 2) the logarithmic singularities of the inner-solution at the panel edges.

The composite solution retains the outer solution's $O(\epsilon \ln \epsilon)$ portion on the axis of symmetry while smoothly blending in the two-dimensional inner-solution in place of the singularity at $r_1 = 0$ before decaying off faster than the two-dimensional solution. Notice that the inner-solution is displaced, representing the speed of the self-induced translation of the vortex panel.

2.3.3. The Self-Induced Velocity

An important result of the preceding analysis is the self-induced velocity of a vortex band. The motion of the vortex band is defined at the mid-point of the band. Thus, using Equation (2.51), the axial speed of the panel center is found to be

$$\begin{aligned} v_{\text{band}} &= \frac{\partial}{\partial x} \psi(x=0, y=0) \\ &= \frac{\kappa a}{2\pi R} \left\{ \ln \frac{8R}{a} + \frac{1}{2} \right\}. \end{aligned} \quad (2.52)$$

The radial velocity at the panel center is zero for any orientation. Thus, for the present order of accuracy, $O(\epsilon)$, the self-induced translation of a vortex band, defined at the center of the band, is purely axial and independent of the panel orientation.

By applying (2.44) to equate the circulations, this result can be compared to the self-induced velocity of a uniform vorticity vortex ring, where $\frac{\omega}{R+x}$ is constant, [21, 22]

$$v_{\text{ring}} = \frac{\kappa a}{2\pi R} \left\{ \ln \frac{8R}{r_0} - \frac{1}{4} \right\}. \quad (2.53)$$

Thus, the core radius of an "uniform" vortex ring must be

$$\begin{aligned} \frac{r_0}{R} &= e^{-1/2} \frac{a}{R} \\ &\approx 0.707 \frac{a}{R} \end{aligned} \quad (2.54)$$

in order to translate at the same velocity as a vortex panel of the same circulation and radius. Since the self-induced velocity reflects the energy of the vortex element, the ratio pursued by equating the known energy of a vortex disk with the energy numerically integrated for a set of equally spaced vortex rings. The core diameter of

the vortex rings giving the same amount of energy is obtained numerically and the ratio is the quotient of this value over the ring spacing. By increasing the number of vortex rings, the ratio was found to converge to about 0.50 [26].

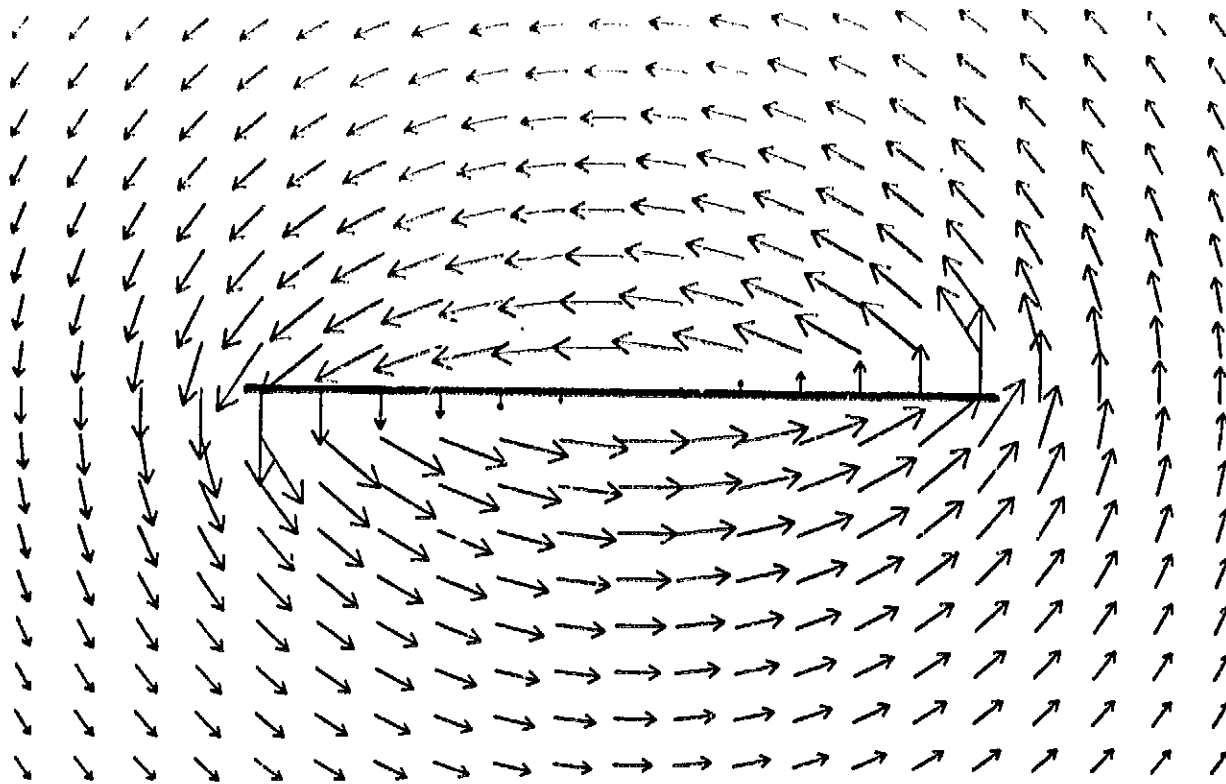


Figure 2-1: Velocity Vectors Associated with a Vortex Panel

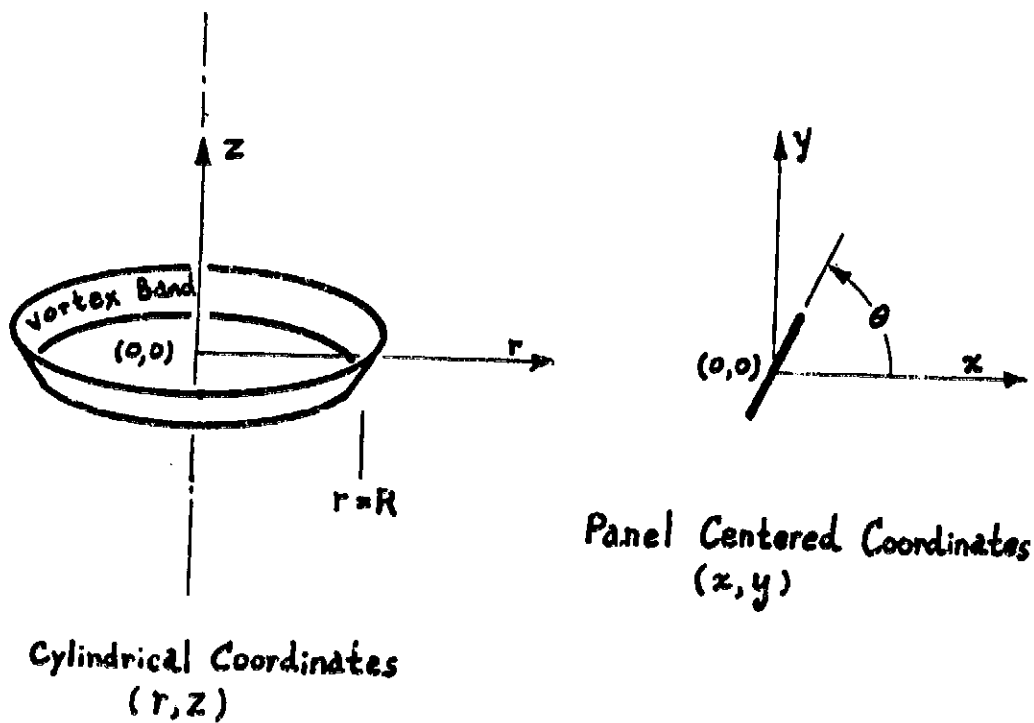


Figure 2-2: The Coordinate System

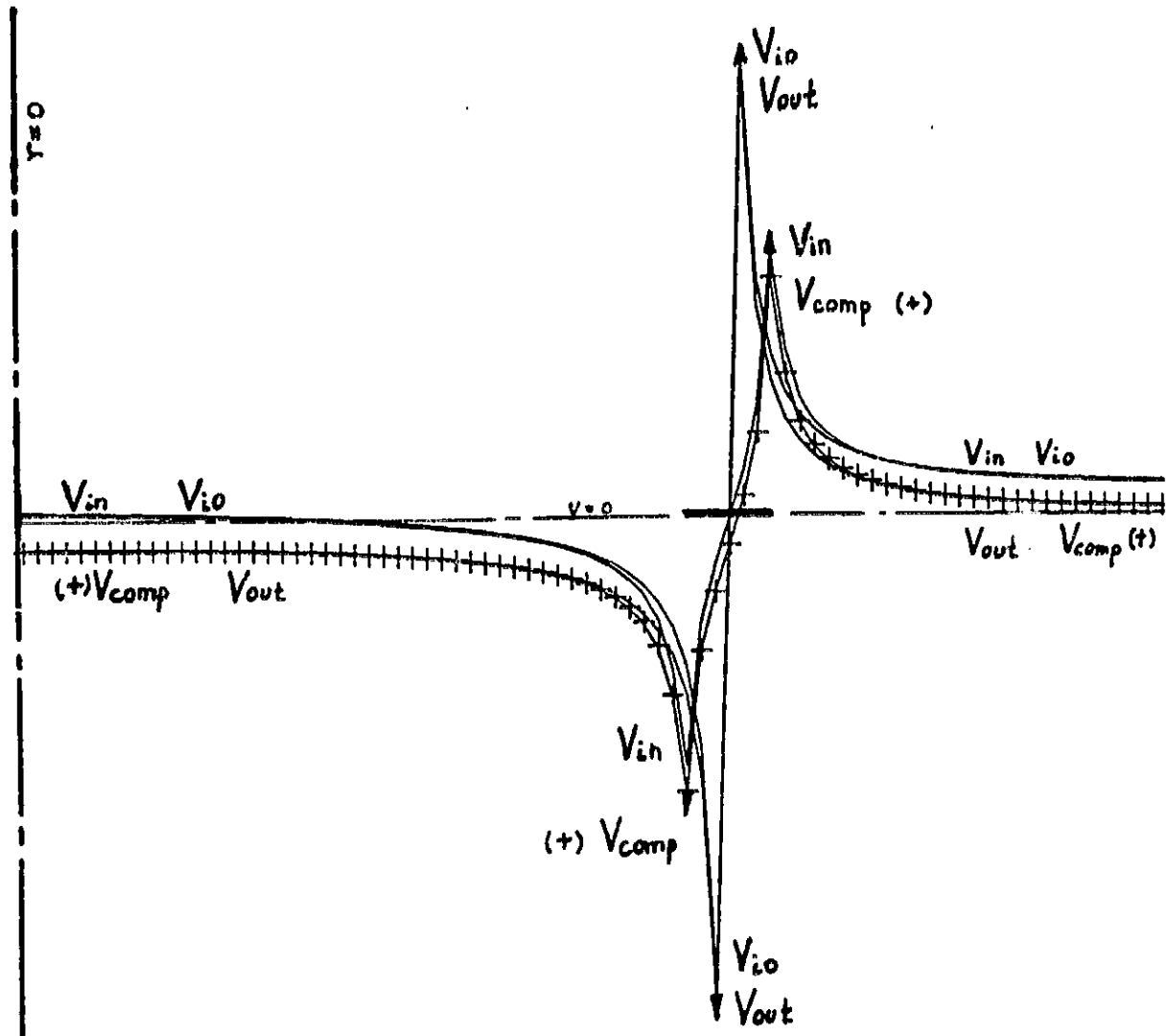


Figure 2-3: Plot of the Axial Velocity and its Constituent Parts

Chapter 3

Numerical Behavior of Vortex Elements

The FORTRAN subroutines for calculating the velocities induced by different vortex elements are presented in Appendix A. In this section, the differences between vortex elements will be explored.

3.1. The Velocity Profiles of Two-Dimensional Elements

Figures 3-1 and 3-2 show velocity profiles for vortex panels. The velocities are perpendicular to the panel-centered coordinate axes because of the panel's uniform circulation distribution. The most important feature is the lack of a strong singularity in the panel velocity profile. However, the normal velocity has a logarithmic singularity at the edges of the panel and no singularity in the tangential velocity, the latter being double-valued but finite on the panel itself. Away from the panel, the velocity profile quickly approaches the point vortex profile. The difference in the effect on the adjacent vortex elements is not obvious in this representation.

3.2. The Velocity Profiles of Axisymmetric Elements

Figures 3-3, 3-4, 3-5, and 3-6 show the velocity profiles along the panel axes of vortex bands with inclinations of 0 and 90 degrees. The centerline to the right denotes the location of the axis of symmetry with respect to the width of the panels. The self-induced translation velocity of the vortex band appears as the non-zero axial velocity at the midpoint of the panel.

3.3. Integration of Vortices in the Form of a Vortex Panel

As a simple test of integrating vortex elements to simulate a vortex sheet, vortex elements were arranged to form a vortex panel. The flow produced by a vortex panel of uniform circulation is described completely by Equation (2.13) and provides a baseline for the flow induced by the integration of vortex elements. Figure 3-7 shows the velocity vectors of flow around the baseline panel. The figures 3-8 and 3-9 shows the flow induced by four and ten point vortices, respectively, arranged to simulate a vortex panel. The accuracy in reproducing the baseline flow demonstrates the gain in accuracy achieved by integrating more point vortices. Of special importance is the velocity induced on the panel represented by the point vortices. The velocities induced on the point vortices are shown along the dashed line representing the vortex panel the point vortices replaces. For four point vortices, the singular nature dominates the velocity near the panel. For ten point vortices, the velocity field has a closer resemblance to the baseline flow. In comparison, Figures 3-10 and 3-11 show the flow field induced by two and ten vortex panels respectively. Unlike the previous plots, the velocity along the integrated panel is determined along the coordinate grid, they do not necessarily represent the velocities at the centers of the panels. The uniform distribution of velocity along the integrated panel shows the effective cancellation of the logarithmic singular behavior at the panel edges. The overall velocity fields are identical, indicating the validity of replacing a vortex sheet with an integration of vortex panels.

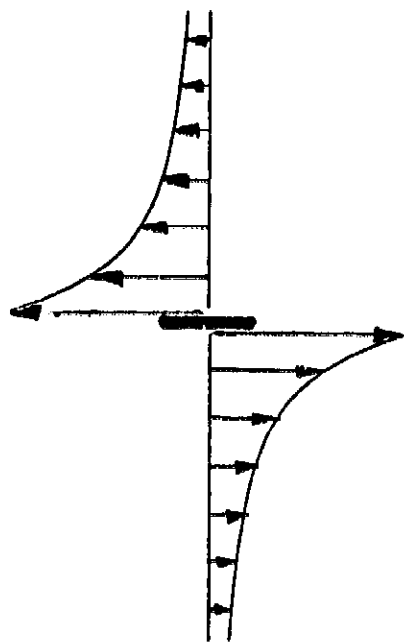


Figure 3-1: The velocity profile on axis tangential to the vortex panel

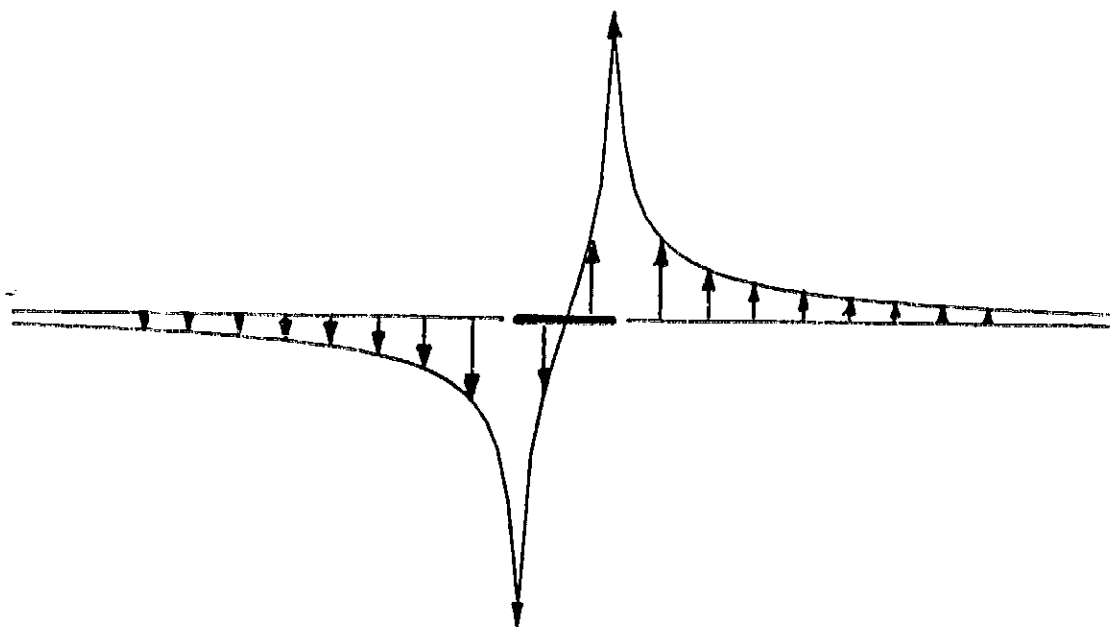


Figure 3-2: The velocity profile on axis normal to the vortex panel

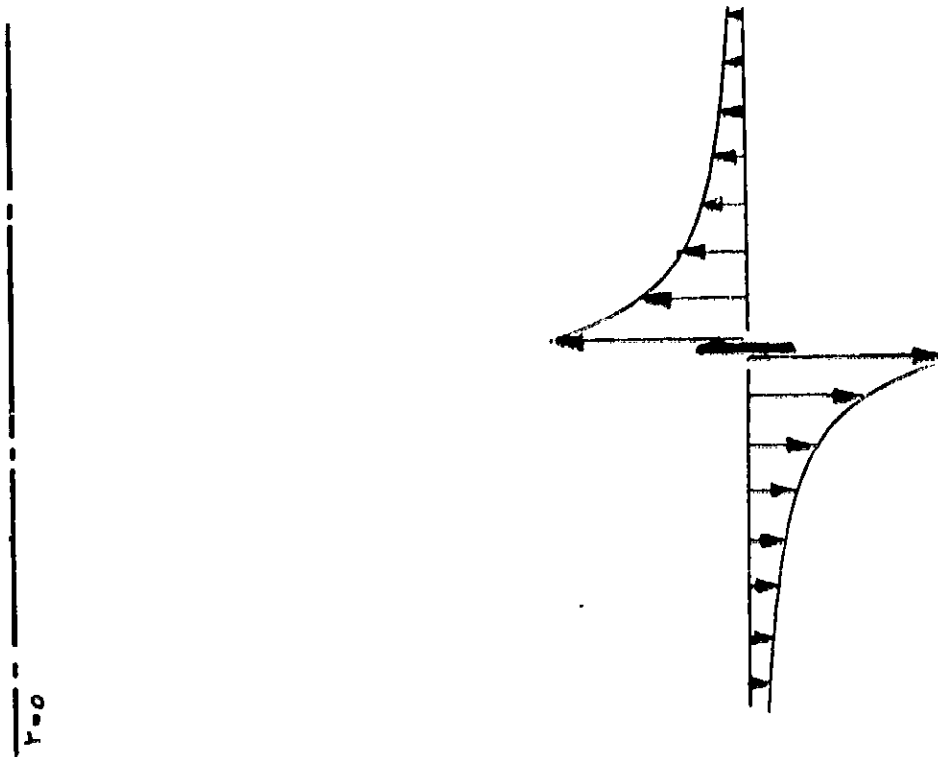


Figure 3-3: The radial velocity profile of a 0 deg vortex band

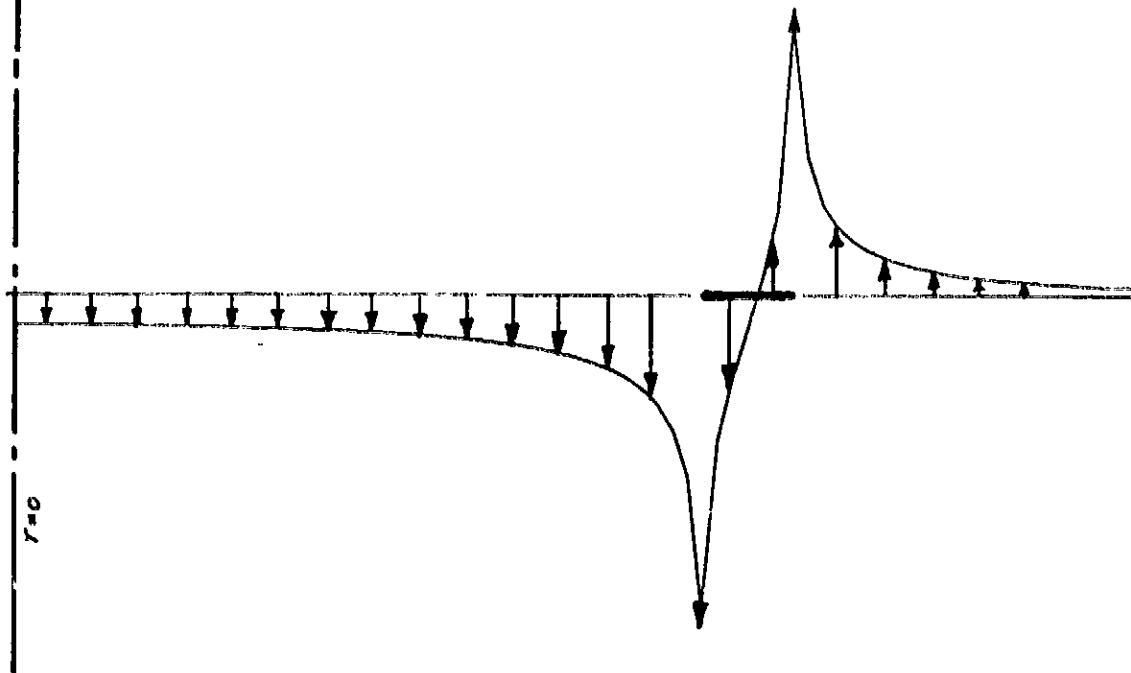


Figure 3-4: The axial velocity profile of a 0 deg vortex band

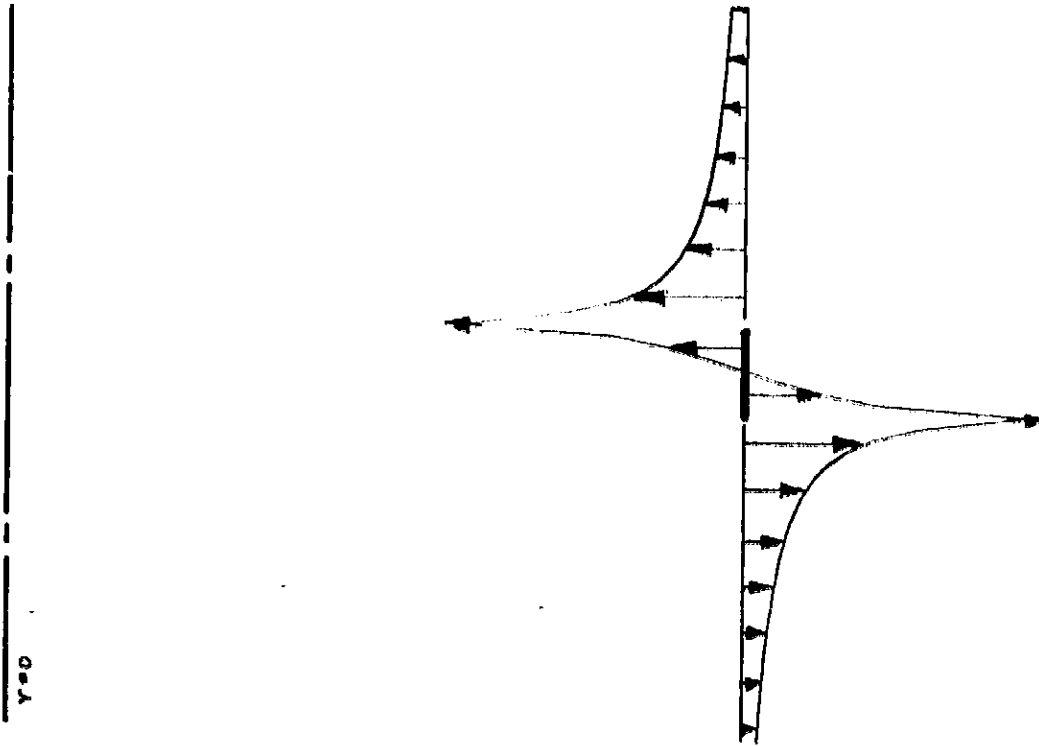


Figure 3-5: The radial velocity profile of a 90 deg vortex band

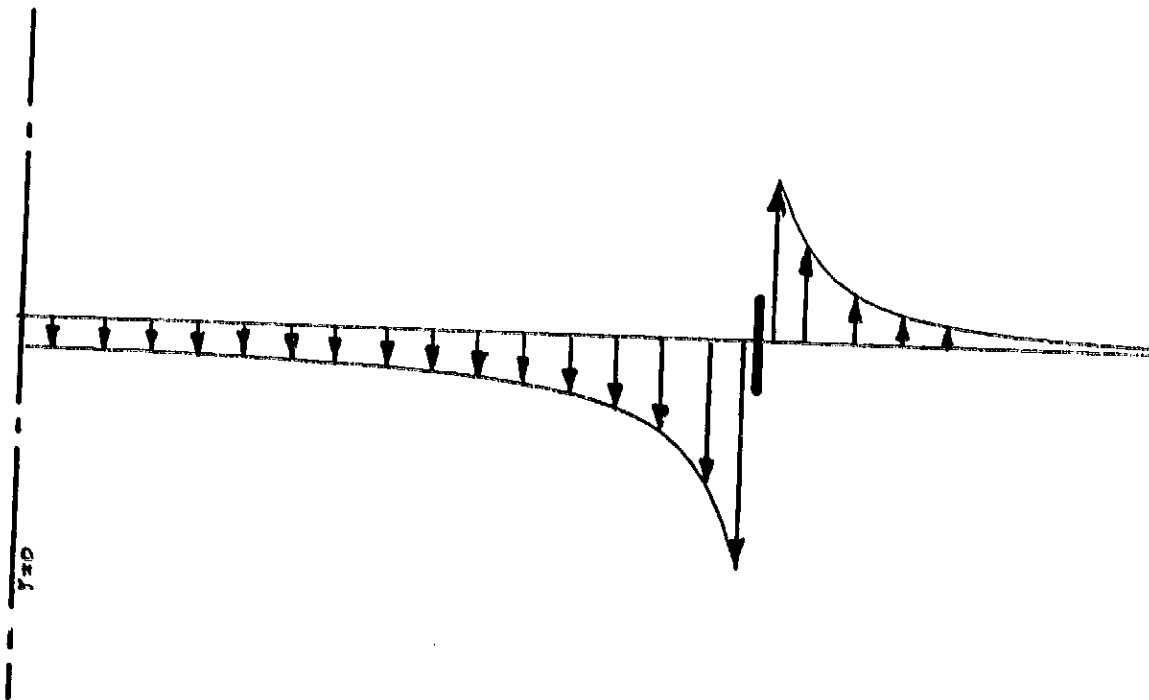


Figure 3-6: The axial velocity profile of a 90 deg vortex band

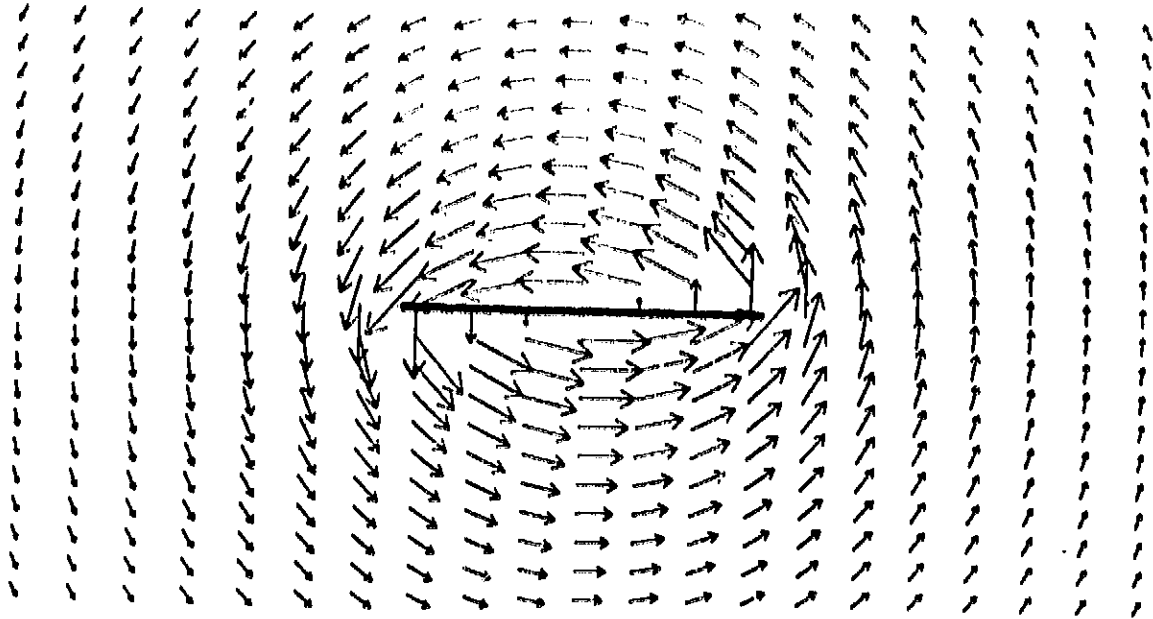


Figure 3-7: Baseline Flow: a single vortex panel spanning $x = \pm 1$

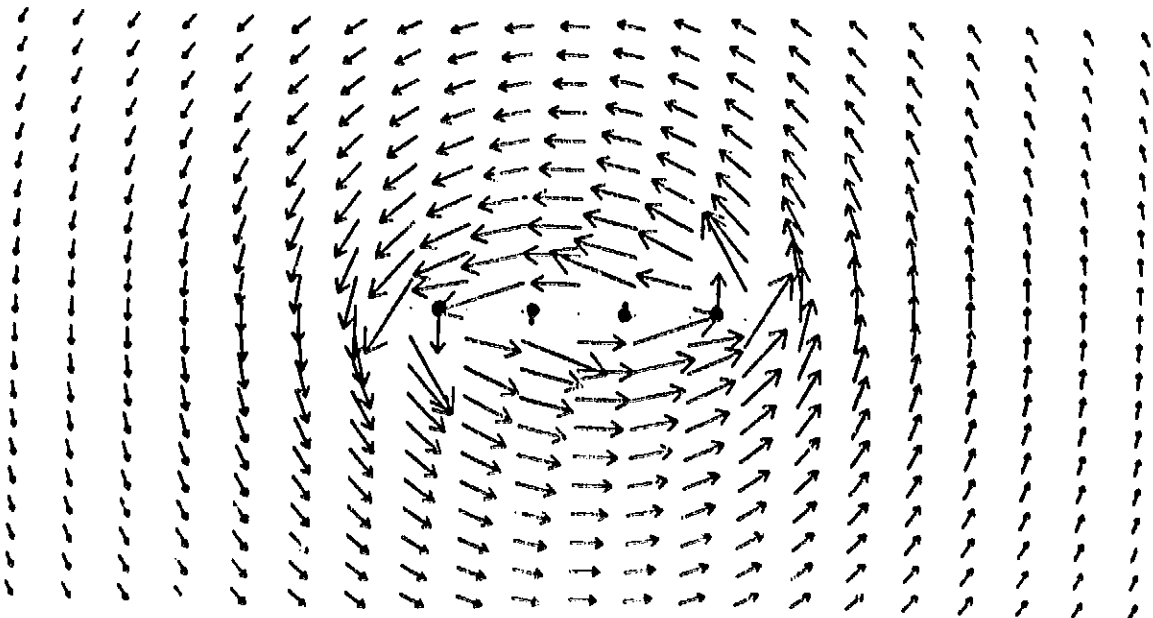


Figure 3-8: Point Vortex Flow: 4 vortices

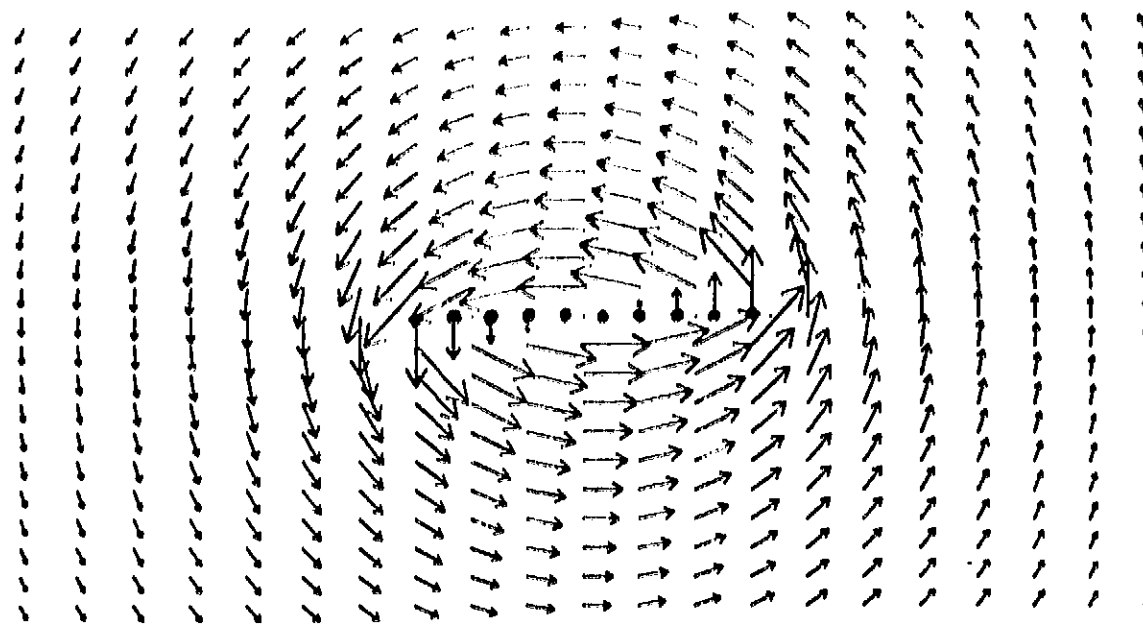


Figure 3-9: Point Vortex Flow: 10 vortices

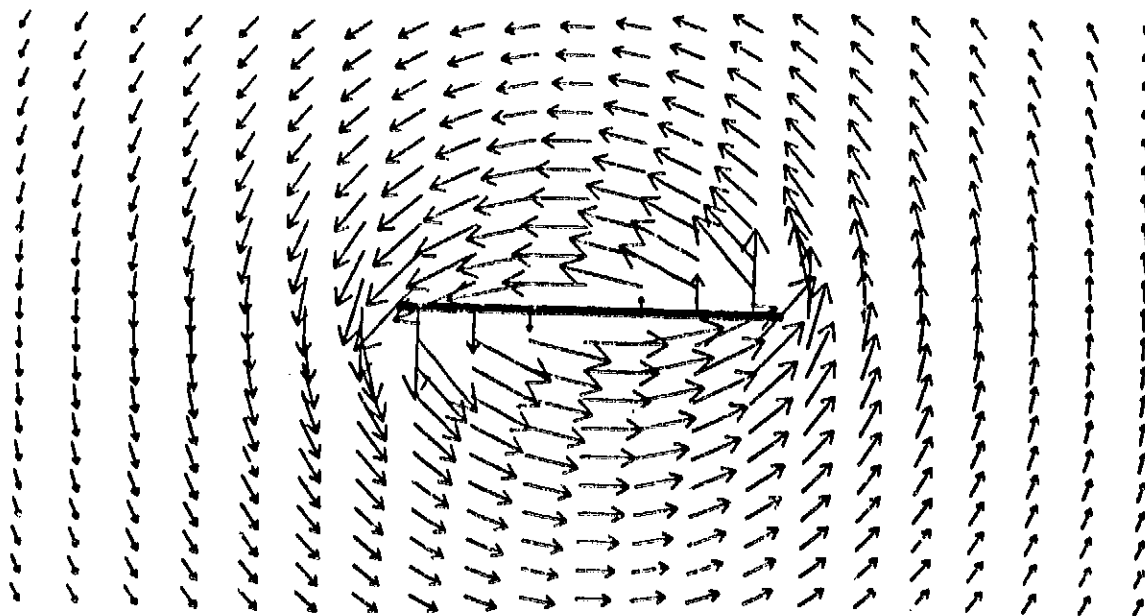


Figure 3-10: Vortex Panel Flow: 2 panels

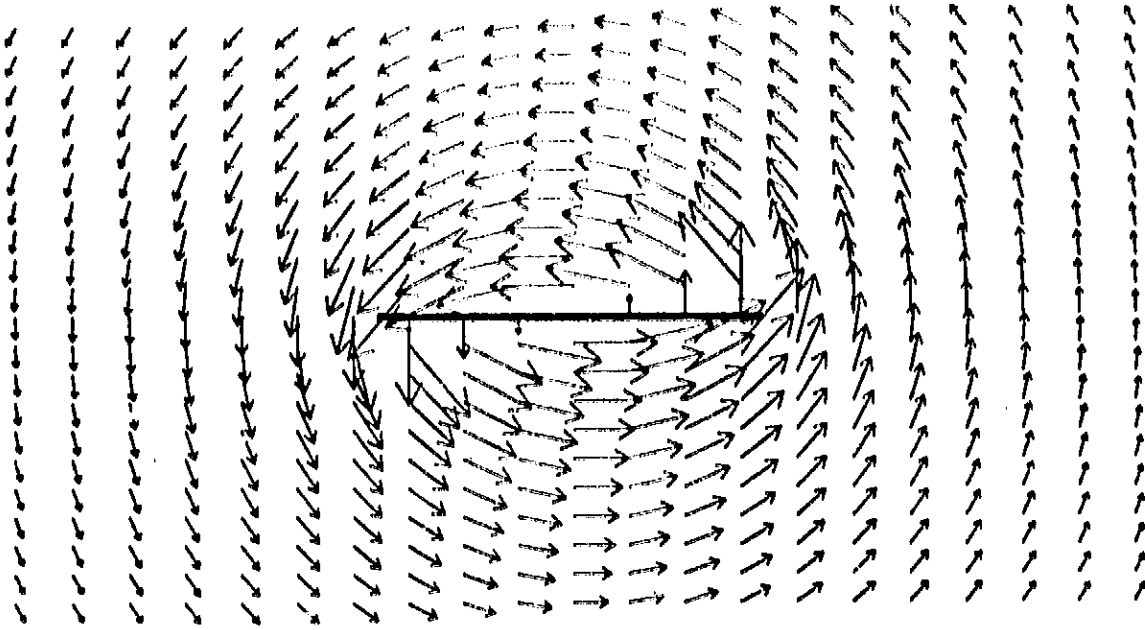


Figure 3-11: Vortex Panel Flow: 10 panels

Chapter 4

Discrete Numerical Approximation of a Vortex Sheet

4.1. The Uniform Downwash Solution for Discretized Vortex Sheets

The simulation of the vortex sheet trailed by a wing with an elliptic loading has been the most popular application for numerical vortex sheet methods. This popularity is not only due to the practical significance of the elliptic loading but also because the loading is predicted to generate only one pair of roll-up spirals.

An elliptically loaded lifting line, with semi-span b , possesses the circulation distribution of the form

$$\Gamma(x) = \Gamma_0 \left[1 - \frac{x^2}{b^2} \right]^{1/2}. \quad (4.1)$$

A straight lifting line with this distribution will generate a uniform downwash and a flat vortex sheet into which the bound vorticity is lost as one proceeds outward from mid-span. Thus the strength of the sheet is given by

$$\begin{aligned} \kappa(x) &= - \frac{\partial \Gamma}{\partial x} \\ &= \Gamma_0 \frac{x}{b^2} \left[1 - \frac{x^2}{b^2} \right]^{-1/2} \end{aligned} \quad (4.2)$$

Because of the singularities at the tips, the sheet will immediately roll-up into exponential spirals. The rolling-up of the sheet relieves the discontinuities in the vertical velocity profile.

Numerical simulations of the wake sheet dynamics usually ignore the fluid dynamics of the vortex sheet formation. For purposes of numerical analysis, it is important to know the initial geometry of the sheet and the flow associated with it. In many Lagrangian approaches to roll-up, an initial distribution of discrete vortices is selected

without checking its accuracy in modelling the initial state of the vortex sheet, and the merits of the analysis are judged by the quality of the resulting roll-up.

A flat vortex sheet which induces a velocity field which is constant along the sheet and singular at the tip is not adequate as the initial condition for a roll-up calculation. For a realistic model, the flat vortex sheet model can only be relied for an "outer-solution", valid away from the singular discontinuity at the edge of the sheet. Then an "inner-solution" at the edge is needed to give the effect of the sheet roll-up which is expected to form immediately upon the formation of the vortex sheet. Thus, a realistic simulation of the wing wake must begin with some sort of roll-up to replace the tip singularity. The same conclusion appears to have been reached empirically by Hooijmakers and Vaastra [16]

4.1.1. Point Vortex Representations of the Vortex Sheet

For Lagrangian simulation of vortex sheets, the initial downwash profile is represented by the velocities induced on each vortex element. Surprisingly, past investigators did not evaluate or comment upon the accuracy of the vortex sheet model to duplicate the initial condition. The only published result which gives the initial downwash profile is Westwater's pioneering work. In Westwater's initial vorticity distribution, an error in the position of three point vortices produced a "kink" in the initial downwash profile as shown by Figure 4-2. The total circulation contained by the sheet is 1.0, resulting in the uniform downwash result of 0.5 for a continuous, flat wake vortex sheet. Although the kink is apparent at the beginning of the tabulated results [12], Westwater proceeded with the tedious manual calculations without correcting the error. Unfortunately, even though the initial downwash profile can indicate the accuracy of the vortex sheet model and the validity of the subsequent roll-up, such results have not been published with the results of other roll-up calculations.

There are two approaches to representing a vortex sheet using point vortices. Westwater introduced the method of dividing the sheet into strips of equal circulation and replacing them by a point vortex at the centroid of vorticity of the strip. The other method, used successfully by Fink and Soh, replaces strips of equal width with a point vortex of equivalent circulation at the center of the strip. Westwater's method

was popular for a long time since it concentrates the vortices, and also serves as tracer particles, where most action is expected. Pink and Soh, on the other hand, designed their method to approximate an integration of flat panels. The downwash profile calculated using these two methods are shown in Figures 4-3 and 4-4. Both methods share the smooth, yet large, deviation from the uniform downwash value of 0.5, which is improved by increasing the number of vortices used. The exaggerated smoothing of the velocity discontinuity appears to be responsible for the extremely smooth roll-up obtained using point vortices. Figure 4-4 displays a secondary deviation by the velocity of the inner-most point vortex of the distribution. This error is caused by the proximity to the mirror image of the vortex which, having opposite circulation, adds a significant contribution on the downward velocity of the inner-most point vortex. In Figure 4-3, where there is more separation between the inner-most vortex and its adjacent vortices, thus no deviation is observed. Overall, the deviations from the predicted value of the uniform downwash are surprisingly large. Point vortex correction derived by Van der Vooren¹, as presented by Moore [4], is not applicable for the equal space discretization. Application of Van der Vooren's correction to the equal strength discretization did not improve the calculated downwash profile.

Instead of using the velocities induced on the point vortices to calculate the motion of the vortex sheet, the downwash can be defined to be the velocities obtained at points half-way between equally spaced vortices. This is the two-dimensional equivalent of the quadrilateral vortex-lattice (or "dipole") method which is often used for three-dimensional flow simulations. Figure 4-5 shows the velocities at points half-way between point vortices representing an elliptically loaded wing wake. The vortices are equally spaced as in Figure 4-4. The downwash profile obtained by this method differs substantially from the uniform lifting line downwash (0.5) and displays a character different from Figures 4-3 and 4-4. The "dip" in the downwash at the end of the profile is the result of the large step increase in the vortex strength at the tip.

¹Van der Vooren's correction involves the gradient of the vorticity distribution, resulting in an additional point vortex-like contribution to the velocity induced on each vortex.

4.1.2. Vortex Panel Representation of the Vortex Sheet

The downwash profiles corresponding to Figures 4-3 and 4-4 for integrations of vortex panels are shown in Figures 4-6 and 4-7 respectively. The figures show that an integration of panels will produce much better approximation of the downwash profile expected for a flat vortex sheet than possible using the same number of point vortices. Near the tip, the deviations from the uniform downwash result reflects the large step increase in the discretized distribution of the vortex sheet strength. The equal circulation panel distribution, Figure 4-6, produces less panels where the sheet is weak, resulting in the inaccurate velocity on the left-most panel. Since the velocity of a vortex panel is obtained at the center of the panel, which are half-way between the logarithmic singularities at the panel edges, features found in the velocities obtained between point vortices are expected. The only observed common feature is the "kink" in the profile at the next-to-the-last panel also found in Figure 4-7. However, the kink in the velocity induced by panels is less severe than that for the velocities midway between point vortices. This reflects the difference in degree of singularity possessed by the two vortex elements.

The downwash profile for the integration of equal width vortex panels closely resembles the uniform downwash produced by an elliptically loaded lifting line except at the tip. The discontinuous nature of the downwash inhibits the smooth roll-up of a sheet modelled using only vortex panels. If the downwash induced on the panels (disregarding the last panel at the tip) is taken to represent the outer-solution, then an inner-solution must be superposed to represent the roll-up at the tip. The tip roll-up can be represented by replacing the last panel on the sheet with a vortex core of the same strength, positioned in accordance to the Kaden's similarity solution (See Appendix B for details). Figure 4-8 shows the resulting smooth downwash profile. The right-most point in the profile is the downwash on the last panel and its "relief" in the downwash profile is significant; the velocity of the tip roll-up core is positive and lies outside of the plot.

The downwash profile for the integration of equal strength vortex panels appears to show the effect of a point vortex near the tip, the virtual core. The effect of such a core can be demonstrated plotting the downwash profile calculated with a point vortex of the opposite sign at the tip to cancel out the virtual core effect (Figure 4-9). The

shape of the downwash profile near the tip is not sensitive to the number of panels, suggesting some sort of similarity solution at the tip. The velocities induced on the last three panels by the integration of 5 to 100 panels were used to determine the strength and position of the point vortex needed to cancel out the deviation from the uniform downwash value. The results, plotted in Figures 4-10 and 4-11, shows that the vortex must be positioned 0.204 times the half-width of the last panel from the edge of the last panel and contain about 0.0547 times the circulation contained in one panel.

4.1.3. Vortex Band Representation of the Vortex Sheet

The axisymmetric equivalent of the wake vortex sheet of an elliptically loaded lifting line is the disk of axisymmetric vortex sheet with a translation of a disk in a fluid at rest. The first theoretical study of this flow was made by G.I. Taylor [27]. The vorticity distribution necessary to obtain a uniform velocity profile on the disk of vorticity is equivalent to Equation (4.2). The only difference is the factor of $\frac{\pi}{2}$ greater downwash induced by the same amount of total circulation. This means that using the same vorticity distribution as before, we expect the uniform velocity to have the value of $\frac{\pi}{4} = 0.7854$.

The straightforward discretization of the axisymmetric vortex sheet into circular line vortices will not be meaningful due to the infinite self-induced velocities of the vortices. However, if the circular line vortices are replaced by vortex rings with a finite core dimension r_0 , then the self-induced velocity of the vortices will be $O(\sigma \ln \sigma)$, where σ is the ratio between the core dimension and the ring's radius. In addition, since the core represents a section of the sheet of approximately the same size, the self-induced velocity is expected to be $O(\sigma^2 \ln \sigma)$ when compared to the $O(1)$ velocity induced by the total disk of vorticity. Thus, if σ is small, the effect of the self-induced velocity is expected to become negligible. If we hypothetically allow the infinite self-induced velocities of the circular line vortices to be neglected, then the discretized disk of vorticity will induce the downwash profile shown by Figure 4-12. The downwash profile for a set of equally spaced circular line vortices is surprisingly uniform and near the correct value, thus demonstrating the insignificance of the self-induced velocity.

If the moving disk is discretized by vortex bands, the self-induced velocities of the bands may be included. The resulting downwash profile is shown in Figure 4-13. Except for the magnitude of the velocities, the profile displays the same features found in the wing wake profile. However, it should be noted that the accuracy of the velocities does not uniformly improve with the increase in the number of vortex bands. Figure 4-14 shows the use of a tip-core to approximate the inner-solution representing the roll-up of the tip (See Appendix B for details). The shape of the resulting downwash profile near the tip does not agree with the two-dimensional equivalent produced by Kaden's similarity solution (Figure 4-8). This may be an indication that the core is positioned too far away from the rest of the sheet in the approximation used to model the tip region of an axisymmetric vortex sheet. Since the approximation is not a similarity solution for the geometry of the tip roll-up, the geometrical error will be reflected in the distance between the edge of the last panel and the tip-core.

4.2. Summary

The calculated velocities of the vortex elements can be used to test the accuracy of the vortex sheet model if the velocities of the actual vortex sheet are known. For elliptical loading cases discussed above, the velocities for each section of the vortex sheet can be predicted. These cases also represent the initial conditions for interesting problems in vortex sheet dynamics. The above results show the accuracy of equal width panels in reproducing the flow field away from the singular tip of the vortex sheet. A near-field solution for the flow around the tip of the vortex sheet can then be approximated using a core of vorticity. The importance of the tip core is also suggested by the virtual core effect in the downwash calculated for the equal circulation segmentation of the same vortex sheet. The incorporation of a tip core in the equal width panel method represents a straightforward modelling of the vortex sheet with results which are more realistic than the results obtained using point vortices alone.

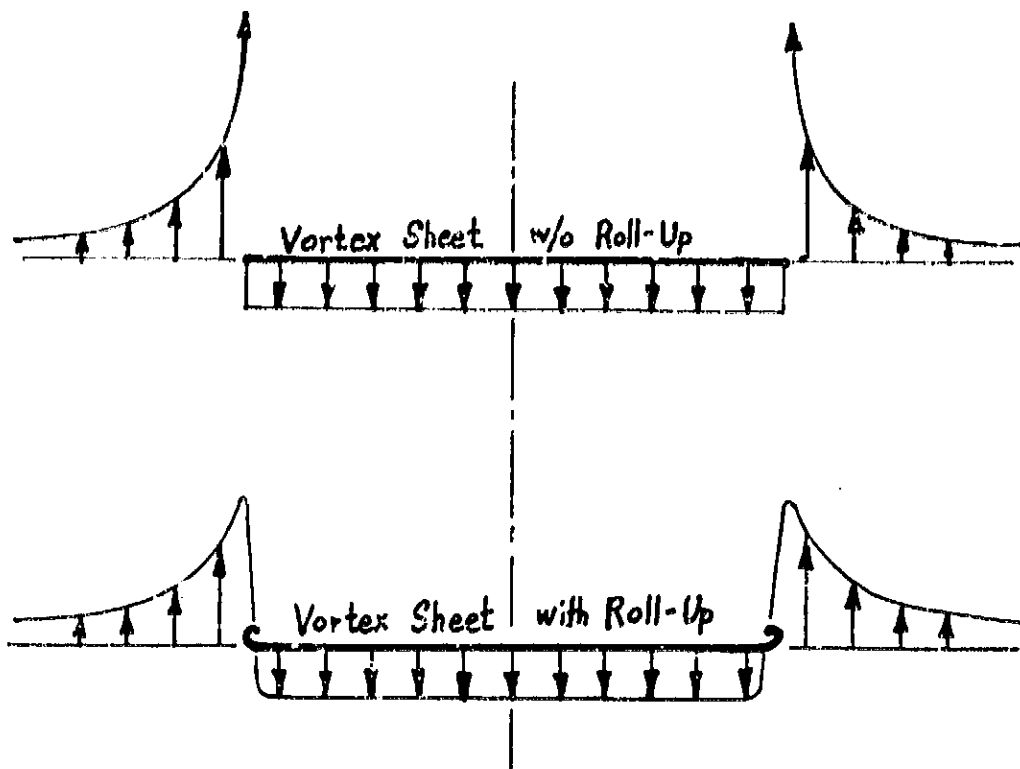


Figure 4-1: Vertical velocity profile for elliptic loading

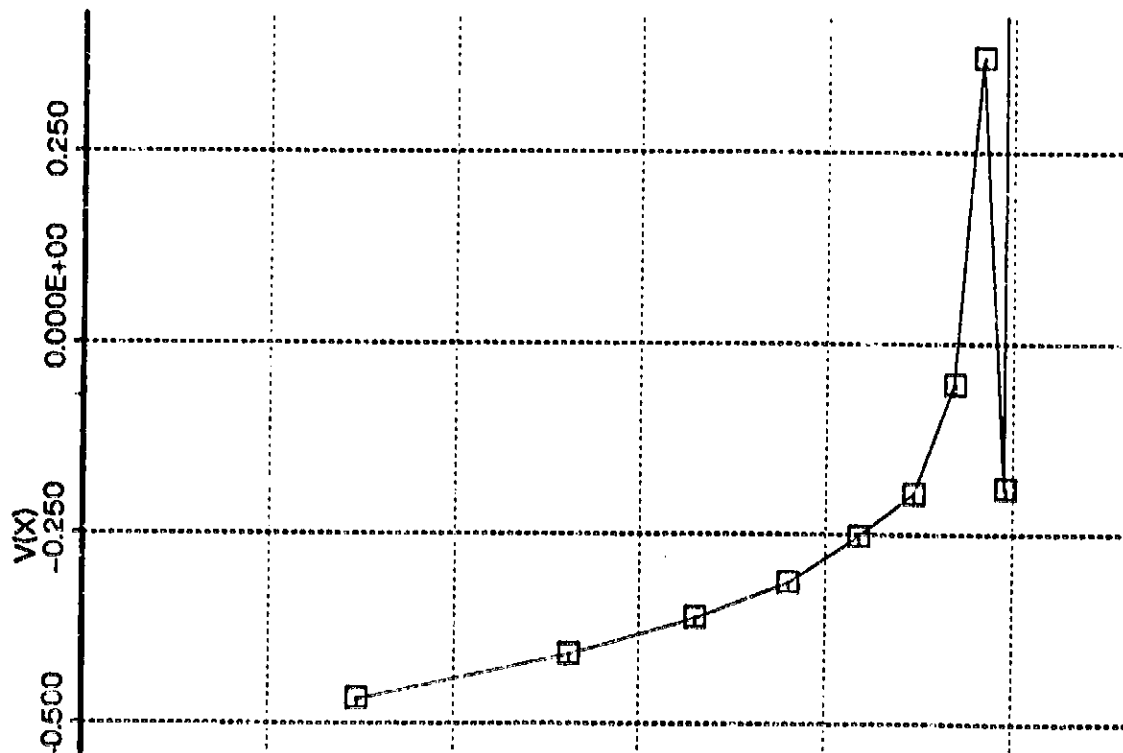


Figure 4-2: The downwash profile for Westwater's initial distribution

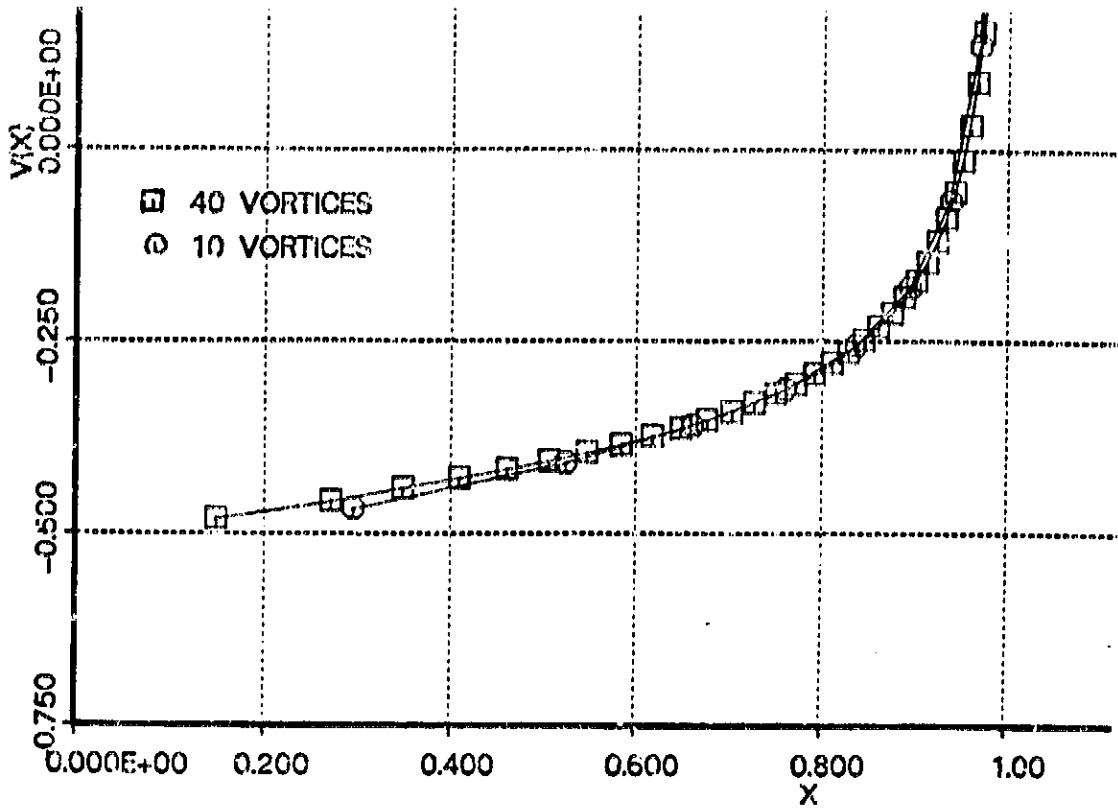


Figure 4-3: Downwash Profile: Integration of equal strength vortices

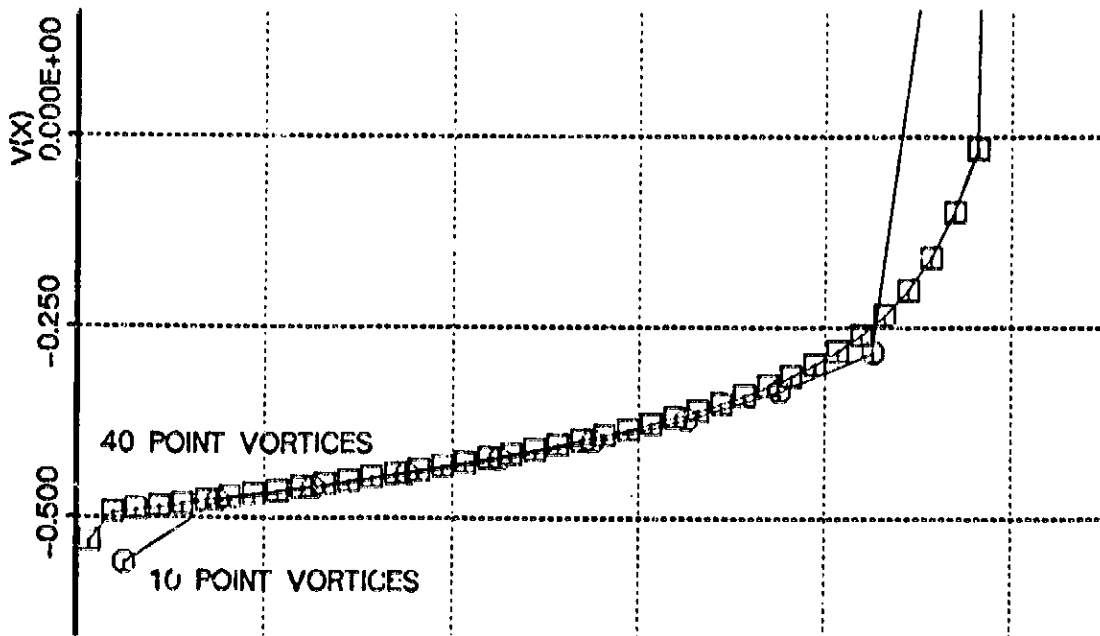


Figure 4-4: Downwash Profile: Integration of equally spaced vortices

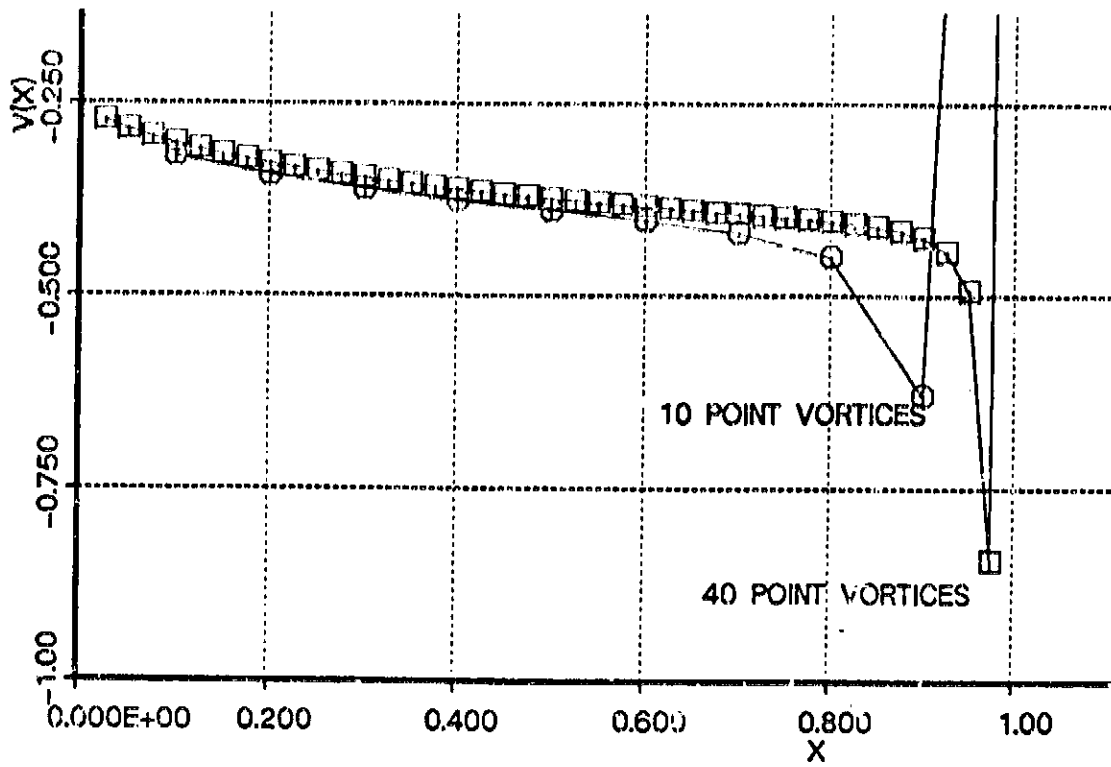


Figure 4-5: Velocities half-way between equally spaced vortices

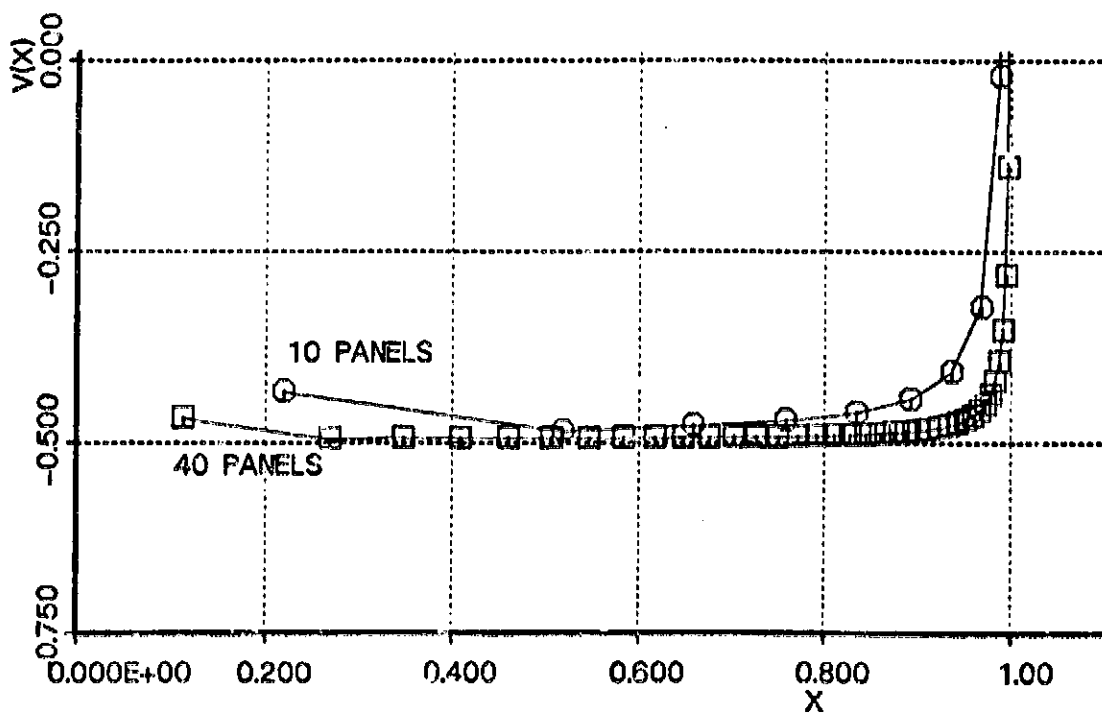


Figure 4-6: Downwash Profile: Integration of equal strength vortex panels

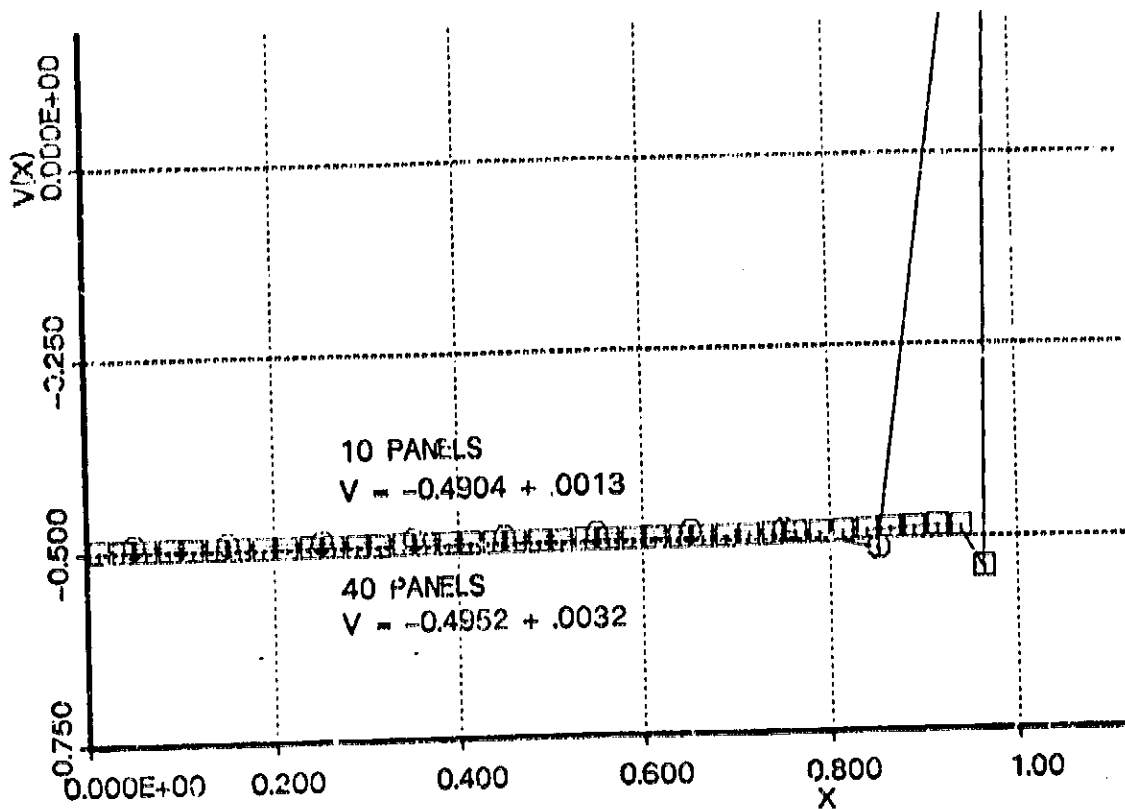


Figure 4-7: Downwash Profile: Integration of equal width vortex panels

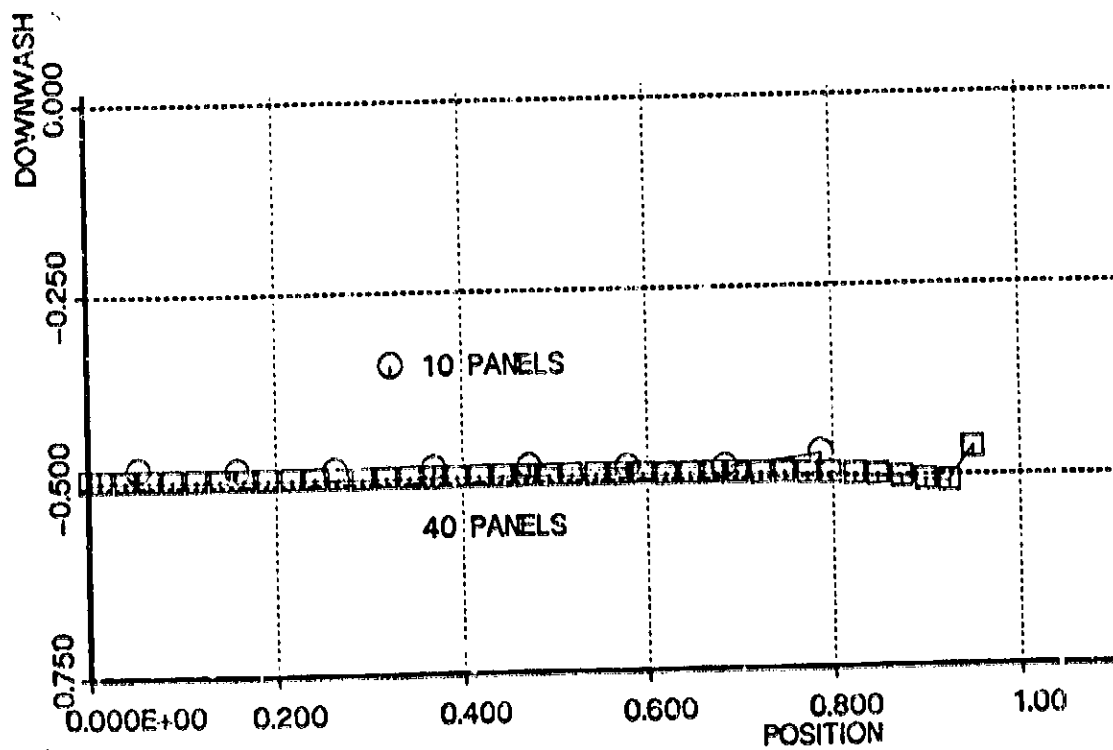


Figure 4-8: Downwash Profile: Equal width panels with roll-up model

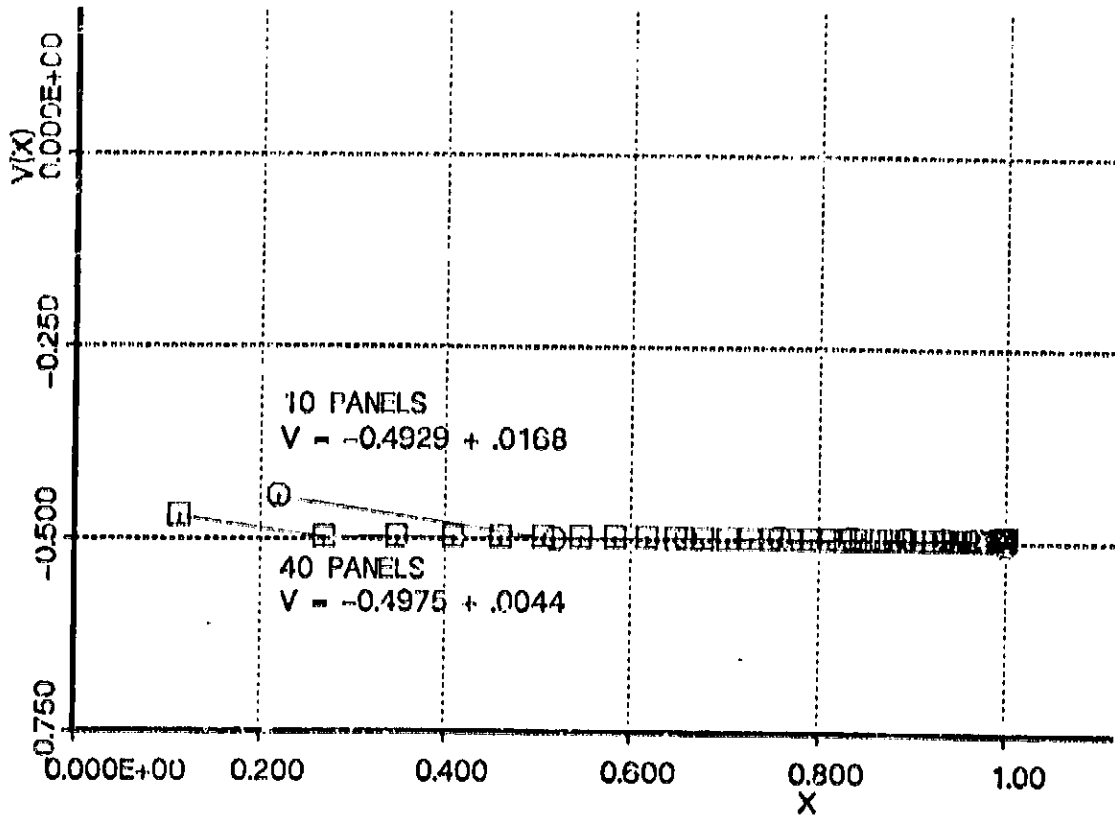


Figure 4-9: Downwash Profile: The effect of virtual core

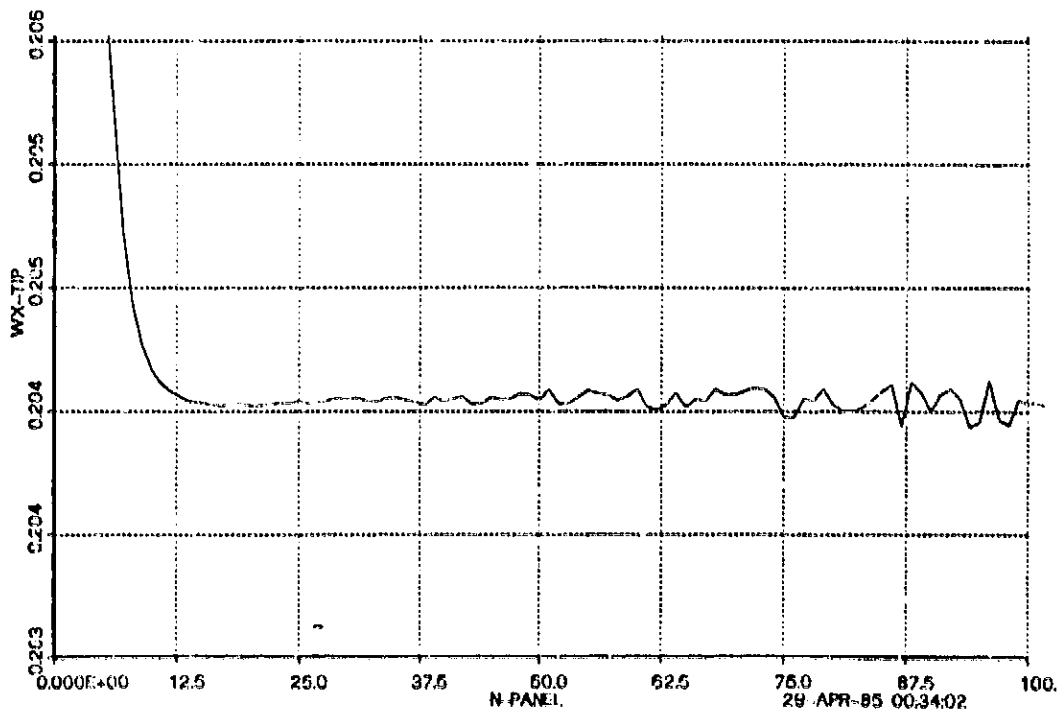


Figure 4-10: Virtual-Core Location: Normalized w.r.t. the tip panel

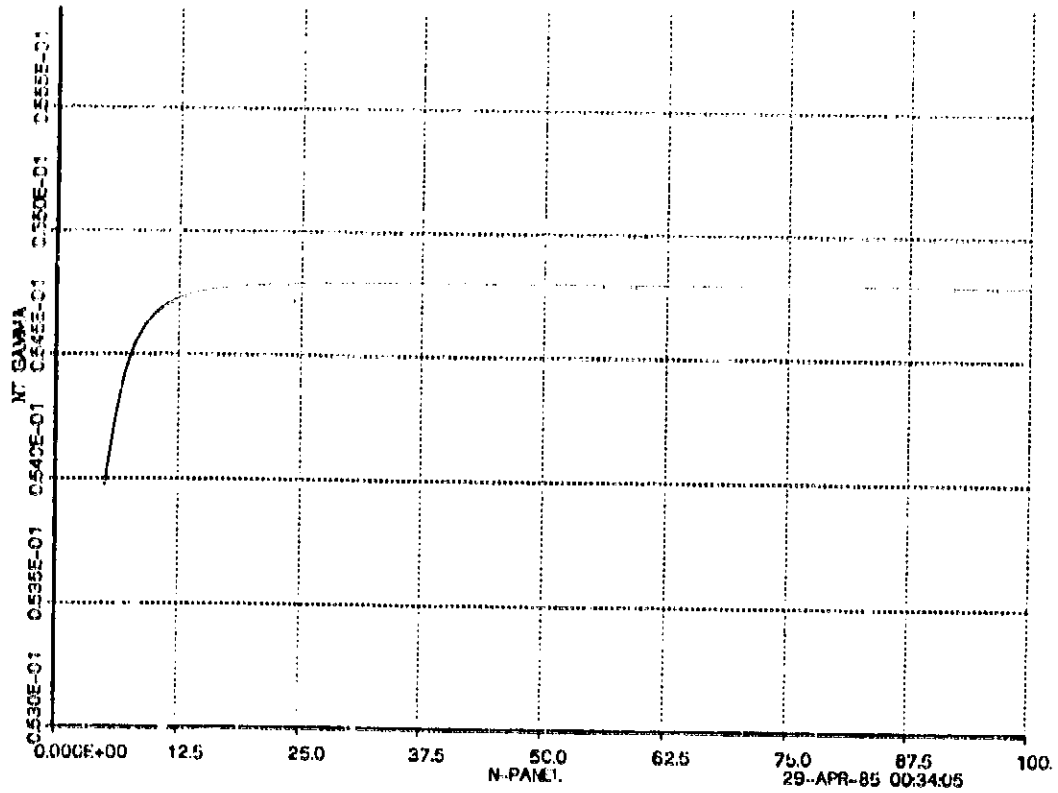


Figure 4-11: Virtual-Core Strength: Normalized w.r.t. the tip panel

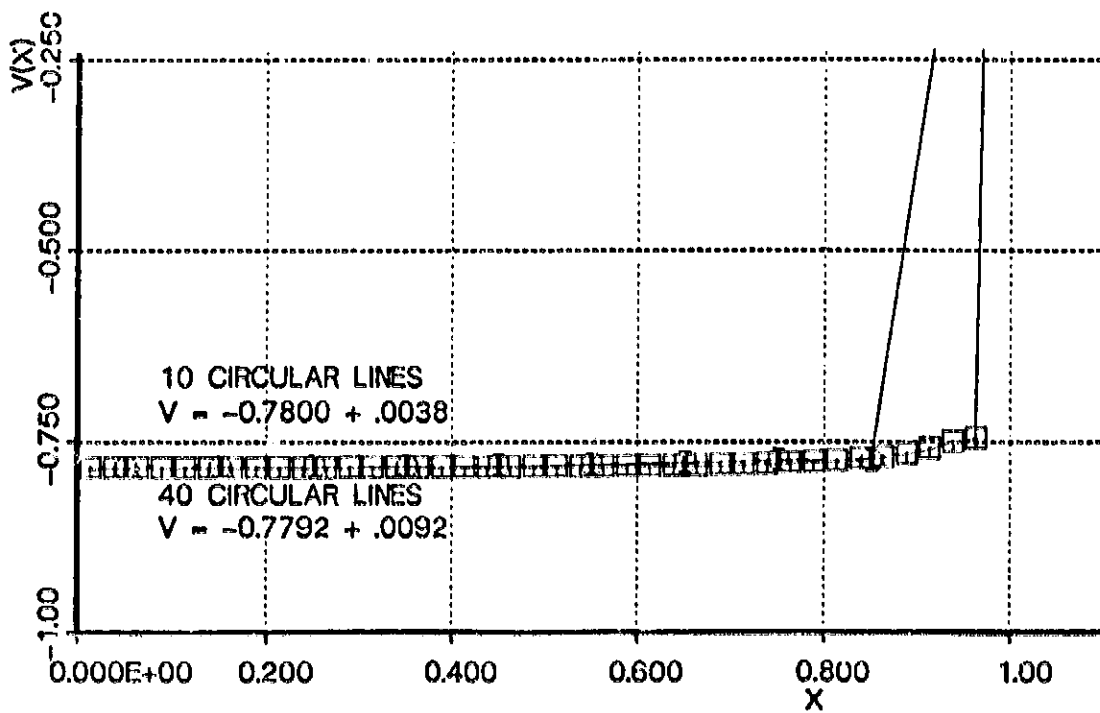


Figure 4-12: Moving Disk: Circular line vortex representation

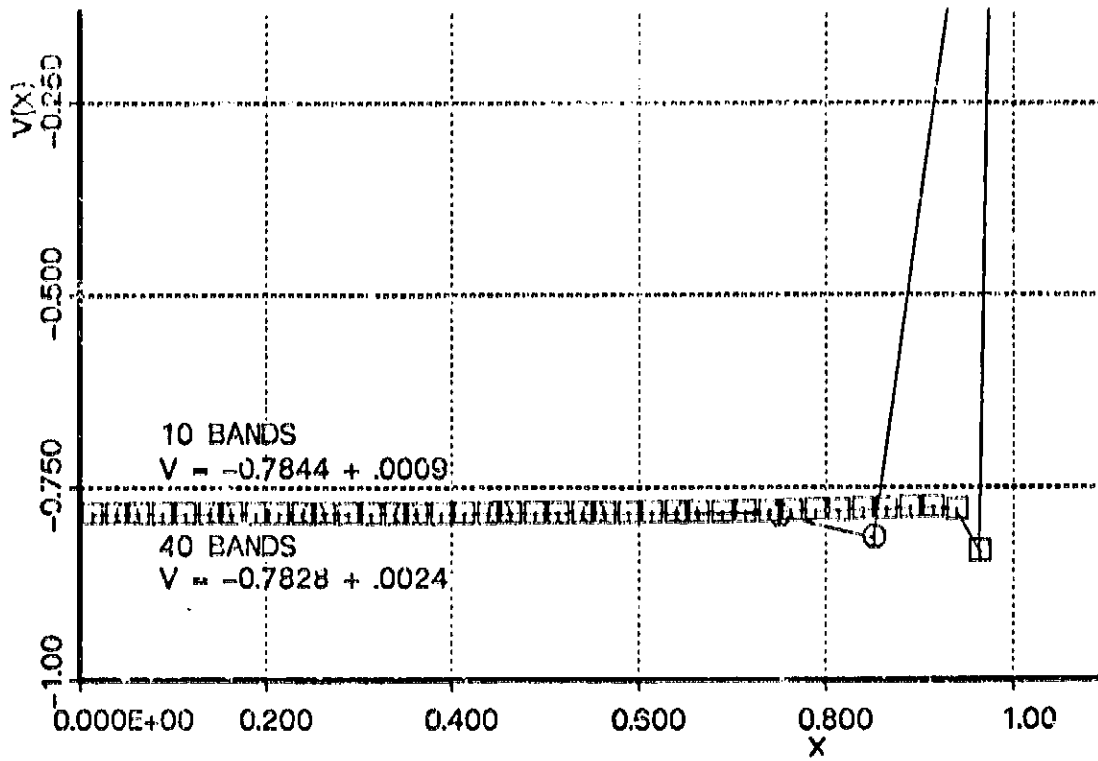


Figure 4-13: Moving Disk: Vortex band representation

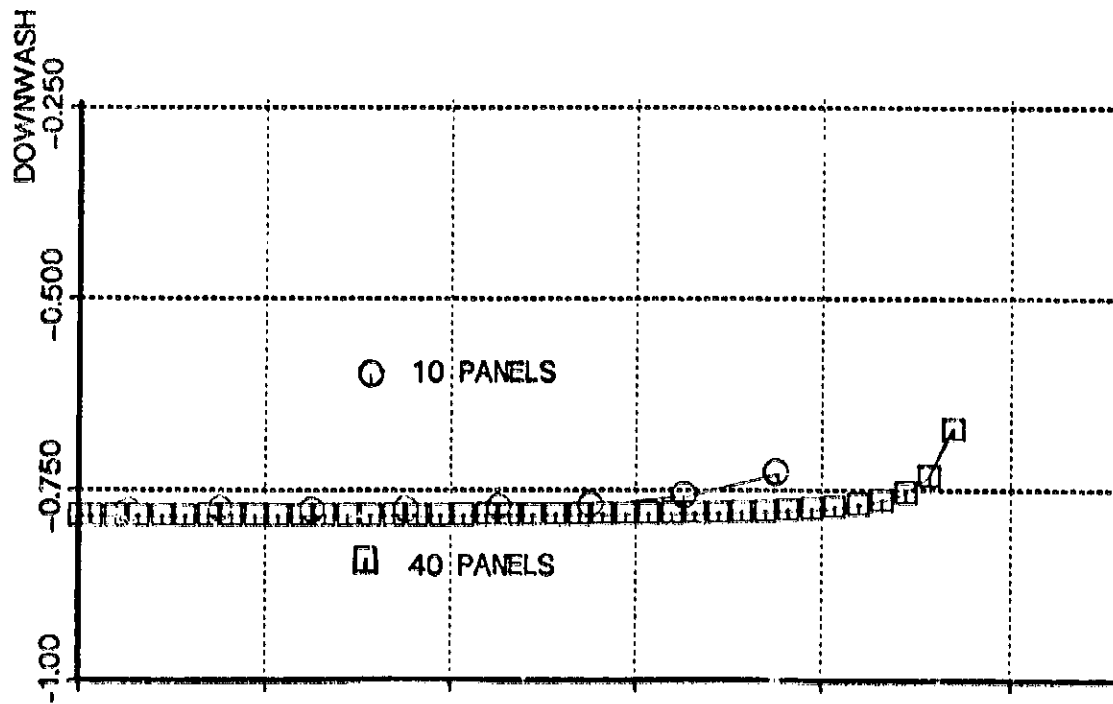


Figure 4-14: Moving Disk: Vortex bands with tip core

Chapter 5

Numerical Simulation of Vortex Sheet Dynamics

5.1. The Numerical Roll-Up of Vortex Sheets

The roll-up of two-dimensional and axisymmetric vortex sheets were simulated using vortex panels. The changing shape of the vortex sheet is determined in a Lagrangian fashion by following the vortex panels throughout cycles of numerical time integration. Accuracy of the method is maintained by reconstructing and rediscrctizing the sheet time integration cycle in the manner prescribed by Fink and Soh [13]. A first-order Runge-Kutta scheme is used for each time integration cycle. The main difference between the panel method and the point vortex method is the amount of data which must be handled to describe the sheet. Since the orientation and the width for each panel must be recorded, the amount of geometrical data is effectively doubled. The numerical scheme for following the dynamics of the vortex sheet is summarized by the flow chart in Figure 5-1.

5.1.1. The Time-Integration Scheme

The centers of the vortex panels are translated using the Runge-Kutta scheme during each cycle of time integration. A vortical flow system is characterized by gradients in velocity resulting in curved trajectories of the convected vortices. The Runge-Kutta scheme is generally more efficient in describing curved trajectories than the simpler Euler scheme [28]. Euler scheme translates the control points for an short increment in time along a straight trajectory based on the velocity at the beginning of each cycle. Runge-Kutta scheme, on the other hand, uses more than one set of velocity data to approximate a curved trajectory during each time integration cycle. If only one additional velocity input is used, the Runge-Kutta scheme is refered to as being of the first order. The panel method, unlike the point vortex methods, requires the size and the orientation for each panel in order to calculate meaningful velocities. Since

only the centers of the panels are tracked by the time integration, the entire sheet must be reconstructed in order to obtain the size and the orientation of the panels. However, a rigorous reconstruction of the sheet is highly computation intensive. Probably for this reason, Hoijmakers and Vaatstra [16] used the Euler scheme with their panel method, while Fink and Soh [14] were able to use a Runge-Kutta scheme with their improved point vortex scheme.

In the first-order Runge-Kutta scheme used in this study, a simple approximate reconstruction of the intermediate vortex sheet geometry is used to provide additional velocity data. At the beginning of the integration cycle, the vortex panels are arranged by the rediscrretization scheme to form a continuous vortex sheet and the initial set of velocities are obtained. Then the intermediate positions of the panel centers are derived using the Euler scheme. To obtain the intermediate velocity, the changes in the orientation and size of the panel due to the initial deformation of the sheet must be derived. The intermediate panels are oriented parallel to the line spanning the positions of the two adjacent panels centers (Figure 5-2). The width of the intermediate panel is taken to be half the distance between the adjacent panel centers. The new positions of the panel centers are obtained by averaging the initial and intermediate velocities and by translating the panels by the corrected velocity for twice the time increment used to obtain the intermediate solution.

5.1.2. The Reconstruction and Rediscrretization of the Vortex Sheet

The reconstruction and rediscrretization of the vortex sheet are performed after each cycle of time integration. The rediscrretization procedure allows the vortex sheet to be reproduced by vortex panels of equal widths. This scheme also helps to maintain the accuracy of the panel representation of the vortex sheet and helps dampen short wavelength instabilities. The damping of the vortex sheet is achieved by reconstructing the vortex sheet using only the positions of the panel centers. A parabolic spline, selected in order to rule out non-physical wiggles between the control points, is fitted to represent the vortex sheet (Figure 5-3). At the same time, a linear interpolation is used to represent the distribution of circulation in the sheet. The new vortex panels, having equal widths, are made to span segments of the vortex sheet (Figure 5-4). The circulation contained in the segments of the vortex sheet is transferred to the panels spanning them. Although this procedure reduces the effective radius of curvature of

the vortex sheet by shifting the panels inside a curved spline representing the vortex sheet, the effect can be minimized by decreasing the size of the panels. In any case, because straight segments are being used to represent a curve, small panel width is necessary to maintain the geometrical accuracy of the panel representation. The size of the segments are also adjusted to maintain a certain relative distance between the outer-most panel and the vortex representing the inner region of the roll-up spiral.

5.1.3. The Treatment of the Inner Roll-Up Region

As shown previously, the vortex panels alone can at most reproduce the outer solution for the flow induced by a vortex sheet. This is inadequate as an initial condition without a model to represent the initially infinitesimal roll-up at the end of the sheet. Thus, the simulation of vortex sheet rollup begins by replacing the singularity at the edge of the sheet with a core representing the initial roll-up of the sheet edge (Figure 5-5). The placement of the tip roll-up core for the two-dimensional wing wake follows the result presented by von Karman of Kaden's analysis for roll-up by a parabolically loaded vortex sheet. For the roll-up of axisymmetric vortex sheets, due to the lack of a similarity solution, the a much simpler tip core is used. The details of the initial conditions are described in Appendix B. Such models for the initial condition of the vortex sheet is necessary for a realistic numerical approximation of the flow when using vortex panels to model the vortex sheet.

The core is a model for a tightly rolled-up section of vortex sheet, the core center representing the center of the spiral. By knowing the position of the center of rollup, the inner-most resolvable section of the vortex sheet in the spiral can be handled more accurately. The spline representing the vortex sheet is derived from the panel centers, the location of the edge of the last panel, corresponding to the end of the sheet and the inner-most resolvable section of the spiral, is uncertain. (See Figure 5-6.) Since the roll-up should be in the form of an exponential spiral with the core at its center, the orientation of the last panel may be used to blend the resolved section of the spiral with the core. It also possible to truncate inner-most section of the resolvable vortex sheet and dump the circulation, momentum, and energy of the truncated section into the core. (Although both methods may be used concurrently, core jumping was not used in any of the results presented below.) Core dumping is attractive for numerical reasons since the size of the panels can be kept relatively small even as the

sheet stretches without being limited by computer memory size. As vorticity is dumped into the core, the conservation of circulation, momentum and kinetic energy determines the strength, position, and size of the core respectively.

5.2. Results of the Roll-Up Calculations

The numerical scheme described above has been applied to simulate the roll-up of two-dimensional and axisymmetric vortex sheets. All roll-up simulations were initiated with a model representing a small amount of roll-up already in place at the edge of the vortex sheet.

5.2.1. Two-Dimensional Roll-Up

The roll-up of a two-dimensional vortex sheet trailed by a flat, elliptically loaded wing is the classical test case for numerical vortex sheet methods. In order to simulate the geometry of the sheet, the Trefftz plane method, originally introduced to roll-up studies by Westwater [12], is used. Each cross-section of the wake vortex sheet is treated as an unsteady two-dimensional vortex sheet. Thus, as described above, the sheet is replaced by a series of equal width flat panel of constant vorticity. Unlike the axisymmetric flow system, this two-dimensional roll-up requires the program to account for the mirror-image contribution across the plane of symmetry. The time integration cycle is begun with a flat sheet at $y = 0$ and a tip core positioned at the center of Kaden's spiral for roll-up of the outer 5% of the vortex sheet. There are 76 panels describing the sheet initially, the number increasing as the sheet stretches; the size of the panel is kept constant. In this simulation, roll-up of the sheet has been allowed to take place without core dumping to demonstrate the robustness of the model. The panel widths have been kept constant.

Figure 5-7 shows the geometry of the sheet after every ten time integration cycles, each cycle representing a nondimensional elapsed time² of the the of 0.005. The initial location of the roll-up core is given by a small circle, partly hidden by the inner regions of the spirals, at about $x = 0.97$. Although the inner region of the spiral is obscured by the overlapping, smooth rollup of the outer region can be seen.

²The time is nondimensionalized by the time scale, $t' = r_0/b^2$

The core representing the inner region of the spiral initially moves inward and upward to conserve impulse. As the core approaches the centroid of vorticity for the complete vortex system, $x_0 = 0.7854$, the upward movement ceases and begins moving downward while asymptotically approaching x_0 .

Figure 5-8 shows the amount of circulation contained by the sheet outboard of a given panel. The horizontal axis gives the panel index, and since the panels are constant in width, this is equivalent to the arc length along the sheet. Values of circulation are negative since the panels' κ were defined to be positive. The y-intercept shows the total circulation of the system which has been defined to be 1.0. The first curve, the start-up distribution, is elliptical and the strength of the tip core appears as the jump from the end of the curve to $\Gamma = 0$. The lessening of the gradient indicates the stretching of a section of the sheet. Stretching is extreme in the inner-most region of the spiral as indicated by the nearly horizontal inclination of the curve while the outer portion is still relatively unaffected by the rollup. Slight bumps in the curves therefore show regions of differential stretching associated with the rollup.

The roll-up of a vortex sheet must conserve circulation and momentum. The total circulation computed for the numerical model of the vortex sheet as it deforms with time shows a negligible fluctuation of about .01% per time step from the expected value of 1.00. The program maintained this value to better than 0.001% accuracy, representing only the fluctuations due to numerical round-off errors. Calculated centroid of vorticity for a smooth elliptical distribution is 0.7854. For the numerical model of the initial condition used, the centroid of vorticity was found to be 0.7925. During the subsequent steps in time, the centroid value was found to decrease by less than 0.05% per time integration cycle, or time step. The steady decrease in centroid appears to be connected with the additional panels used to represent the stretching of the vortex sheet.

Betz [10] has shown that the circulation within the spiral, measured from the center of the spiral, should approach a constant distribution. Figure 5-9 shows the distribution of circulation versus the distance from the position of the roll-up core for each time step plotted in Figures 5-7 and 5-8 along with a plot of the approximate solution found by Betz. Each curve represents the sheet for increments of 0.100 in

nondimensional time. Since each cycle of time integration covers 0.005 in nondimensional time, each curve represents the result of 20 time steps. Some of the deviation from Betz's result can be explained by the fact that Betz did not use Kaden's similarity solution but placed his hypothetical roll-up at the end of the sheet. Figure 5-10 shows the blow-up of the region covered by the spiral. In both figures, the area over which the circulation is integrated increases to the right of the plot; thus each curve will converge on the total circulation of the sheet, which in this case is unity, toward the right of the plot. Although Betz's solution shows the general trends, the numerical solution exhibits a tendency toward higher concentration of circulation inside the roll-up spiral.

Figure 5-11 shows the geometry of the sheet at elapsed time of 1.00. The spiral planform generally agrees with those generated by other investigators, the weakness in the flat panel method is apparent in the tightly wound spiral. As the spiral tightens near the center, the number of panels become insufficient to adequately resolve the spiral. In this case, there are approximately 11 panels describing the inner-most turn of the spiral. Due to the ambiguity in the radial position caused by spanning flat panels across a tight curve, the end of the sheet has crossed over several turns of the spiral (Figure 5-12). When this happens, the closed section of the vortex sheet stops stretching and becomes roughly equivalent to a core of vorticity.

While sheet crossing represents a violation of the physical nature of vortex sheet, the simulation can become unrealistic much earlier. When the panels forming one turn of the spiral roughly overlap with the panels forming an adjacent turn, the geometry of the section have been found to stabilize in this configuration. Since the phenomenon is produced by the flat geometry of the panels, this behavior is uncharacteristic of a smooth vortex sheet. For this reason, the width of the panels must be reduced in order to accurately resolve the inner regions of the spiral.

5.2.2. Roll-Up Produced by an Impulsive Movement by a Disk

The problem studied by Taylor [27] is demonstrated by performing the elliptically loaded wing wake with axisymmetric vortex bands. The motion of the disk is modelled by a flat axisymmetric vortex sheet. A rough approximation of the initial roll-up of the tip is used (see Appendix B). The axisymmetric tip core, unlike the

two-dimensional core, has a self-induced velocity which must be determined using the conservation of energy. The subsequent roll-up of the vortex sheet into a vortex ring proceeds smoothly as shown in the figures. As with the wing wake, the simulation begins with 80 panels with the outer 1.25% of the vortex sheet transformed into the initial roll-up core with no subsequent core dumping.

Figure 5-13 shows the roll-up of a vortex sheet produced by an impulsive motion of a flat disk. There are 10 plots, each representing elapsed time of .05, and the initial configuration, with the tip core shown as a small circle, shown in this plot. The rollup is similar to the wing wake roll-up with one important difference, the spiral translation is augmented by the self-induced velocity. The spiral is behaving essentially as a ring vortex. Figure 5-14 shows the circulation distribution corresponding to the geometries above. The gap between the first curve, showing the initial circulation distribution, and the rest of the curves is due to the decrease in panel size and a proportional increase in the number of panels imposed by the program in the first few time steps. This is performed when the distance between the core and the end of the sheet is reduced below defined limits. Otherwise, all of the features of the wing wake case can be observed.

Centroid of vorticity for an axisymmetric vortex sheet is the radius of a vortex ring with the same impulse. The calculated value for the centroid of a continuous vortex sheet is $x_c = 0.8165$; the total circulation should be 1. The panel-method introduces a error in the centroid to give the computed value of 0.882 for the initial vortex sheet. However, the important criteria for the accuracy of the numerical simulation is the invariance of these values as the roll-up proceeds. The total circulation was found to fluctuate by less than 0.001% while the centroid of vorticity was maintained to about 0.05% change per time step where each time step is equal to elapsed time of 0.005. In addition, if the roll-up simulation is perfectly accurate, Betz hypothesized that the circulation integrated away from the center of roll-up should approach a final distribution. A test of the hypothesis is shown by Figure 5-15. The circulation distribution in the spiral, which is the region toward the left, appears to converge on a relatively steep slope which reflects a high concentration of vorticity. This feature is more apparent here than in the two-dimensional case because of the faster rate of roll-up. Figure 5-16 shows the blow-up of the circulation distributions in the region covered by the spiral.

Figure 5-17 shows in detail the sheet geometry at elapsed time of 0.550 . As compared to the wing wake roll-up at the same stage of roll-up, the spirals are looser but more turns of the spirals are present. The invariant tip roll-up core is shown with its calculated cross-sectional radius which, as can be observed, is very small; it represents the tip 1.25% of the initial vortex sheet. Due to the higher rate of inward motion in the spiral, the inner-most turn has already reached the point where the panels are inadequate to resolve the curvature and a sheet crossing has taken place.

5.2.3. Roll-Up of a Helicopter Wake

The evolution of the wake produced by a single rotation of a helicopter rotor was simulated by imposing an approximate rotor loading

$$\Gamma(x) = \Gamma_0 x^2 \left[1 - \frac{x^2}{b^2} \right]^{1/2} \quad (5.1)$$

on the initially flat axisymmetric vortex sheet. This load distribution is shown graphically in Figure 5-19. The downwash profile induced by vortex bands, without a tip roll-up model, for this distribution is shown in Figure 5-20. The numerical result for the velocity at the center of the disk agrees well with the theory, which comes out to be 0.3927 if the contributions of all of the infinitesimal circular line vortices are integrated analytically.

Figure 5-21 shows the roll-up simulating the evolution of a wake due to one rotation of the helicopter rotor at increments of 0.05 in nondimensional time. The tip core contains the circulation of the outer 1.25% of the flat vortex sheet and each time step represents nondimensional elapsed time of 0.005 . A prominent feature of the vortex sheet geometry is the stationary point near the midpoint on the sheet. This feature was also found in a similar investigation by John Kantelis [26] using a collection of vortex rings to represent the vortex sheet. It is noticed that the steepening of the circulation curve, indicating a concentration of vorticity which should eventually lead to another roll-up of the vortex sheet, only develops at the center of the axisymmetric vortex sheet. Thus, although the vortex sheet contains regions with vorticity of opposite signs, the sheet does not appear to roll-up into two separate vortex rings. The circulation plot (Figure 5-22) shows a significant decay of the trough in the circulation curve during the first ten or so time steps. This is a numerical error due the inaccuracy introduced by the linear interpolation of circulation used in the reconstruction of the vortex sheet after each time step.

The validity of the simulation is indicated by the invariance of total circulation, equal to zero, and the impulse of the vortex sheet. Total circulation and total impulse are found to be conserved to within 0.001% and .0025% respectively during each time integration cycle. In addition, the circulation distribution away from the roll-up center is expected to converge on a final curve. Figure 5-23 shows the distribution of circulation integrated away from the center of the roll-up for each time step in Figures 5-21 and 5-22 overlapped to show the comparative deviations. The blow-up of the region covered by the spiral is shown in Figure 5-24.

The geometry of the vortex sheet at elapsed time of 0.50 is shown in Figure 5-25. The panel which represents the minimum in the circulation distribution curve (Figure 5-22) has been circled to show the extent of the negative vorticity in the roll-up. Tip roll-up is much faster than the two previous cases since there is more circulation concentrated in the tip region. The blow-up, Figure 5-26, shows extensive sheet crossing for the inner-most turns of the spiral. Tip core, which appears as a dot in the middle of the spiral, is shown with its cross-sectional radius in scale.

5.2.4. Kelvin-Helmholtz Instability

The instability, which is discretized from of the underlying Kelvin-Helmholtz Instability, becomes evident under special conditions. A wake vortex sheet which is very finely discretized reached the geometry shown in Figure 5-27 after ten time steps. During each time step, the panels were allowed to move the maximum of 0.1 times the panel width. The circle on the right represents the location of Kaden's core model. If the sheet is magnified in the vertical direction, the development of Kelvin-Helmholtz-type instability becomes visible (Figure 5-28). Further magnification shows the waves to have a period of 11 panels and the scales to be within the 8 digit accuracy of the computer.

The damping of Kelvin-Helmholtz Instability in the numerical simulation is in the form of low-pass filtering the waviness in the vortex sheet. This filtering occurs as the panels span across crests and troughs of short wavelength waves. Due to the stretching of the sheet, the panels which describe the geometry of the vortex sheet following a time integration cycle will be slightly displaced from the previous panels. The amount of this displacement determines the amount of filtering which takes place.

This is because waviness in the displacement of a sheet formed by panels can not be resolved unless the the next set of panels overlap the displaced panels. For this reason, the instability appears when the amount of displacement, limited by the amount of time elapsed in one cycle, is kept small. This is what happened in Figure 5-28.

The filtering effect can also be suppressed by continuously increasing the spatial resolution of the panel-method. An example of this numerical behavior is shown in Figure 5-29. The initial conditions on the sheet and the time integration cycles are identical to the disk wake roll-up case presented earlier. To illustrate the filtering effect, the size of the panels were constantly reduced to about one half that of the panel used for Figure 5-13. This is accomplished by specifying $GFAC = 2$ instead of $GFAC = 1$; see Appendix C. This effectively suppressed the filtering and the small instabilities are able to grow more freely. As the roll-up proceeds, the secondary roll-up spirals are amalgamated into the tip roll-up spiral and the secondary spirals are also stretched as they spiral into the tip roll-up spiral. This behavior can be observed directly above the main spiral where stretching has deformed the secondary spiral. Plot of the circulation distribution, Figure 5-30, shows jumps in circulation which corresponding to each secondary roll-up. The circulation distribution in this plot was initially elliptical like those in Figure 5-14. Except for the existence of the secondary roll-up, the simulation proceeded no differently than the previous case. The computer program maintained the invariance of circulation and momentum with the same degree of accuracy as before. Distributions of circulation taken from the center of the main roll-up spiral is shown in Figure 5-31. Figure 5-32 shows the blow-up of the region covered by the main roll-up spiral. They are no different from the previous results except for the effects of secondary roll-up in the circulation distribution.

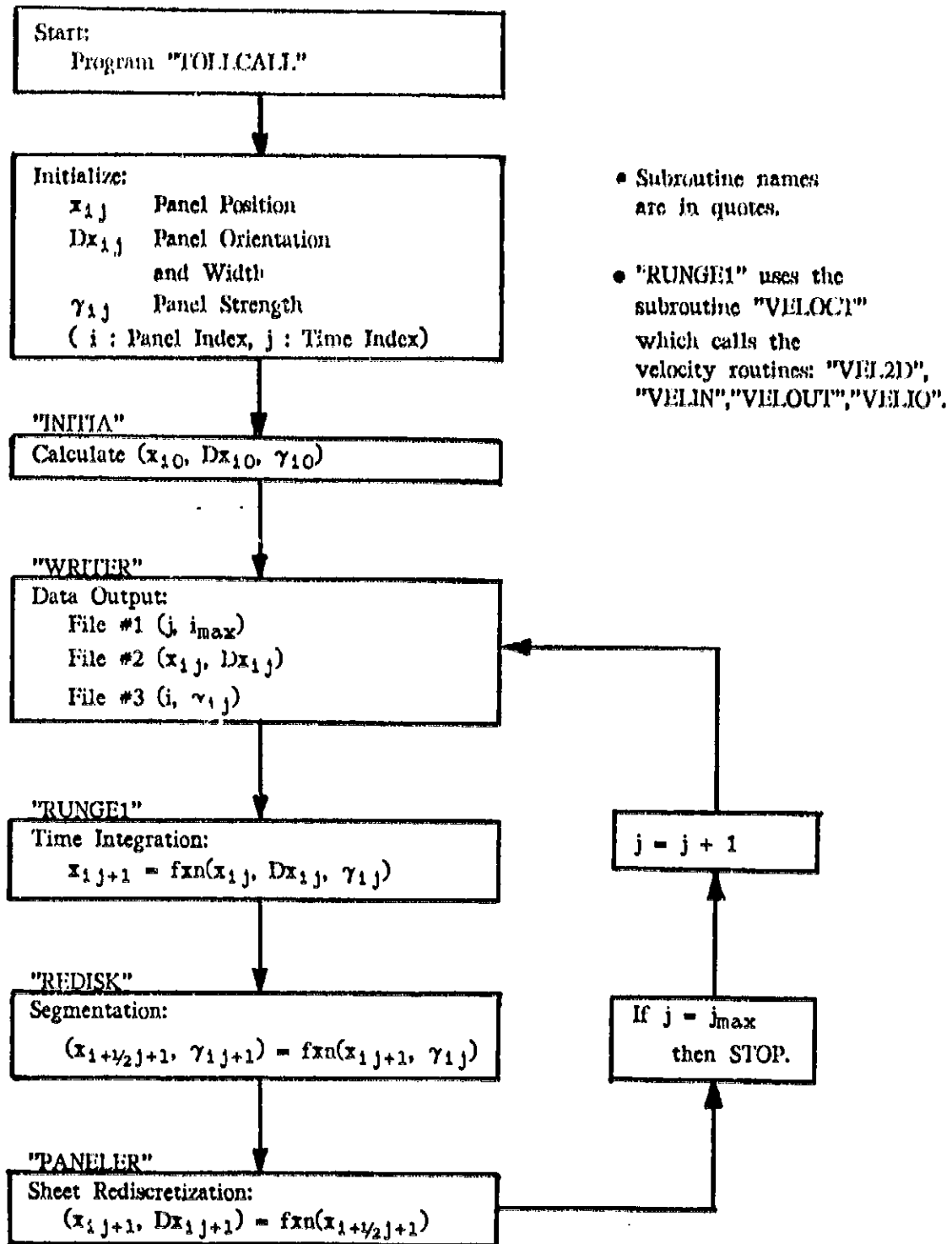
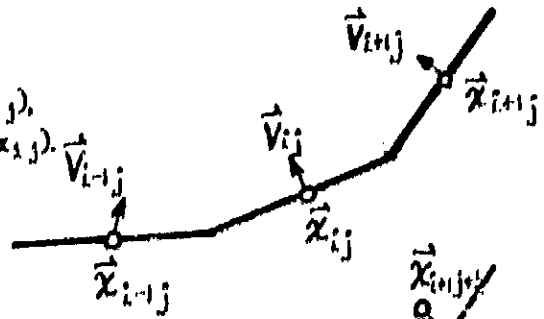
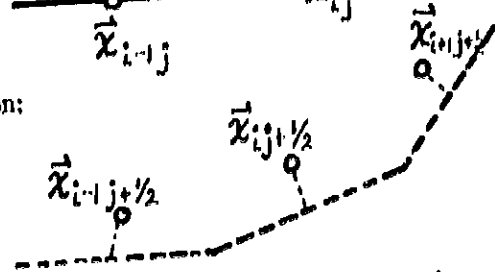


Figure 5-1: Flow Chart of the Vortex Dynamics Program

1. Given Initial Configuration: (x_{1j}, Dx_{1j}) ,
Calculate Velocity: $v_{1j} = f_{xn}(x_{1j}, Dx_{1j})$.



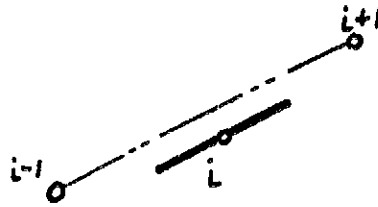
2. Translation to the Intermediate Position:
 $x_{1j+1/2} = x_{1j} + v_{1j} \Delta t/2$.



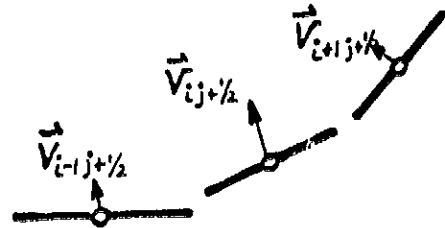
3. Approximate Intermediate Panel Inclination:
 $\arg(Dx_{1j+1/2}) = \arg(x_{i+1j+1/2} - x_{i-1j+1/2})$.



4. Approximate Intermediate Panel Width:
 $|Dx_{1j+1/2}| = 1/2 |x_{i+1j+1/2} - x_{i-1j+1/2}|$



5. Calculate Intermediate Velocity:
 $v_{1j+1/2} = f_{xn}(x_{1j+1/2}, Dx_{1j+1/2})$.



6. Combine Velocities,
e.g. $v_{1c} = (v_{1j} + v_{1j+1/2})$, for
Translation to the Final Position:
 $x_{1j+1} = x_{1j} + v_{1c} \Delta t$.

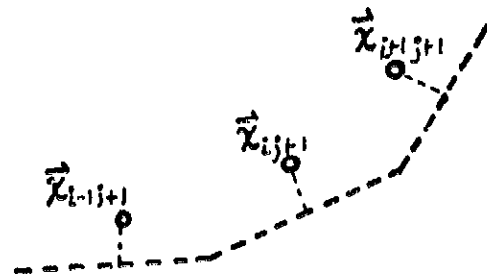


Figure 5-2: The First-Order Runge-Kutta Scheme

To fit a spline between points i and $i+1$.

1. Obtain adjacent points (Extrapolate at the ends).
2. Slopes at i and $i+1$ are obtained from the tangents to the arcs $(i-1, i+1)$ and $(i, i+2)$.
3. A parabola is fitted between i and $i+1$ to fit the slopes.

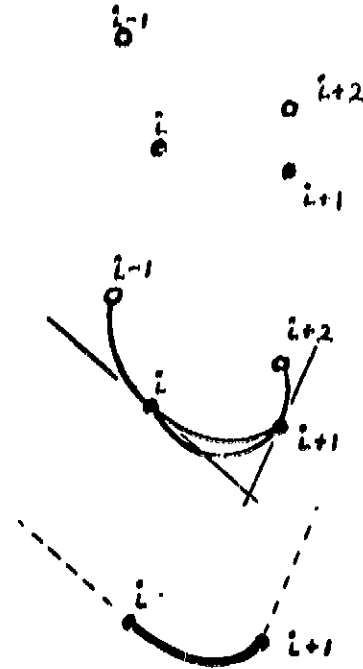


Figure 5-3: The Reconstruction of the Vortex Sheet

Subroutine "RUNGE1" gives the translated panel centers, x_{1j+1} .
 Subroutine "REDISK" splines the panel centers and determines the spatially equidistant points, $x_{1+\frac{1}{2}j+1}$, along the spline.
 Subroutine "PANELER" spans points $x_{1-\frac{1}{2}j+1}$ and $x_{1+\frac{1}{2}j+1}$ with panel i .

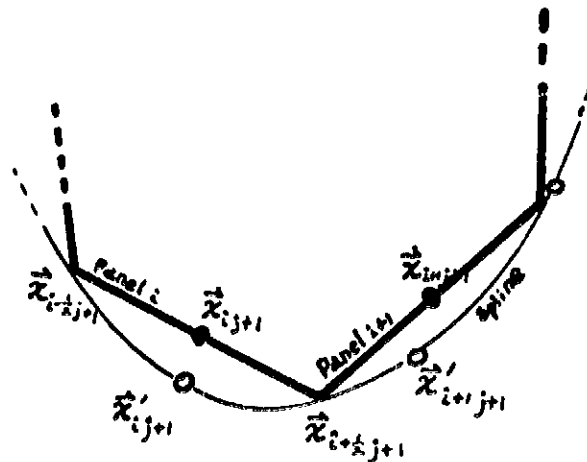
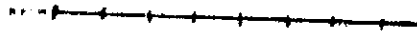


Figure 5-4: The Rediscretization of the Vortex Sheet

Equal width panel discretization
of a flat wake vortex sheet.



The remaining sheet is
stretched (rediscretized)
so the edge is under the core.



Equiv. Kaden's Soln.

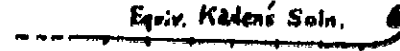


Figure 5-5: Initial Configuration of the Vortex Sheet and Roll-Up

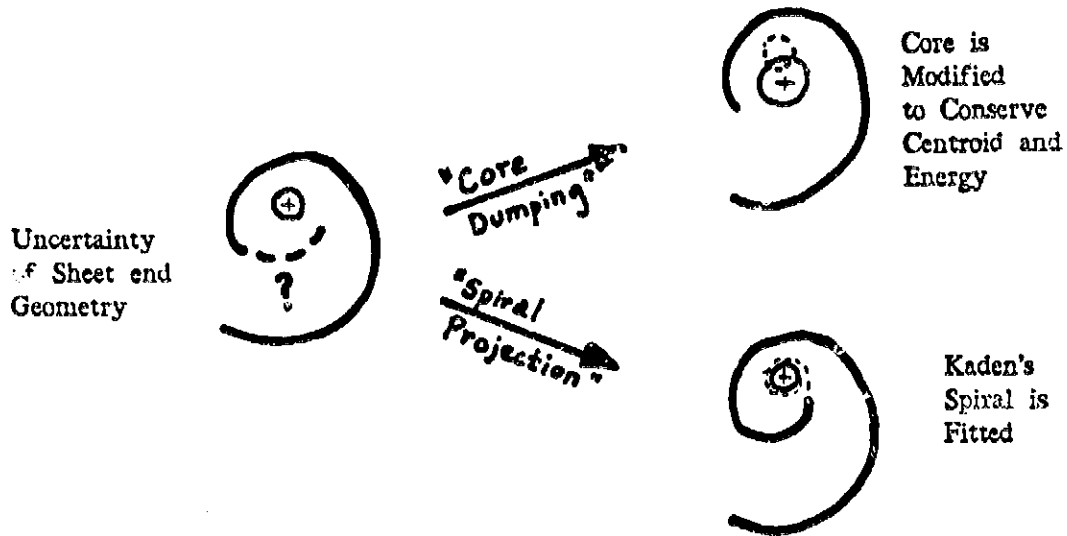


Figure 5-6: The Core Dumping Approach

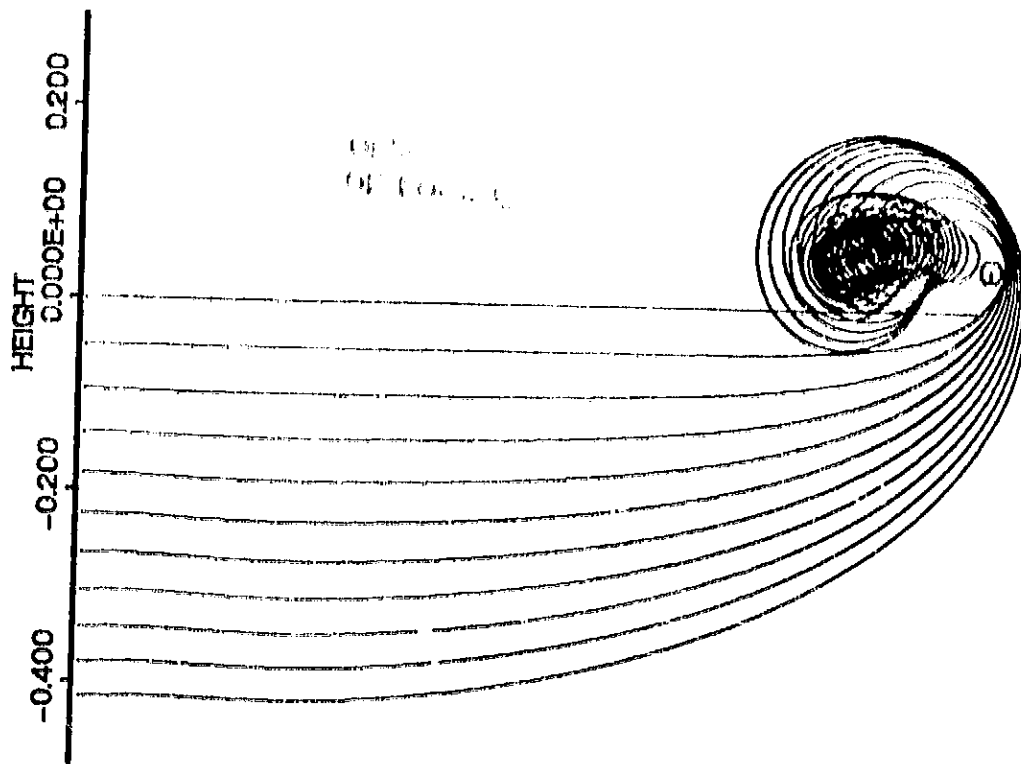


Figure 5-7: Roll-Up of Elliptically Loaded Wing Wake

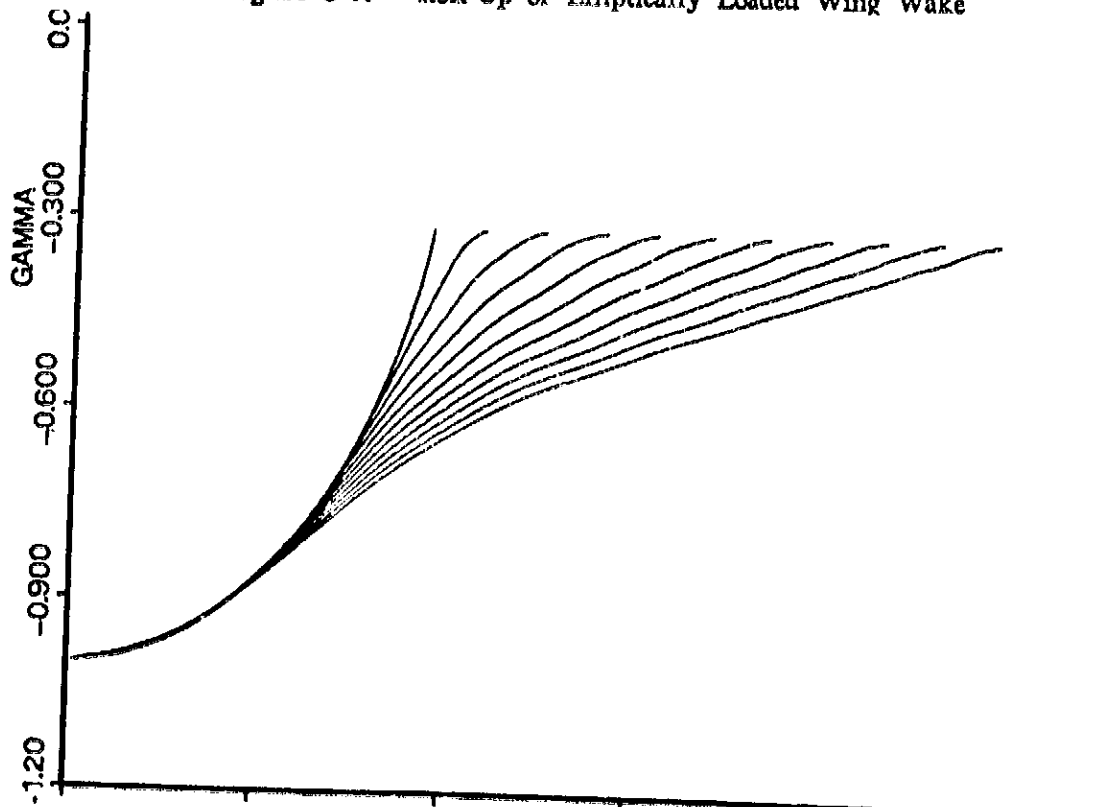


Figure 5-8: The Corresponding Circulation Distribution

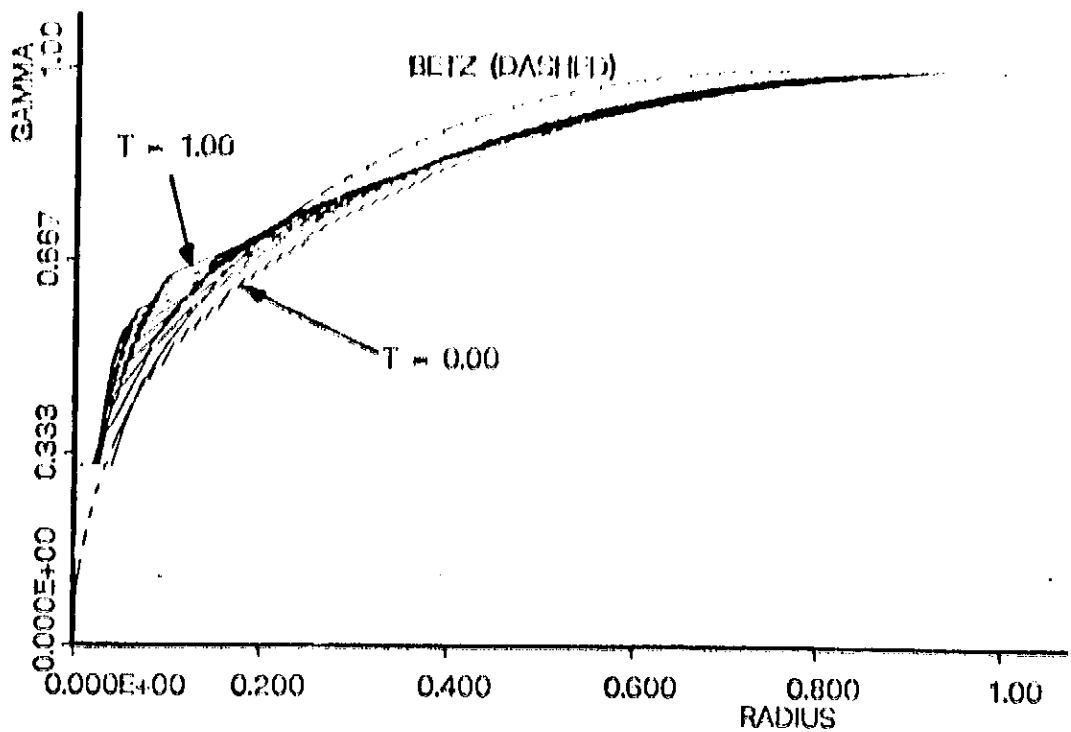


Figure 5-9: Distribution of Circulation Surrounding the Roll-Up Core

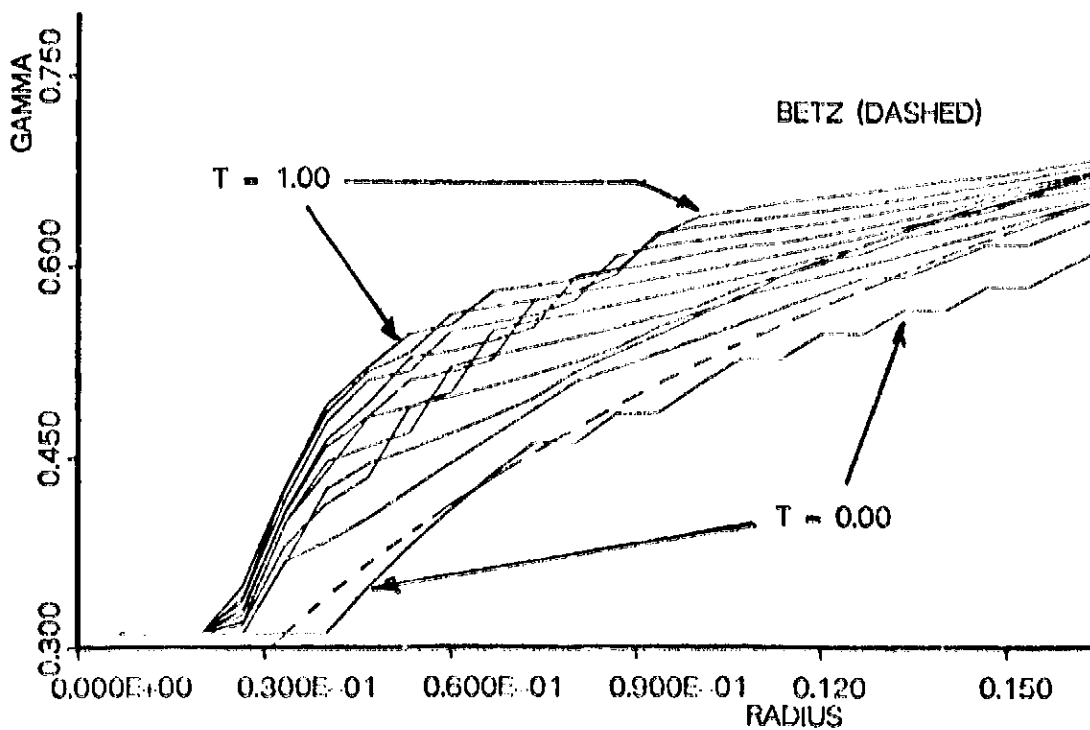


Figure 5-10: Blow-up of Fig. 5-9

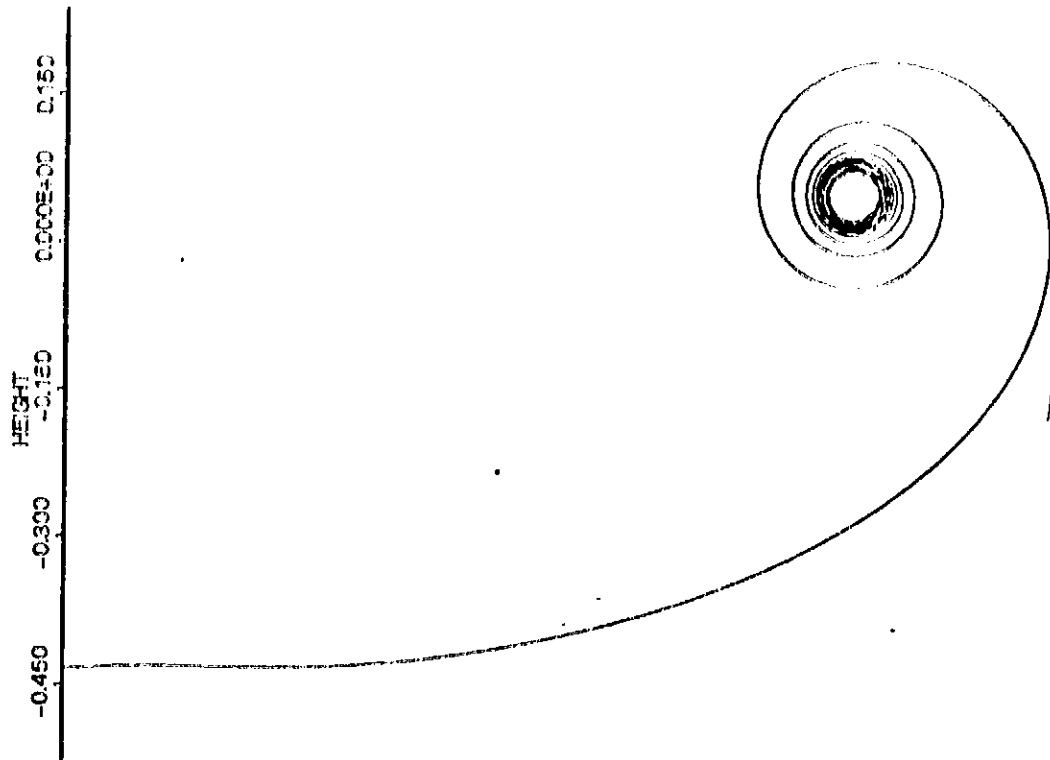


Figure 5-11: Roll-Up of Wing Wake at T = 1.00

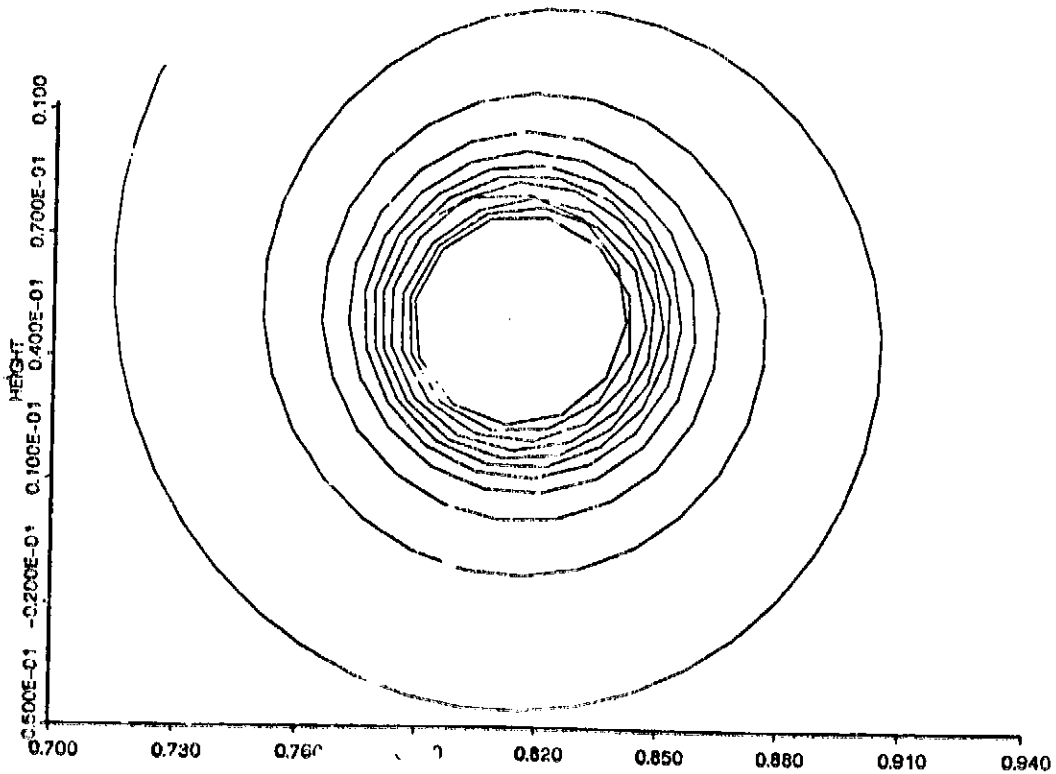


Figure 5-12: Detail of Figure 5-11

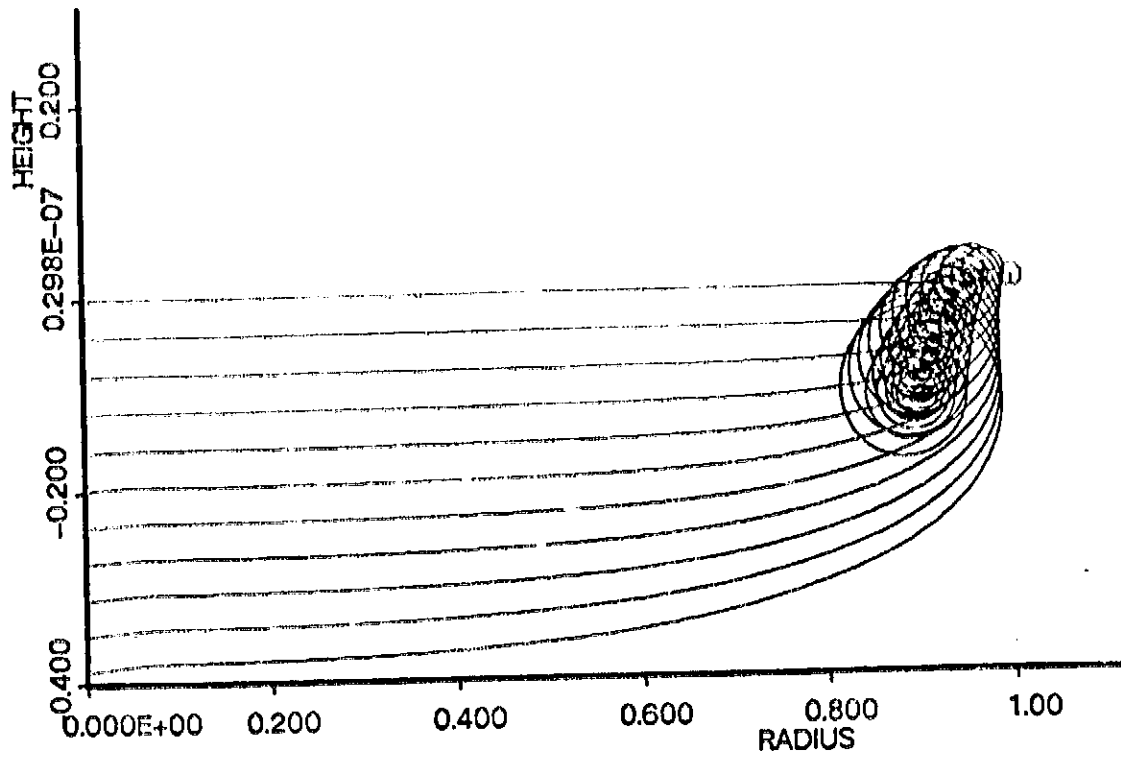


Figure 5-13: Roll-Up Produced by a Moving Disk

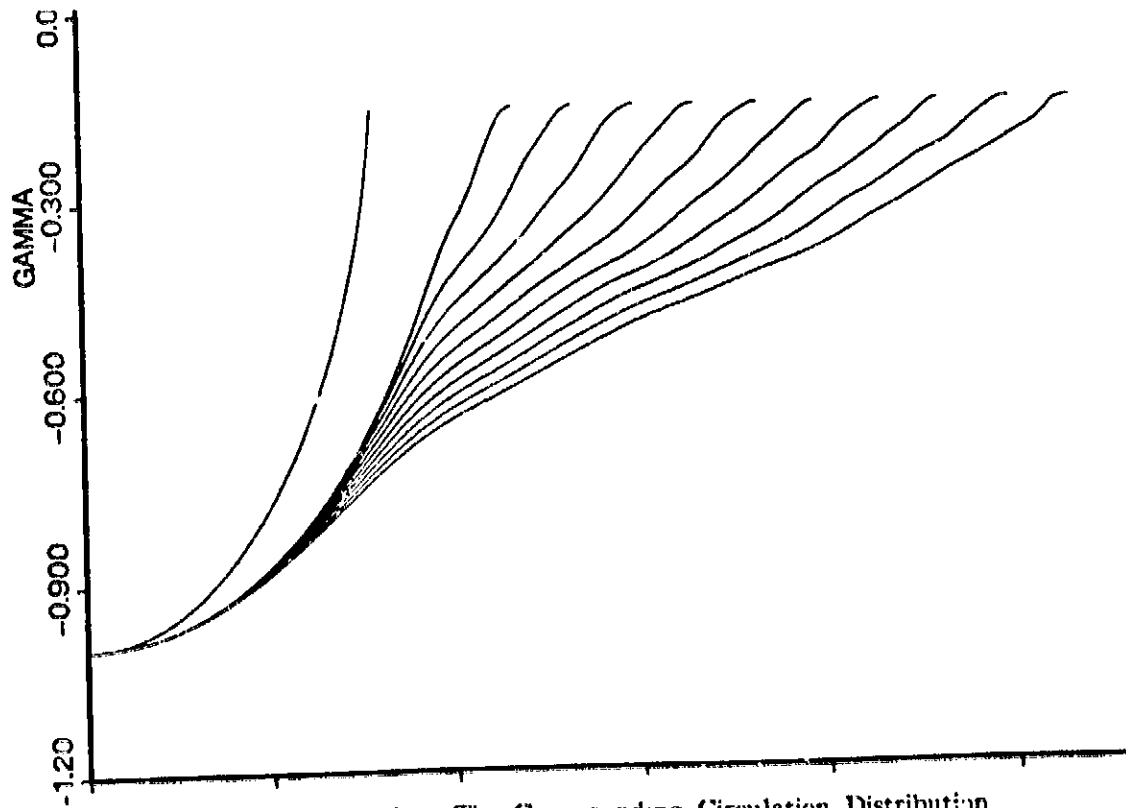


Figure 5-14: The Corresponding Circulation Distribution

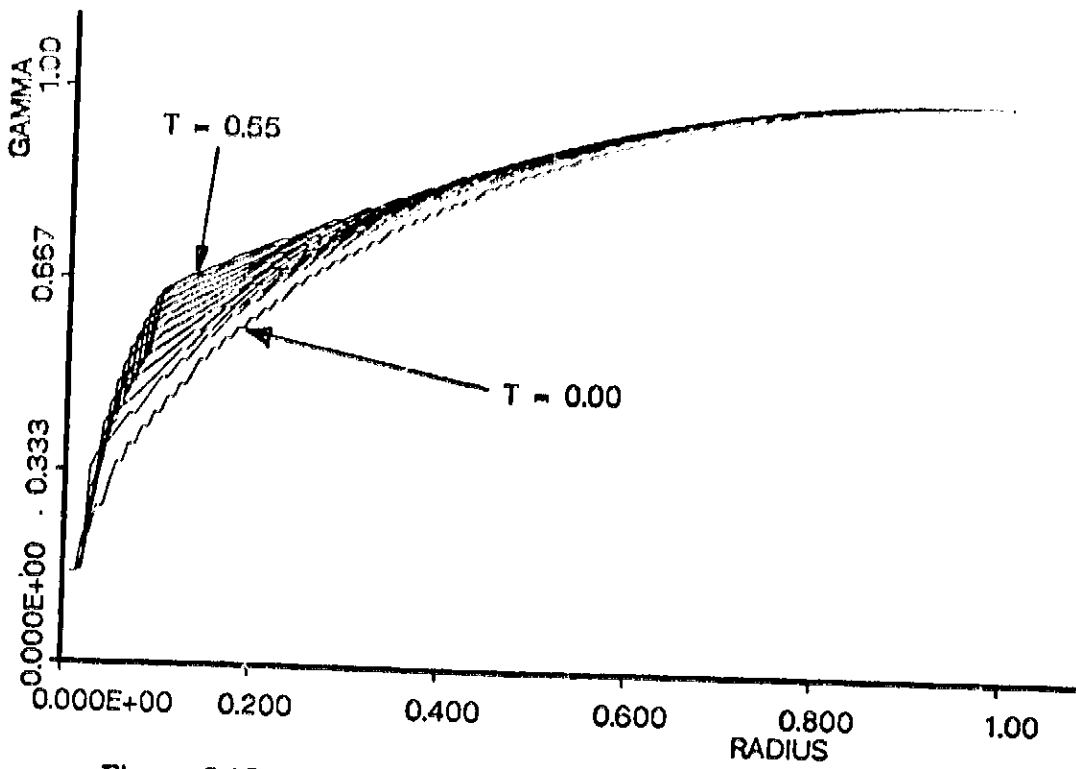


Figure 5-15: Distributions of Circulation Surrounding the Roll-Up Core

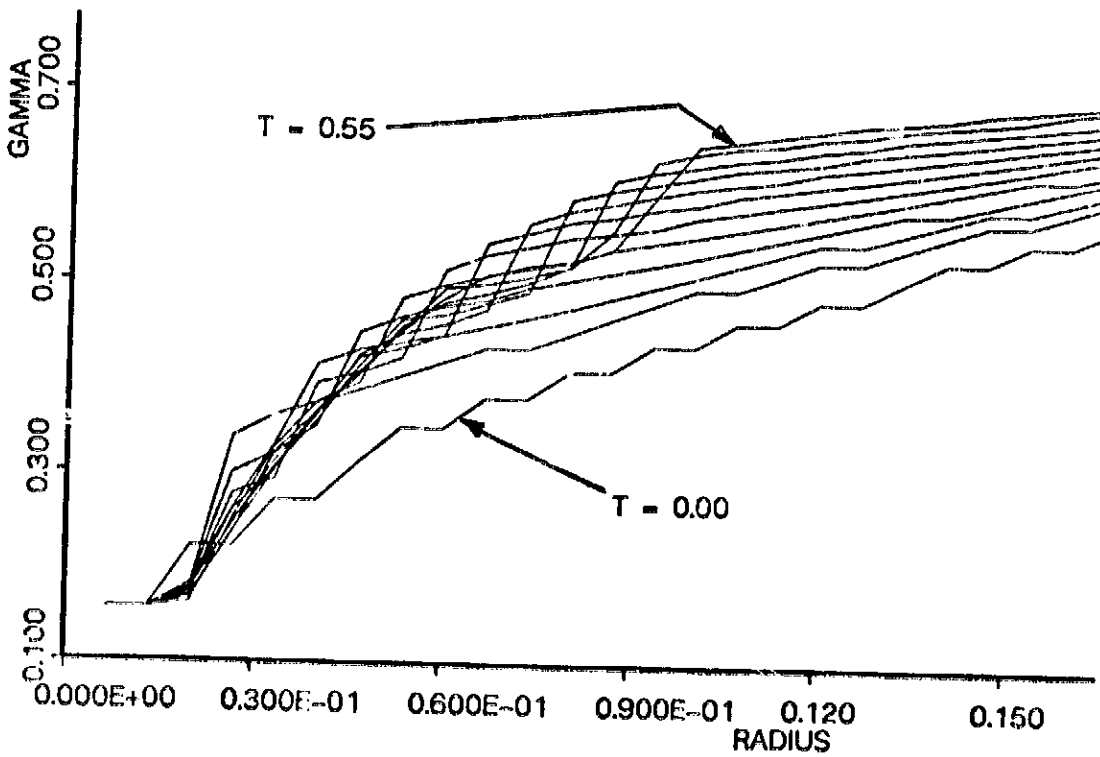


Figure 5-16: Detail of Fig. 5-15

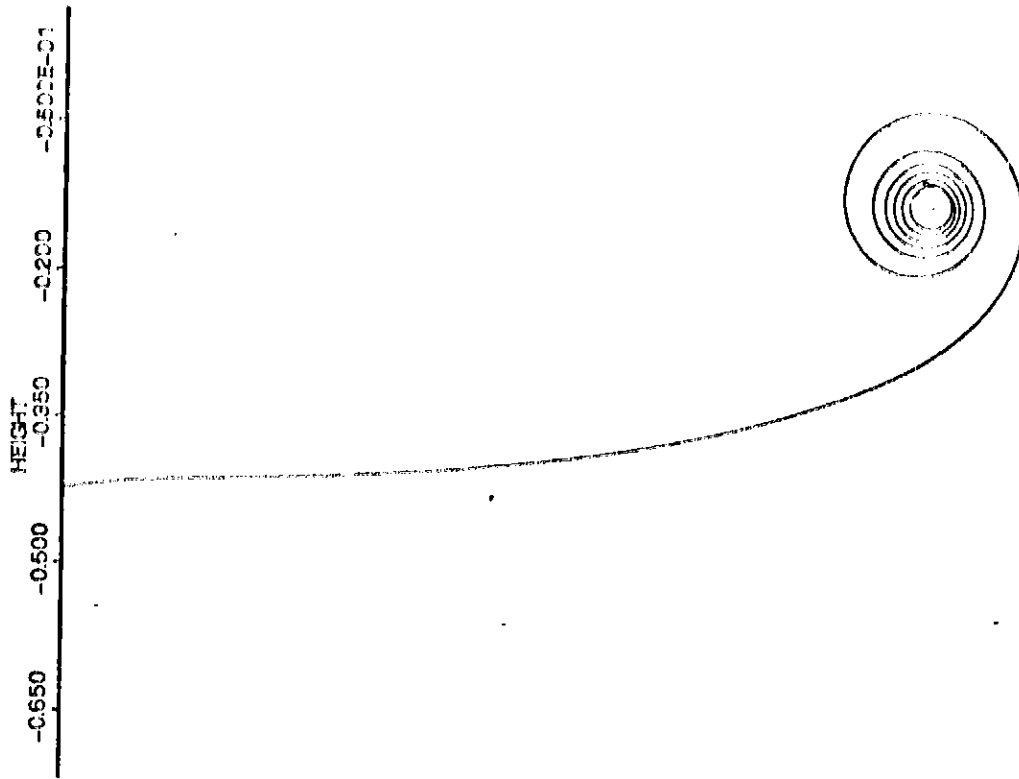


Figure 5-17: The Sheet Geometry: $T = 0.55$

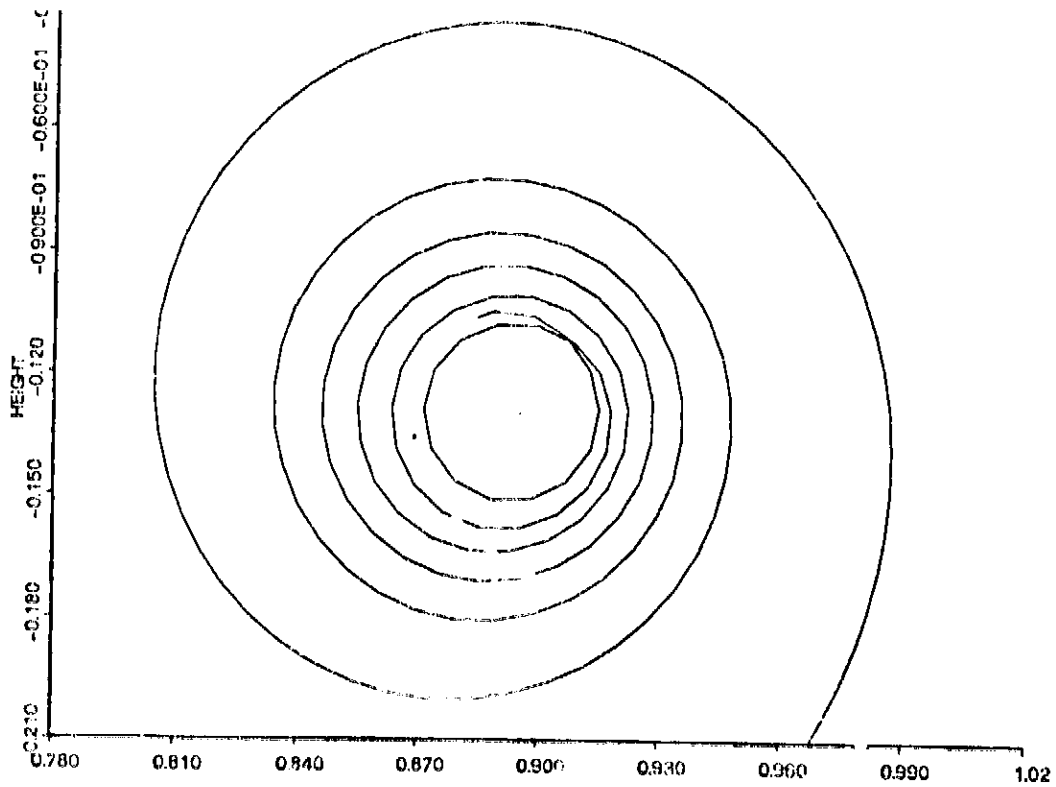


Figure 5-18: The Blow-Up of the Spiral

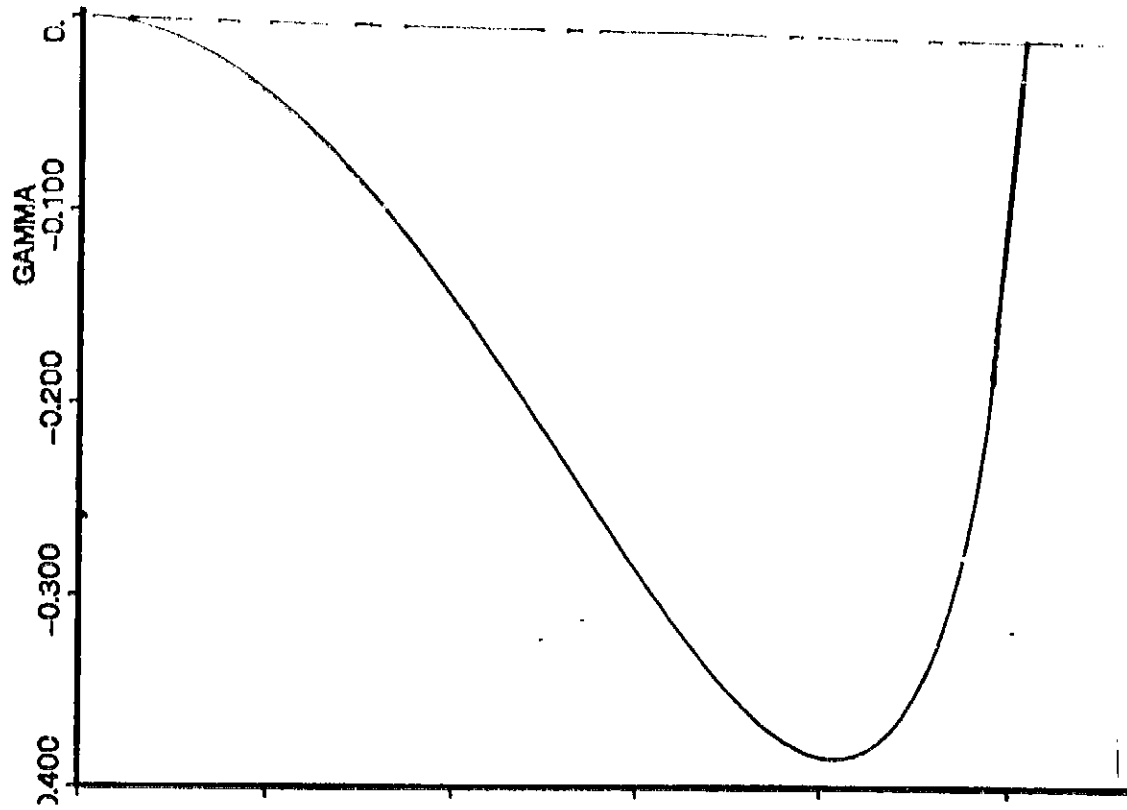


Figure 5-19: Helicopter-type Loading Distribution

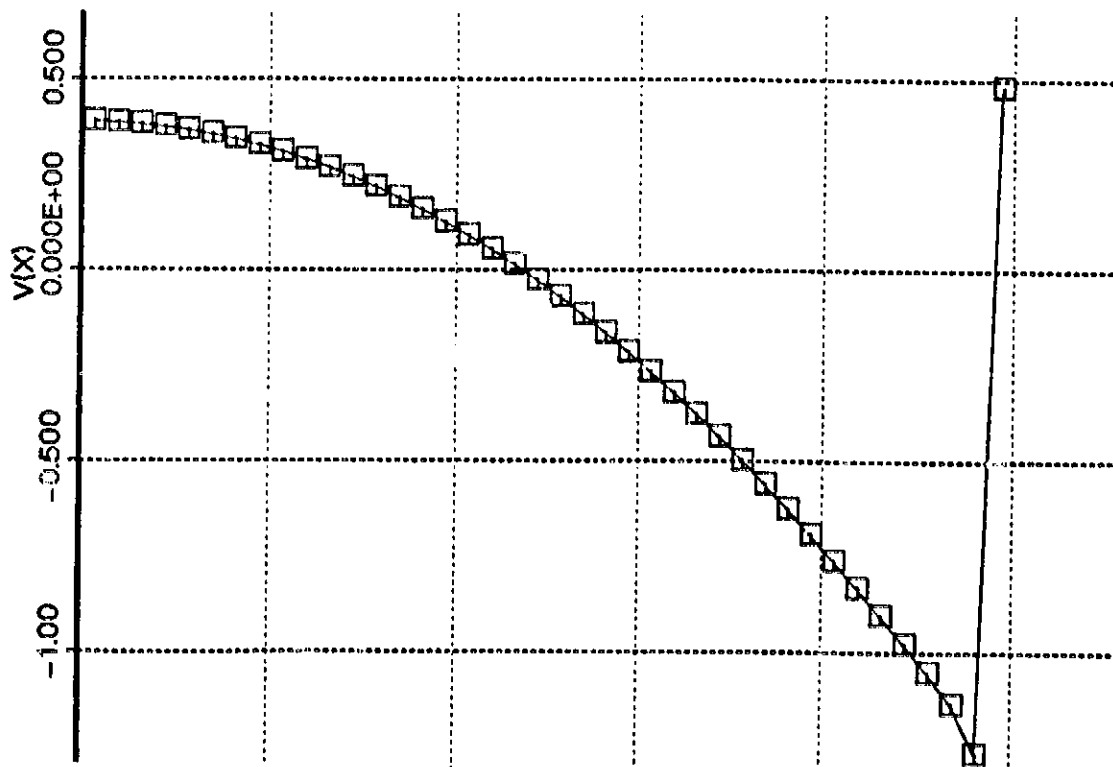


Figure 5-20: Downwash Profile: Vortex Bands with the Above Loading

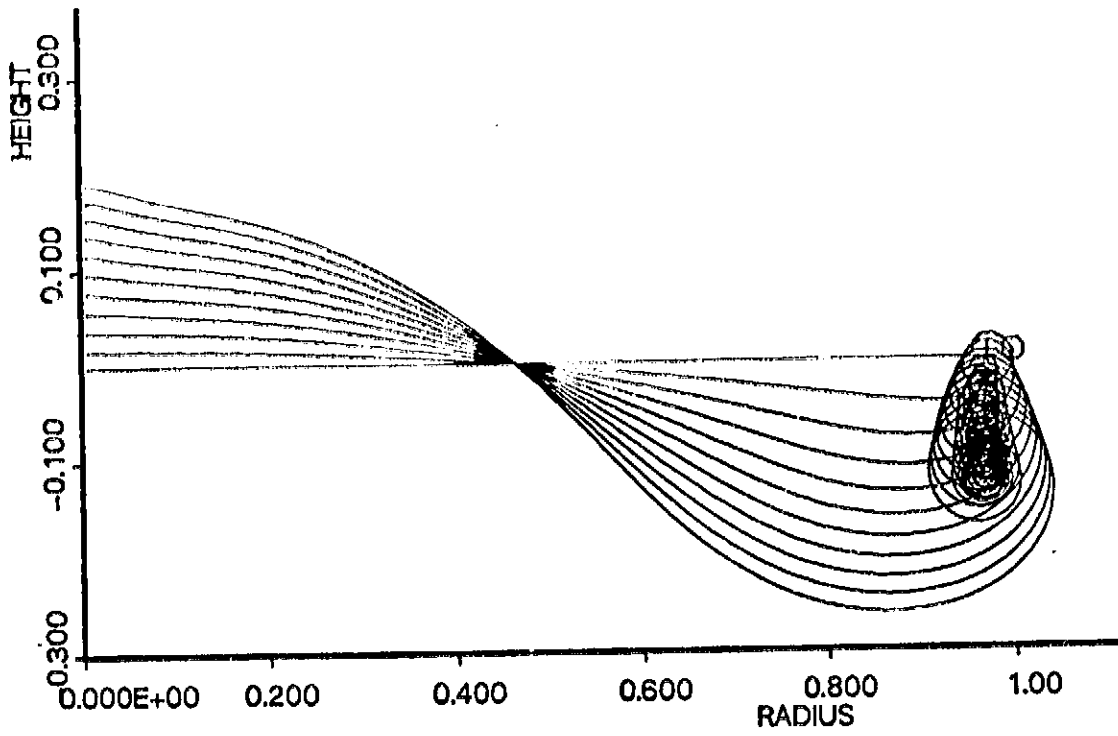


Figure 5-21: Roll-Up for a Helicopter Type Loading

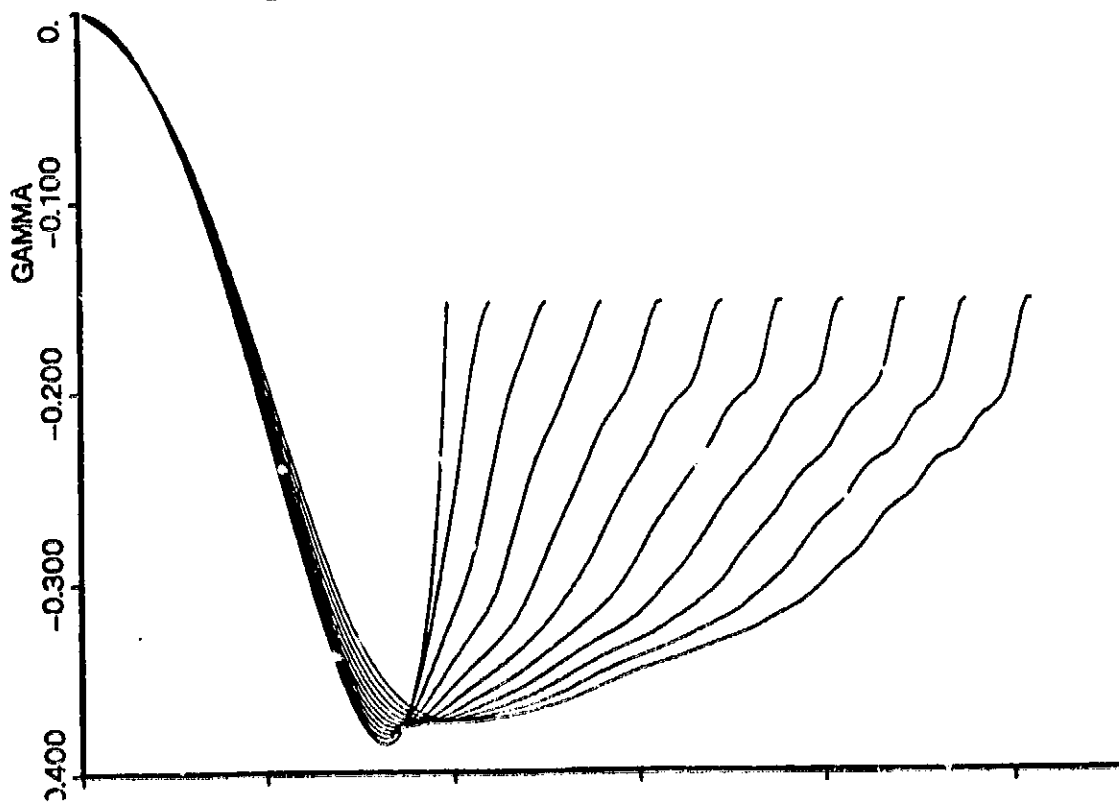


Figure 5-22: The Corresponding Circulation Distribution

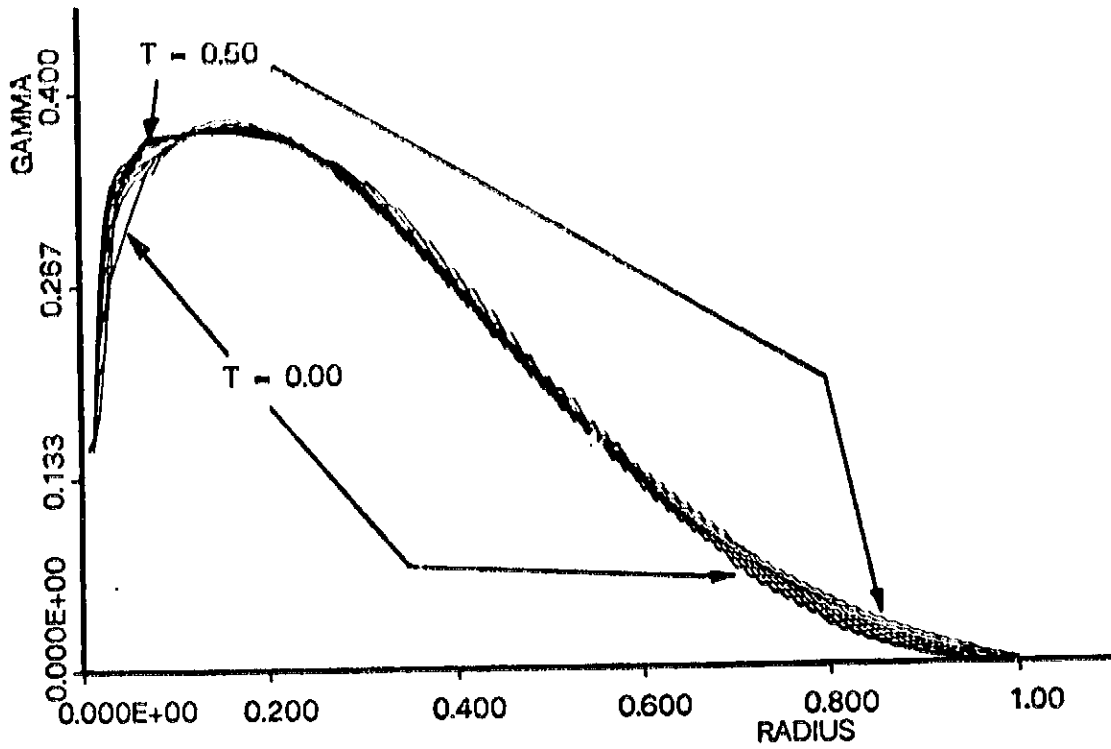


Figure 5-23: Distribution of Circulation Surrounding the Roll-Up Core

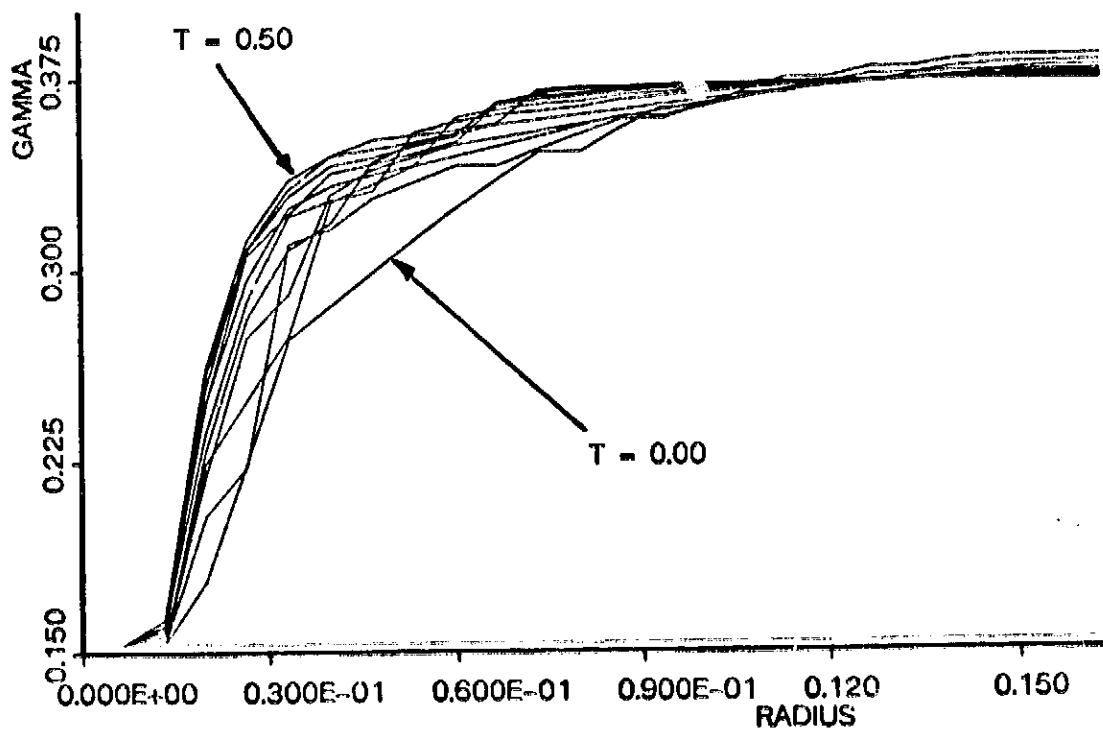


Figure 5-24: Detail of Fig. 5-23

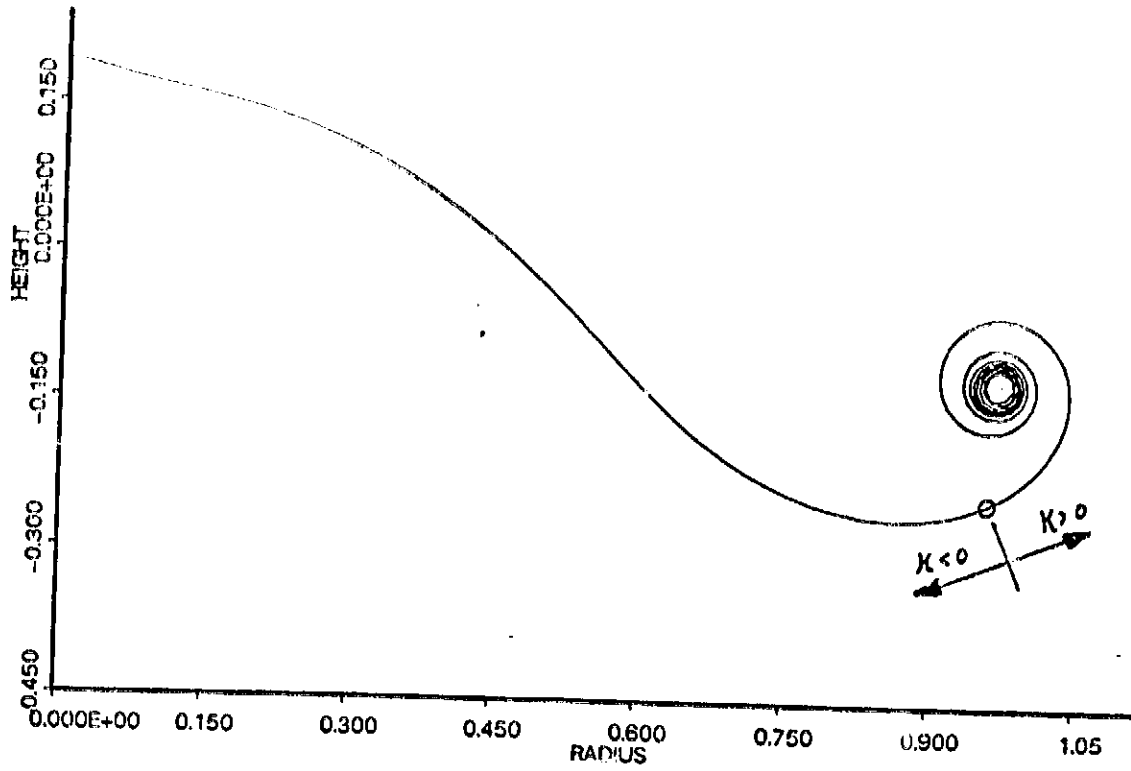


Figure 5-25: Helicopter Roll-Up: T = 0.500

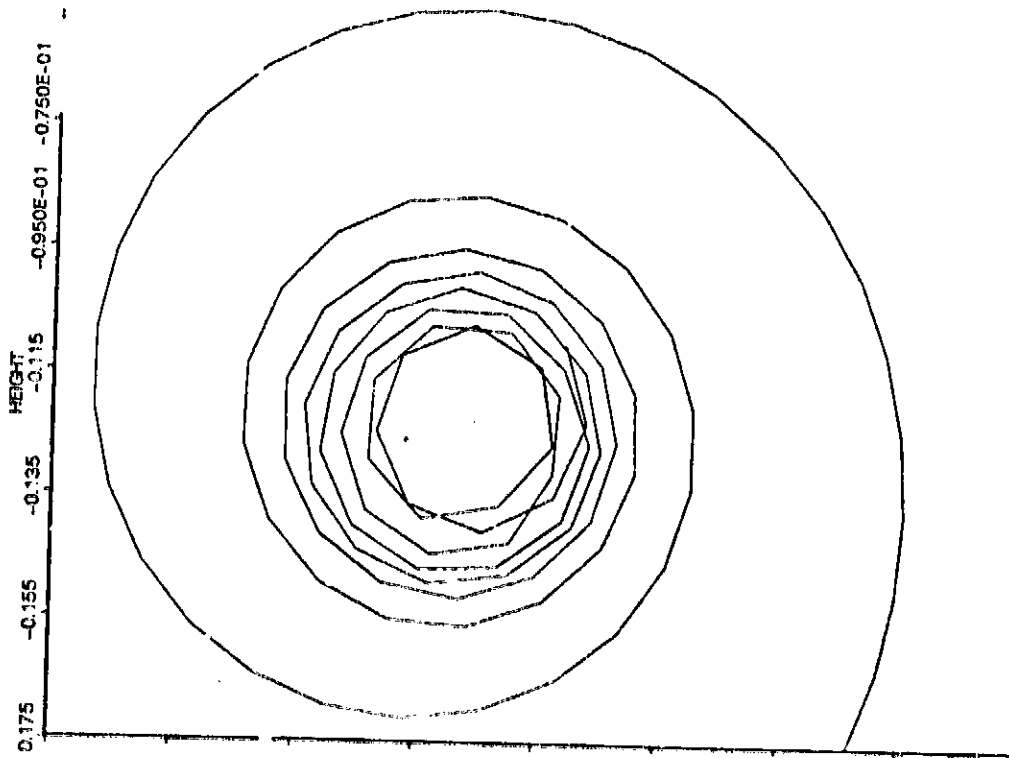


Figure 5-26: Blow-Up of the Tip Spiral in Fig. 5-25

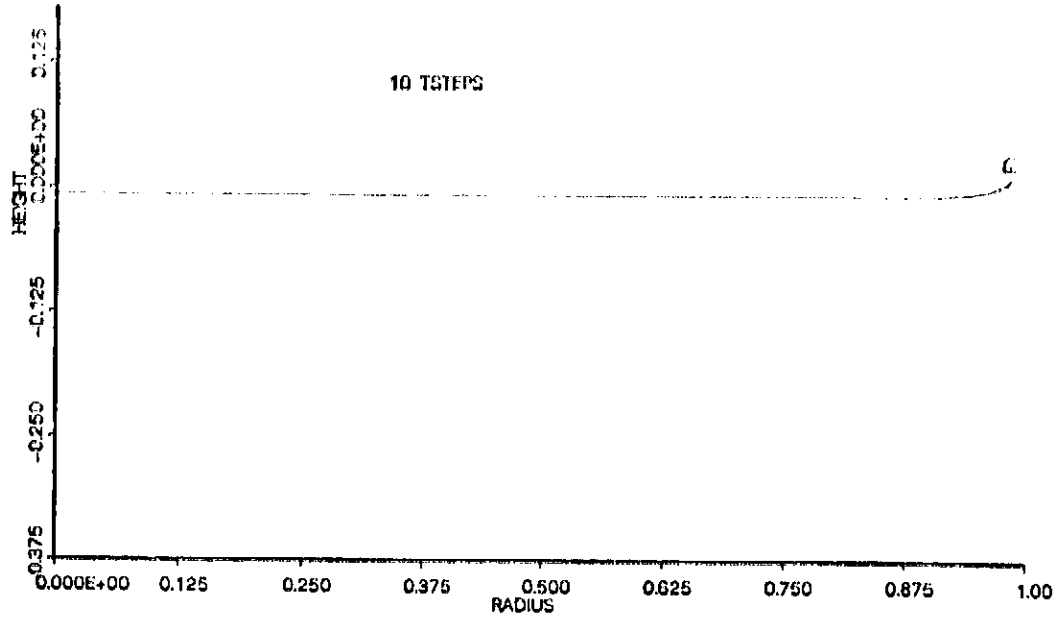


Figure 5-27: Geometry of the Wake Vortex Sheet

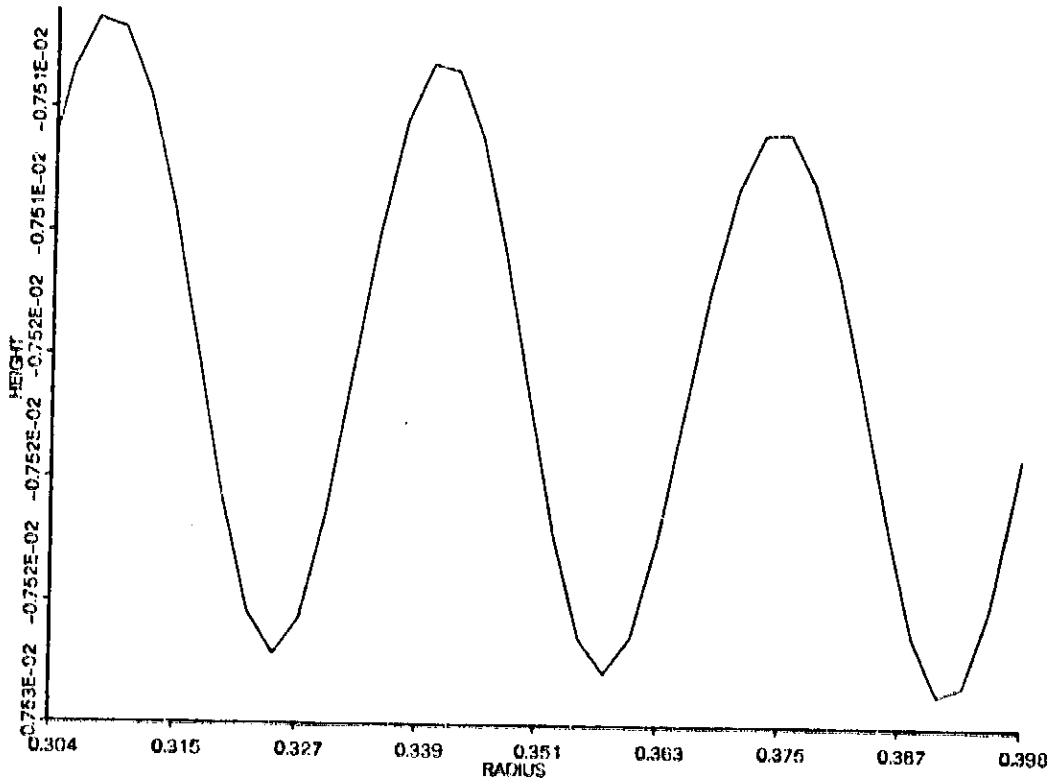
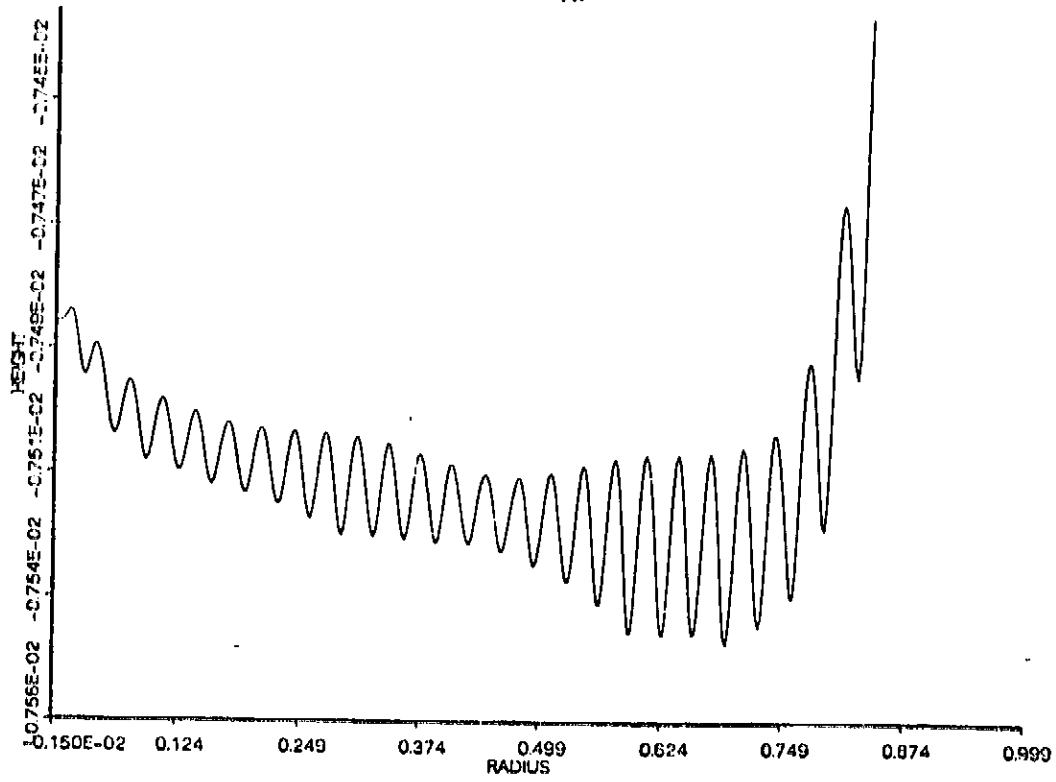


Figure 5-28: Repeated Magnification of a Section of Vortex Sheet

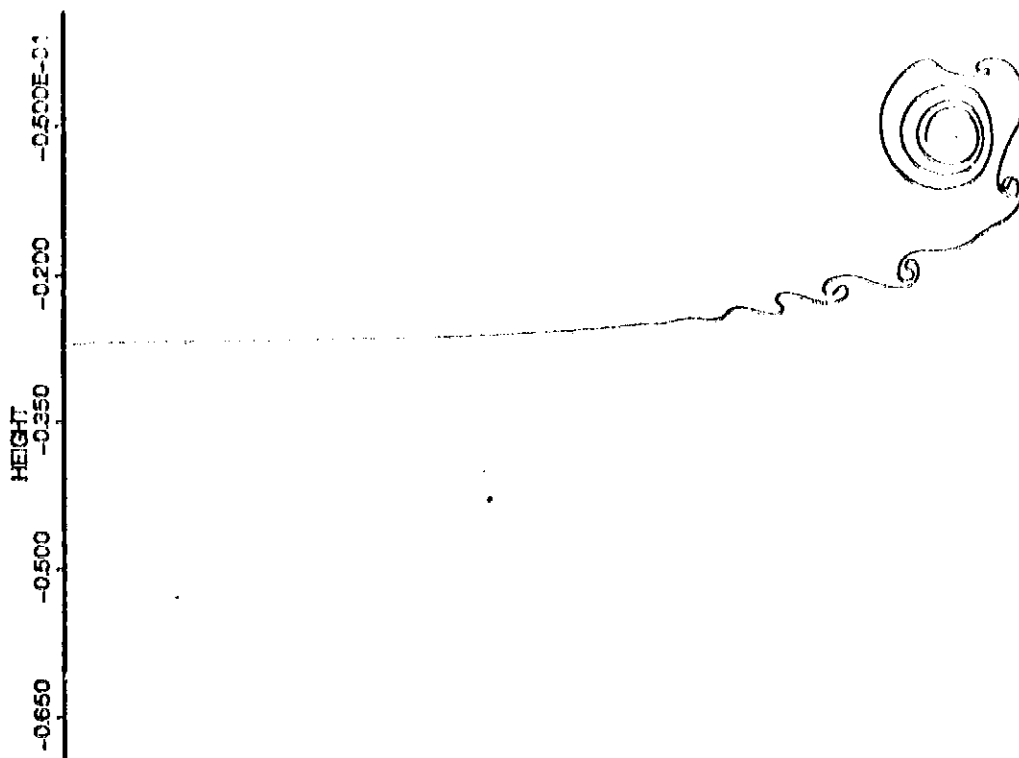


Figure 5-29: Repeat of Fig. 5-13 with Finer Paneling: $T = 0.350$

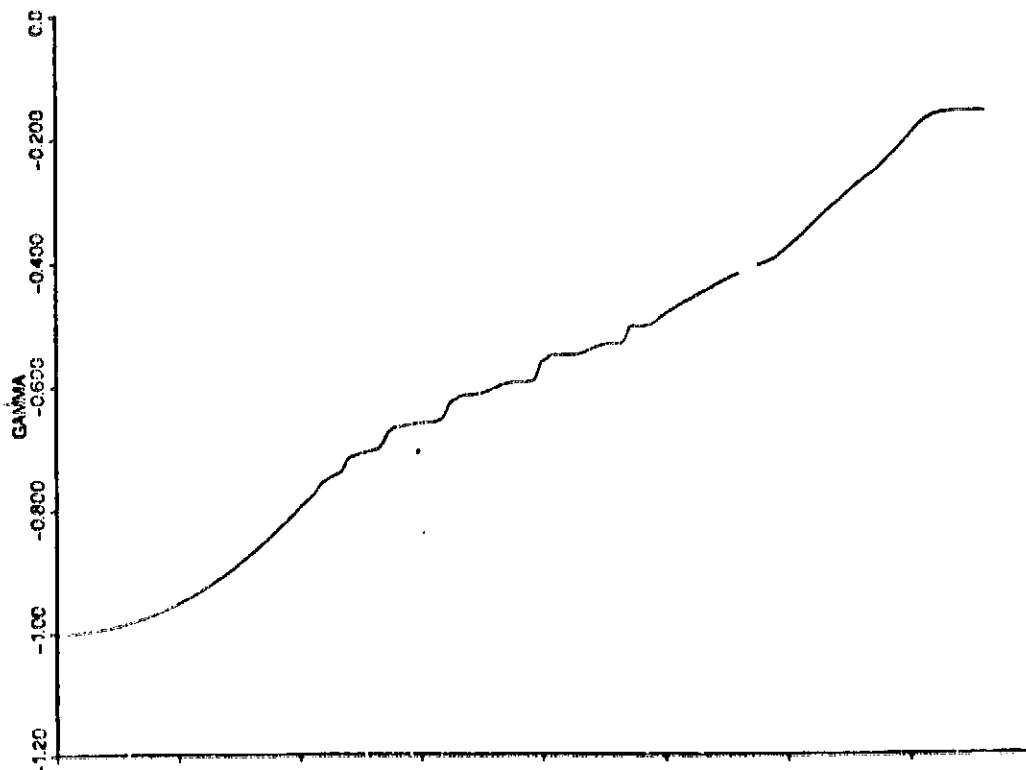


Figure 5-30: The Corresponding Circulation Distribution

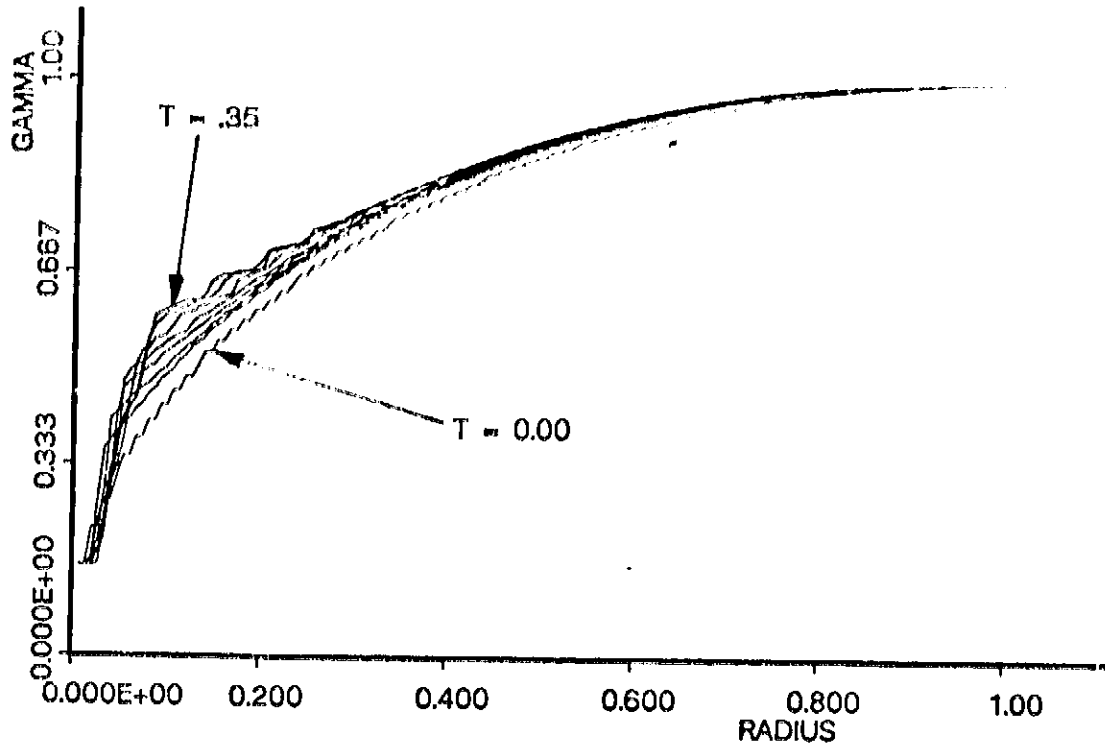


Figure 5-31: Circulation Distribution Around the Main Roll-Up

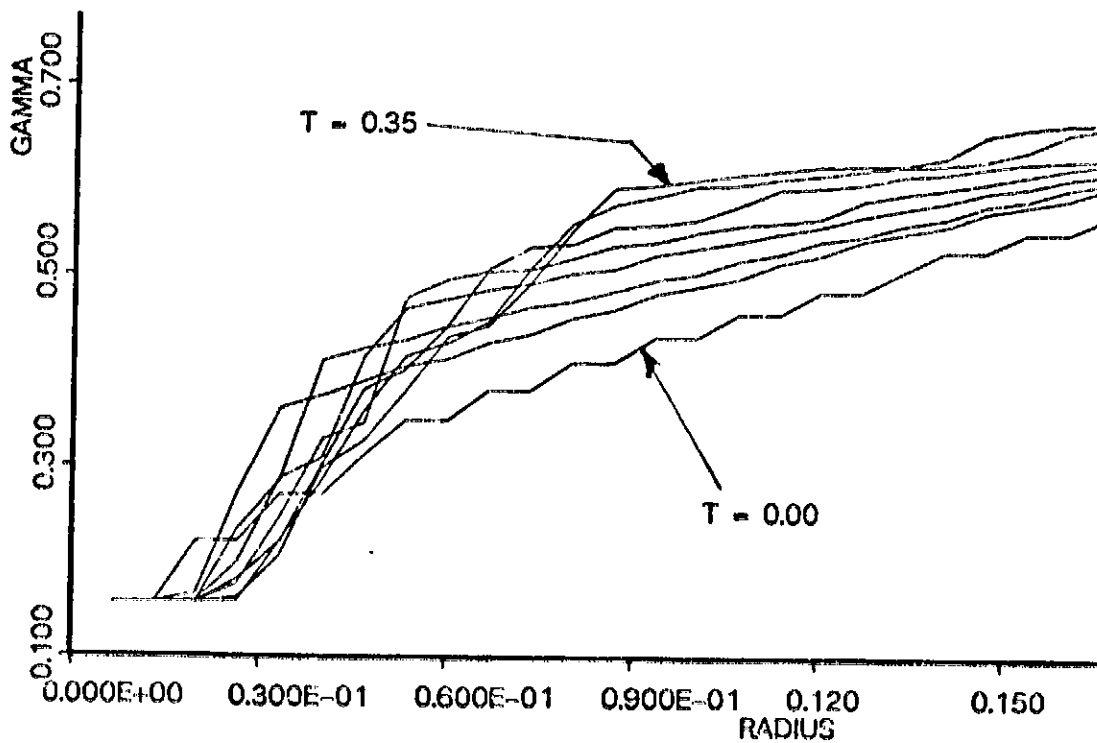


Figure 5-32: Detail of Fig. 5-31

Chapter 6

Conclusions

The behavior of vortex sheets with axisymmetric geometry presents the next frontier in the study of vortical flows. Axisymmetric flow lies between the relatively well understood two-dimensional flows and the complex three-dimensional flows. For this reason, understanding of axisymmetric vortex sheets is useful before completely three-dimensional vortex sheets can be modelled. Due to the complexity imposed by the increase in number of variables as the number of dimensions are increased, three-dimensional models using discrete vortices or dipoles are more desirable than panel methods. However, the use of simpler models would be meaningless unless the accuracy of the models can be determined. For this reason, the axisymmetric panel method was developed as a higher-order model to test the accuracy of simpler axisymmetric vortex models.

To accurately formulate the behavior of an axisymmetric vortex panel, a flat strip of a uniform two-dimensional vortex sheet, called the vortex panel, was first studied. The calculations of the velocity field show that an assemblage of panels will mutually induce motions which are more representative of a vortex sheet than an assemblage of point vortices. Even when reproducing a vortex sheet with non-uniform vorticity and curved geometry, the panel method performs no worse than the discrete vortex method. The simple geometry of the vortex panel allows a straightforward derivation of a matched asymptotic solution for the flow induced by an axisymmetric equivalent of the vortex panel, the vortex band. Vortex bands can be assembled to accurately represent an axisymmetric vortex sheet, limited by the geometric inaccuracy in representing a smooth curve using straight line segments and, at least for this study, the non-smoothness of the vorticity distribution. Both of these weaknesses are problems of spatial resolution which can be alleviated by increasing the number of elements. Thus, panel-method can be used to accurately simulate the evolution of an axisymmetric vortex sheet.

The vortex sheet dynamics calculation is an initial condition problem. One important result has been the accuracy of the panel-method in reproducing the flow induced by a flat vortex sheet which is the initial state of the vortex sheet in many problems of interest. In the present study, the singularity at the edge of the vortex sheet was modelled using a simple discrete vortex. While the introduction of a tip vortex core was necessary for the accurate reproduction of the global flow field, it is also useful for the numerical simulation of the self-induced deformation of the vortex sheet.

The self-induced velocity of curved vortices have inhibited the study of the dynamics of axisymmetric vortex sheets. By using the method of matched asymptotic expansion, the self-induced velocity of an axisymmetric vortex panel consistent with the kinetic energy of a section of an axisymmetric vortex sheet was found. The axisymmetric panel-method was used to simulate the roll-up caused by the impulsive motion of a circular disk and the roll-up of a vortex sheet with a loading which approximates that of a helicopter rotor. In both cases, smooth roll-up was observed and both total circulation and impulse were conserved. By relaxing the low-pass filtering inherent in the numerical method, secondary roll-up due to Kelvin-Helmholtz instability can be observed. This feature for an axisymmetric vortex sheet was simulated numerically using the panel-method described above.

References

1. Rosenhead, I., "The Formation of Vortices from a Surface of Discontinuity", *Proc.R.Soc.London Ser.A*, Vol. 134(1931), pp. 170-92.
2. Eirikhoff, G., Fisher, J., "Do Vortex Sheets Roll Up?", *Circ.Mat.Palerno*, Vol. 8(1959), pp. 77-90.
3. Saffman, P.G., Baker, G.R., "Vortex Interactions", *Ann. Rev. Fluid Mech.*, Vol. 11(1979), pp. 95-122.
4. Moore, D.W., "On the Point Vortex Method", *SIAM J.Sci.Stat.Comp.*, Vol. 2(1981), pp. 65-84.
5. Baker, G.R., "The Cloud-in-Cell Technique Applied to the Roll-Up of Vortex Sheets", *J.Comp.Physics*, Vol. 31(1979), pp. 76-95.
6. Murman, E.M., Stremel, "A Vortex-Wake Capturing Method for Potential Flow", *AIAA Paper*, No. 82-0947, June (1982).
7. Moore, D.W., "The Spontaneous Appearance of a Singularity in the Shape of an Evolving Vortex Sheet", *Proc.R.Soc.London Ser.A*, Vol. 365(1979), pp. 105-119.
8. Meiron, D.I., Baker, G., Orzsag, S.A., "The Analytical Structure of Vortex-Sheet Dynamics. Part 1. Kelvin-Helmholtz Instability", *J.Fluid Mech.*, Vol. 114(1979), pp. 283-298.
9. Karman, Th. von, Burgers, J.M., *Aerodynamic Theory*, Springer, (1935), pp. 320-325, See also Westwater¹²
10. Betz, A., "Behavior of Vortex Systems", *NACA TM-713*(1933).
11. Pullin, D.I., "On a Generalization of Kaden's Problem", *J. Fluid Mech.*, Vol. 104(1981), pp. 45-53.
12. Westwater, F.L., "Rolling Up of the Surface of Discontinuity Behind an Aerofoil of Finite Span", *Aero.Res.Comm.R&M*, No. 1692(1935).
13. Fink, P.T., Soh, W.K., "Calculation of Vortex Sheets in Unsteady Flow and Applications in Ship Hydrodynamics", *Proc. 10th Symp. Naval Hydrodynamics*, Cambridge, Mass., (1974), pp. 463-488.
14. Fink, P.T., Soh, W.K., "A New Approach to Roll-Up Calculations of Vortex Sheets", *Proc.R.Soc.London Ser.A*, Vol. 362(1978), pp. 195-209.
15. Baker, G., "A Test of the Method of Fink & Soh for Following Vortex Sheet Motion", *J. Fluid Mech.*, Vol. 100(1980), pp. 209-220.

16. Hoelmakers, H.W.M., Vaatstra, "A Higher-Order Panel Method Applied to Vortex Sheet Roll-Up", *AIAA Paper*, No. 82-0096(1982).
17. Higdon, J.L., Pozrikidis, C., "The Self-Induced Motion of Vortex Sheets", *J. Fluid Mech.*, Vol. 150(1985), pp. 203-231.
18. Morky, M., "Calculation of Vortex Sheet Roll-Up in a Rectangular Wind Tunnel", *J. Aircraft*, Vol. 12, No. 9(1975).
19. Batchelor, G.K., *Introduction to Fluid Dynamics*, Cambridge University, (1957).
20. Widnall, S.H., Tsai, C.Y., "The Instability of the Thin Vortex Ring of Constant Vorticity", *Phil. Tran. R. Soc. Lond.*, Vol. 287(1977), pp. 273-305.
21. Lamb, H., *Hydrodynamics*, Dover, (1932).
22. Bliss, D., "The Dynamics of Curved Rotational Vortex Lines", Master's thesis, M.I.T., Aero/Astro, (1970).
23. Bender, C.M., Orszag, S.A., *Advanced Mathematical Methods for Scientists and Engineers*, McGraw-Hill, (1978).
24. Jahnke, E., Emde, F., *Table of Functions*, Dover, (1945).
25. Tung, C., Ting, L., "Motion and Decay of a Vortex Ring", *The Physics of Fluids*, Vol. 10, No. 5(1967).
26. Kantelis, J. Private Communications
27. Taylor, G.I., "Formation of a Vortex Ring Giving an Impulse to a Circular Disk and then Dissolving it Away", *J. Appl. Phy.*, Vol. 24(1953), pp. 104.
28. Roache, P.J., *Computational Fluid Dynamics*, Hermosa Publishing, (1972).

Appendix

The following pages are divided into three sections,

- 1) The listings of the FORTRAN routines for computing the velocity induced by various vortex elements.
- 2) The description of the numerical model of the initial state of the vortex sheet prior to the numerical roll-up simulation and the FORTRAN listing.
- 3) The listing of the FORTRAN program for the numerical simulation of vortex sheet dynamics.
- 4) The inputs for the vortex sheet dynamics simulation program used to generate the figures within the text.

All of the following program listings have been written in FORTRAN 77 Version 3.0 for the Digital Equipment Corporation VAX-750 computer.

Appendix A

The Vortex-Velocity Routines

The velocity induced by a vortex element is calculated using a Cartesian coordinate system, (X,Y), centered on the vortex inducing the flow. The panel's inclination respect to the coordinate system is expressed by (DX,DY), where DY/DX equals the tangent of the angle between the panel and the x-axis. (W) is the half-width of the panel and (G) is the vorticity along the panel. The velocity is obtained as orthogonal components, (u,v).

The names of the two-dimensional velocity routines:

VEL2D : The Vortex Panel Routine

VEL2DF: The Point Vortex Routine

The axisymmetric vortex routines differ from the two-dimensional vortex routines due to the inclusion of the radius of the vortex element, R. The composite solution, V_{comp} , for the velocity induced by a vortex band is

$$V_{comp} = V_{in} + V_{out} - V_{io}$$

where the routine

VELIN computes the inner-solution, V_{in}

VELOUT computes the outer-solution, V_{out}

VELIO computes the intermediate-solution, V_{io} .

(Note: The V_{out} alone gives the velocity induced by a simple vortex ring.)

```

SUBROUTINE VEL2D (UIN, VIN)
.....
*   THIS SUBROUTINE CALCULATES THE VELOCITY FIELD INDUCED
*   BY A FLAT VORTEX STRIP OF
*   WIDTH           : 2W
*   STRENGTH        : G
*   INCLINATION     : ( DX, DY )
*   AT POSITION (X, Y) RELATIVE TO THE STRIP MIDPOINT
*   (DUMMY VARIABLE: RADIUS : R)
.....
C   RELATIVE COORDINATES AND QUADRATIC-POSITION VARIABLES
C
COMMON /VELO/ R, X, Y, DX, DY, W, G
PI = 2*ASIN(1.)
COST = DX / SQRT(DX**2+DY**2)
SINT = DY / SQRT(DX**2+DY**2)
Q5 = (X**2 + Y**2)/W**2
Q4 = (Y*COST - X*SINT)/W
Q3 = (X*COST + Y*SINT)/W
Q2 = Q5 - 2*Q3 + 1.
Q1 = Q5 + 2*Q3 + 1.
.....
CHECK FOR SINGULAR CONDITION
IF (Q4.EQ.0) THEN
  ATN = 0.0
  GO TO 740
END IF
.....
740  ATN = ATAN((1.-Q3)/Q4)+ATAN((1.+Q3)/Q4)
CONTINUE
IF ((Q1.EQ.0).OR.(Q2.EQ.0)) THEN
  UIN = 0
  VIN = 0
  GO TO 750
END IF
.....
C   PERTURBED VORTEX STRIP FORMULA
U1 = -SINT*LOG(Q2/Q1)+2.*COST*ATN
V1 = -COST*LOG(Q2/Q1)-2.*SINT*ATN
UIN = -G / 4. / PI * U1
VIN = G / 4. / PI * V1
750  RETURN
END

```

SUBROUTINE VELOZDF (UIN, VIN)

```

.....
*           THIS SUBROUTINE CALCULATES THE VELOCITY FIELD INDUCED
*           BY A FLAT VORTEX STRIP OF
*           WIDTH           : 2W
*           STRENGTH       : G
*           INCLINATION    : ( DX, DY )
*           AT POSITION (X, Y) RELATIVE TO THE STRIP MIDPOINT
*           (DUMMY VARIABLE: RADIUS : R)
.....
C           RELATIVE COORDINATES AND QUADRATIC-POSITION VARIABLES
C
COMMON /VELO/ R, X, Y, DX, DY, W, G
PI = 3.141592654
QS = SQRT(X**2. + Y**2.)
IF (QS.EQ.0) GO TO 750
COST = X / QS
SINT = Y / QS
.....
U1 = SINT/QS
V1 = COST/QS
UIN = -G/2./PI * U1
VIN = G/2./PI * V1
750  RETURN
      END

```

SUBROUTINE VELIN (UIN, VIN)

```

.....
* THIS SUBROUTINE CALCULATES THE INNER SOLUTION
* OF THE VELOCITY FIELD INDUCED BY AXISYMMETRICALLY
* PERTURBING A FLAT VORTEX STRIP OF
* WIDTH : 2W
* STRENGTH : G
* INCLINATION : ( DX, DY )
* RADIUS : R
* AT POSITION (X, Y) RELATIVE TO THE STRIP MIDPOINT
*
* THE DERIVATIVES OF THE STREAM-FUNCTION HAS BEEN
* DIVIDED INTO TWO PARTS:
* 1 - RECTILINEAR SOLUTION
* 2 - FIRST ORDER PARTICULAR SOLUTION
.....
C RELATIVE COORDINATES AND QUADRATIC-POSITION VARIABLES
C
COMMON /VELO/ R, X, Y, DX, DY, W, G
PI = 3.141592654

COST = DX / SQRT(DX**2.+DY**2.)
SINT = DY / SQRT(DX**2.+DY**2.)
Q5 = (X**2. + Y**2.)/W**2.
Q4 = (Y*COST - X*SINT)/W
Q3 = (X*COST + Y*SINT)/W
Q2 = Q5 - 2.*Q3 + 1.
Q1 = Q5 + 2.*Q3 + 1.
.....
CHECK FOR SINGULAR CONDITION
IF (Q4.EQ.0) THEN
  ATN = 0.0
  GO TO 740
END IF
.....
740 ATN = ATAN((1.-Q3)/Q4)+ATAN((1.+Q3)/Q4)
CONTINUE
.....
C PERTURBED VORTEX STRIP FORMULA
U1 =-SINT*LOG(Q2/Q1)+2.*COST*ATN
V1 =-COST*LOG(Q2/Q1)-2.*SINT*ATN
U2 = (X/2./R) * U1
V2 = (X/2./R) * V1
* + .5*W/R *( LOG(Q2*Q1)
* -Q3*LOG(Q2/Q1)
* +2.*Q4*ATN
* -4.)

UIN =-G / 4. / PI * (U1 + U2)
VIN = G / 4. / PI * (V1 + V2)

750 RETURN
END

```

SUBROUTINE VELOUT (UO, VO)

I ELLIPTIC INTEGRALS I

```

.....
*           THIS SUBROUTINE CALCULATES THE VELOCITY FIELD           *
*           INDUCED BY A VORTEX RING WHICH IS USED AS THE          *
*           OUTER VELOCITY SOLUTION FOR A VORTEX BAND OF          *
*           WIDTH           : 2W                                     *
*           STRENGTH        : C                                     *
*           INCLINATION     : (DX, DY)                             *
*           RADIUS          : R                                     *
*           AT POSITION (X, Y) RELATIVE TO THE BAND MIDPOINT       *
.....
COMMON /VELO/ R, X, Y, DX, DY, W, G
REAL M1, LAM, K0, K1, K2, KL0, KL1, KL2, K, KP
UO = 0.0
VO = 0.0
PI = 3.141592654
.....
R1 = SQRT(X**2.+Y**2.)
R2 = SQRT((X+2.*R)**2.+Y**2.)
LAM = (R2-R1)/(R1+R2)
M1 = 1. - LAM**2.
IF (R1.EQ.0) GO TO 730
IF (LAM.EQ.0) GO TO 730
DXR1 = X/R1
DYR1 = Y/R1
DXR2 = (X+2.*R)/R2
DYR2 = Y/R2
DXL = (DXR2-DXR1)/(R2+R1) - LAM/(R2+R1)*(DXR1+DXR2)
DYL = (DYR2-DYR1)/(R2+R1) - LAM/(R2+R1)*(DYR1+DYR2)
K0 = 1.3862944
K1 = .1119723 * M1
E1 = .4630151 * M1
K2 = .0725296 * M1**2.
E2 = .1077812 * M1**2.
KL0 = .5
KL1 = .1213478 * M1
EL1 = .2452727 * M1
KL2 = .0288729 * M1**2.
EL2 = .0412496 * M1**2
K = K0 + K1 + K2 - (KL0 + KL1 + KL2)*LOG(M1)
E = 1. + E1 + E2 - (EL1 + EL2)*LOG(M1)
KP = E / LAM / M1 - K / LAM
EP = (E - K) / LAM
DXR = DXR1 + DXR2
DYR = DYR1 + DYR2
RR = R1 + R2
.....
UO = G*W/PI/(R+X) * (DYR*(K-E)+RR*(KP-EP)*DYL)
VO = -G*W/PI/(R+X) * (DXR*(K-E)+RR*(KP-EP)*DXL)
730 RETURN
END

```

SUBROUTINE VELIO (UIO, VIO)

```

*****
*           THIS SUBROUTINE CALCULATES THE OUTER LIMIT           *
*           APPROXIMATION OF THE INNER VELOCITY SOLUTION         *
*           GIVEN BY ROUTINE VELIN IN ORDER TO MATCH THE         *
*           OUTER VELOCITY SOLUTION GIVEN BY ROUTINE VELOUT      *
*****
COMMON /VELO/ R, X, Y, DX, DY, W, G
PI = 2* ASIN(1.)
COST = DX / SQRT(DX**2+DY**2)
SINT = DY / SQRT(DX**2+DY**2)
Q5 = (R**2 + Y**2)/W**2
Q4 = (Y*COST + R*SINT)/W
Q3 = (-R*COST + Y*SINT)/W
Q2 = Q5 - 2*Q3 + 1.
Q1 = Q5 + 2*Q3 + 1.
UIO = 0.0
VIO = 0.0

R1 = SQRT(X**2.+Y**2.)
IF (R1.EQ.0.0) GO TO 720
*****
UIO = G*W/PI * ( 1. + X/R/2. ) * Y/R1/R1
VIO = G*W/PI * (( 1. + X/R/2. ) * X/R1/R1 + .5/R*LOG(R1/B/R))
720  VIO = G*W/PI * LOG( B*R/W ) /2 /R
*           + VIO
RETURN

END

```

Appendix B

The Initial Conditions for Roll-Up Simulations

The velocity field induced by a distribution of panels alone precludes a smooth roll-up unless the singularity at the edge of the vortex sheet is correctly modelled. The vorticity singularity at the edge of a vortex sheet is expected to produce an infinitesimal roll-up in an infinitesimal amount of time. Such a roll-up relieves the singular velocity discontinuity which would otherwise exist at the edge of the vortex sheet.

The roll-up simulations uses an initial configuration which represents a vortex sheet with a model for an arbitrary amount of roll-up at the edge of the sheet. The initially rolled-up section of the vortex sheet is replaced by a circular core of vorticity. For the roll-up of the wake vortex sheet shed by an elliptically loaded wing, Kaden's similarity solution for roll-up of parabolic loading is used to approximate the position of the center of the roll-up spiral. The position of the center of the roll-up spiral is given in Reference [9]. Figure B-1 shows Kaden's solution for the roll-up of the outer X_0 segment of the vortex sheet.

$$\begin{aligned} a_0 &= 0.57 X_0 \\ b_0 &= 0.88 X_0 \end{aligned}$$

A significant feature of Kaden's solution is the stretching of the remainder of the sheet up to the point directly under the center of the spiral, as noted by the displacement of point A on the sheet to point A'. This displacement conserves the overall centroid of vorticity since the center of the spiral is less than the centroid for the outer X_0 section of the flat vortex sheet. The numerical model replaces the rolled-up X_0 section with a core at the center and linearly stretches the remaining flat vortex sheet so its edge would come directly under the core. The resulting model reproduces the centroid of vorticity for the elliptic loading, $x_c = \pi/4$, to within 1% accuracy.

While Kaden's method is available to approximate the location of a tip core for two-dimensional roll-up, its application to an axisymmetric roll-up will not conserve impulse. Therefore, a vortex ring with the same impulse and energy as the outer X_0 section of the axisymmetric vortex sheet is used as a core. However, the vertical location of the roll-up core can not be obtained by the conservation equations. Since no theory exists for obtaining the vertical location, the ratio of distances for Kaden's solution was used to approximate the location. In addition, since the core conserves the centroid of vorticity, the remaining sheet was not stretched for this case. Figure B-2 shows the numerical model of the initial roll-up for axisymmetric vortex sheet which represents a translating disk.

$$R_0 = R \left[1 - \frac{2X_0}{3} + \frac{X_0^2}{3R^2} \right]^{1/2}$$

$$c_0 = \frac{88}{57} [R - R_0]$$

$$r_0 = 8R_0 \exp \left[\frac{-\pi^2 R_0}{4(2RX_0 - X_0^2)^{1/2}} - \frac{7}{4} \right]$$

where, R : the radius of the original axisymmetric vortex sheet,
 r_0 : the radius of the roll-up core.

The initialization of the simulation of vortex sheet dynamics is performed by the routine INITIA.

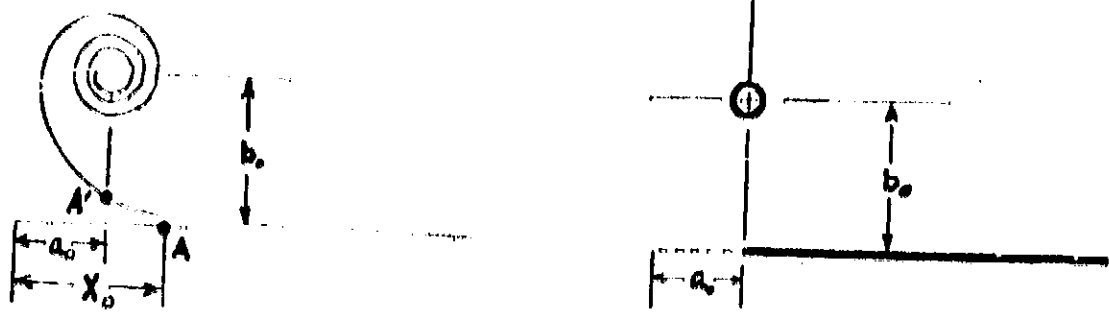


Figure B-1: Kaden's Similarity Solution and its Numerical Model

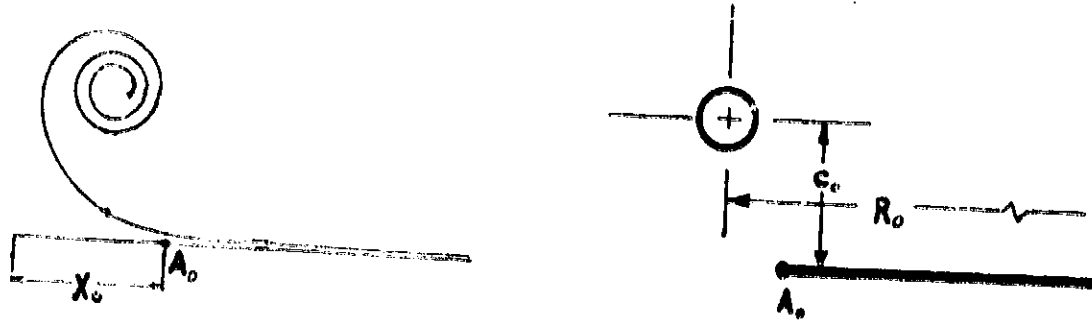


Figure B-2: Initial Roll-Up Model for Axisymmetric Vortex Sheet

SUBROUTINE INITIA (NCORE)

```

| INITIAL VORTEX SHEET GEOMETRY FOR PROGRAM TULLCALL
| modified for complete Kaden's solution and axisymmetric tip cores.
|
| Common block "PANEL" gives the positions (X,Y), the inclination (DX,DY),
| the width (W) and the gradient of circulation (DG).
| Common block "TIME" gives number of panels at each time step and the
| time step data.
| Common block "CORE" gives the information regarding the tip roll-up core.
| Common block "GAMMA" gives the position of each panel on the elliptical
| circulation plot (GS,G).
| Common block "ZOT" specifies the type of roll-up: 0 = 2D elliptic wing
|                                                    1 = uniform disk wake
|                                                    2 = model rotor wake

```

```

COMMON /PANEL/ X(0:505), Y(0:505), DX(0:505), DY(0:505),
               W(0:505), DG(0:505)
COMMON /TIME/ NPANEL, NSTEP, NTIME, TIME, TSTEP
COMMON /CORE/ XC, YC, GC, RC, UC, VC
COMMON /GAMMA/ G(0:505), GS(0:505)
COMMON /ZOT/ ZOT

```

```
PI = 2.*ASIN(1.)
```

```

X(0) = 0
Y(0) = 0
G(0) = -1.
IF (ZOT.GT.1) G(0) = 0.0
GS(0) = 0

```

```

| Equal width segmentation routine.
| R0 and R1 are the positions in span of the inner and the outer edges of
| the panel respectively.

```

```

DO 10 I = 1, NPANEL
X(I) = (FLOAT(I) - .5) / NPANEL
Y(I) = 0.0
R1 = FLOAT(I) / NPANEL
R0 = (FLOAT(I) - 1.) / NPANEL
IF (ZOT.NE.0.AND.ZOT.NE.1) THEN
  IF (R0.EQ.0) THEN
    DG(I) = -(R1**ZOT) * SQRT(1.-R1**2)*NPANEL
  ELSE
    DG(I) = -(R1**ZOT*SQRT(1.-R1**2) - R0**ZOT*SQRT(1.-R0**2))*NPANEL
  END IF
  G(I) = -PI**ZOT*SQRT(1.-R1**2)
ELSE
  DG(I) = -(SQRT(1.-R1**2) - SQRT(1.-R0**2))*NPANEL
  G(I) = -SQRT(1.-R1**2)
END IF
GS(I) = X(I)
W(I) = .5/NPANEL
DX(I) = 1./NPANEL
10 DY(I) = 0.0

```

```
| Tip Core Routines
```

```
| 2D elliptically loaded wing wake.
```

```
IF (ZOT.EQ.0) THEN
```

```

XC = 1. - .57 * ( FLOAT(NCORE) / NPANEL )
YC = .88 * ( FLOAT(NCORE) / NPANEL )
GC = -G(NPANEL-NCORE)

```

```

DXC = XC - X(NPANEL-NCORE) - W(NPANEL-NCORE)
DO 50 I = 1, NPANEL-NCORE
X(I) = DXC * FLOAT(I-1)/(NPANEL-NCORE) + DXC/2/(NPANEL-NCORE) + X(1)
W(I) = DXC /2 / (NPANEL-NCORE) + W(1)
DG(I) = (G(I) - G(I-1)) /2 /W(I)
50 CONTINUE

```

50

```

| Impulsively moved flat disk wake

```

```

ELSE IF (ZOT.EQ.1) THEN

```

```

WC = FLOAT(NCORE) / NPANEL
XC = SQRT( 1. - 2.*WC/3. + (WC**2)/3.)
YC = .88 / .57 * (1. - XC)
GC = -G(NPANEL-NCORE)
RC = B. * XC / EXP( PI**2 /4 *XC /SQRT(2.*WC - WC**2) + 7./4.)
| This is a guess: see Kaden.

```

```

| Model of a helicopter rotor wake

```

```

| ELSE IF (ZOT.EQ.2) THEN

```

```

| WC = FLOAT(NCORE) / NPANEL
| XC = SQRT( 1. - 2.*WC/3. + WC**2/3.) / (1. - WC)
| YC = .88 / .57 * (1. - XC)
| GC = -G(NPANEL-NCORE)
| RC = B. *XC /EXP( PI**2 /4 *R /((1.-WC)**2 /SQRT(2.*WC -WC**2) +7./4.)
| This is only a guess.

```

```

END IF

```

```

| Initial Condition Record

```

```

WRITE(8,*) 'INITIAL SHEET: 1, X(1), Y(1), W(1), DG(1)'
DO 30 I = 0, NPANEL
GS(I) = SQRT(1. - G(I)**2)
30 WRITE(8,*) I, X(I), Y(I), W(I), DG(I)

WRITE(8,*) 'CORE: NCORE, XC, YC, GC, RC', NCORE, XC, YC, GC, RC
WRITE(8,*) ' '

NPANEL = NPANEL - NCORE

RETURN
END

```

Appendix C

The Vortex Sheet Dynamics Program

The program TOLLCALL combines the subroutines listed below to simulate the self-induced motions of a vortex sheet. Input file for the program is stored as device #7. The input file is in the form: (RN, NPANEL, NSTEP, TFAC, GFAC, NCORE, ZOT); RN is the run's identification number, NPANEL is the number of panels initially used to describe the vortex sheet, and NSTEP is the number of time integration cycles for the run. TFAC defines the length of time used in the time integration, TFAC = 1 is equivalent to the nondimensional time span of .005. GFAC defines the size of the panel relative to the distance between the sheet and the center of the roll-up spiral. It is used to insure the accuracy of the tip region as the distance between the sheet and the roll-up core is diminished during the roll-up. NCORE specifies the number of panels describing the initial vortex sheet to be amalgamated into a tip roll-up core. The type of roll-up, as determined by the selected initial condition, is controlled by the parameter ZOT.

- ZOT = 0: Two-dimensional roll-up of wake vortex sheet shed by an elliptically loaded wing.
- ZOT = 1: The roll-up of a vortex sheet simulating the formation of a vortex ring by the impulsive motion of a circular disk.
- ZOT = 2: Axisymmetric roll-up of a circular vortex sheet model of the wake vortex sheet shed by a helicopter rotor.

The program version presented here outputs two files describing the configuration of the vortex sheet after every ten time integration cycles. The file containing the geometrical data of the sheet is in device #9 and the file containing the distribution of vorticity is in device #10. Device #8 holds a utility file describing the execution of the program.

PROGRAM TOLLCALI

I EXECUTIVE ROUTINE FOR ROLLUP PROGRAM

```

COMMON /PANEL/ X(0:505), Y(0:505), DX(0:505), DY(0:505),
               W(0:505), DG(0:505)
COMMON /CONV/ U(0:505), V(0:505)
COMMON /TIME/ NPANEL, NSTEP, NTIME, TIME, TSTEP
COMMON /GAMMA/ G(0:505), GS(0:505)      I GS is a not used
COMMON /CORE/ XC, YC, GC, RC, UC, VC    I   In this version.
COMMON /TFAC/ TFAC, GFAC
COMMON /ZOT/ ZOT

```

```

I Input data read: a. Reference Number (IRUN)
                  b. Number of panels initially in the sheet (NPANEL)
                  c. Maximum number of time steps in the run (NSTEP)
                  d. (.005/TFAC) is the size of each time step
                  e. ({sheet edge to tip core}/GFAC) is the panel width
                  f. Number of cores initially dumped into the tip core
                  g. Type of loading (ZOT)

```

```

READ(7,*) IRUN, NPANEL, NSTEP, TFAC, GFAC, NCORE, ZOT
NINIT = NPANEL

```

I Initialize output file

```

WRITE(8,*) 'ROLL UP PROGRAM FOR VORTEX SHEET, ICHIRO SUGIOKA 37-481'
WRITE(8,*) 'RUN NUMBER: ', IRUN
WRITE(8,*) 'SPLINING BY ROUTINE REDISK'
WRITE(8,*) 'INTEGRATING TIME FACTOR : ', TFAC
WRITE(8,*) 'GEOMETRIC WIDTH FACTOR : ', GFAC
WRITE(8,*) 'INPUTS: (NPANEL, NSTEP) ', NPANEL, NSTEP
WRITE(8,*) 'ZOT FACTOR: LOADING TERM, AXISYMMETRIC IF >1 ', ZOT
WRITE(8,*) ' '

```

I Compute Initial Condition
CALL INITIA (NCORE)

I Time Integration Loop

```

DO 10 NTIME = 0, NSTEP

    CALL WRITER      I Write output data file

    CALL RUNGE1     I Ringe-Kutta time integration scheme
    CALL EULER      I Euler time integration scheme option

    DELTAL = 2. * W(2)      I Panel width parameter (DELTAL)
                           I set to a default panel width

    CALL REDISK (X,Y,G,NPANEL,NPANEL,GMAX,SUML,DELTAL)
                           I Splines and divides the sheet

    CALL PANELER(X,Y,DX,DY,W,DG,G,NPANEL)
                           I Forms the panels

```

10 CONTINUE

End of Loop

CALL WRITER I Record the end results

END

SUBROUTINE WRITER

```

1  This program records the results of toicall on files
1  FOR008.DAT (General accounting information)
1  FOR009.DAT (Geometrical graphics data)
1  FOR010.DAT (Circulation graphics data)

COMMON /PANEL/ X(0:505),Y(0:505),DX(0:505),DY(0:505),
#      W(0:505), DG(0:505)
COMMON /TIME/ NPANEL, NSTEP, NTIME, TIME, TSTEP
COMMON /GAMMA/ G(0:505), GS(0:505)
COMMON /CONV/ U(0:505), V(0:505)
COMMON /CORE/ XC, YC, GC, RC, UC, VC

WRITE(8,*) 'RESULTS FOR NTIME, TIME, NPANEL:', NTIME, TIME, NPANEL

IF (FLOAT(NTIME/10).NE.FLOAT(NTIME)/10.) GO TO 800

WRITE(9,*) NTIME, NPANEL
WRITE(10,*) NTIME, NPANEL

1  Write geometrical data for later graphics.
DO 10 I = 0, NPANEL
WRITE(9,*) X(I), Y(I), DX(I), DY(I), W(I)
10  CONTINUE
WRITE(9,*) XC, YC, RC

1  Write circulation data for later graphics.
DO 20 I = 0, NPANEL
WRITE(10,*) I, GS(I), G(I), DG(I)
20  CONTINUE
WRITE(10,*) GC, RC

800  RETURN
END

```

SUBROUTINE RUNGE1

I This program is a modified Runge-Kutta integration scheme

```
COMMON /PANEL/ X(0:505), Y(0:505), DX(0:505), DY(0:505),
#           W(0:505), DG(0:505)
COMMON /TIME/ NPANEL, NSTEP, NTIME, TIME, TSTEP
COMMON /CONV/ U(0:505), V(0:505)
COMMON /CORE/ XC, YC, GC, RC, UC, VC
COMMON /TFAC/ TFAC, GFAC      I TFAC = FACTOR FOR SIZE OF TIME STEP
COMMON /ZOT/ ZOT
```

I Temporary Buffers

```
DIMENSION X0(0:505), Y0(0:505), DX0(0:505), DY0(0:505),
#           U0(0:505), V0(0:505)
```

```
CALL VELOCT      I Velocities to get to the intermediate points.
```

```
TSTEP = .0025/TFAC      I The intermediate points are at half-way.
```

```
DO 20 I = 0, NPANEL      I Get to the intermediate points.
```

```
X0(I) = X(I)
Y0(I) = Y(I)
DX0(I) = DX(I)
DY0(I) = DY(I)
U0(I) = U(I)
V0(I) = V(I)
X(I) = X(I) + U(I) * TSTEP
Y(I) = Y(I) + V(I) * TSTEP
CONTINUE
```

20

```
XC0 = XC
YC0 = YC
UC0 = UC
VC0 = VC
XC = XC + UC * TSTEP
YC = YC + VC * TSTEP
```

```
DO 25 I = 1, NPANEL-1      I Estimate intermediate panels.
```

```
DX(I) = X(I+1) - X(I-1)
DY(I) = Y(I+1) - Y(I-1)
W(I) = SQRT ((X(I+1) - X(I-1))**2 + (Y(I+1) - Y(I-1))**2)/4.
CONTINUE
```

25

```
I = NPANEL      I Extrapolate at the tip.
```

```
A = (( Y(I-2) - Y(I-1) ) * ( X(I-1)**2 - X(I)**2 )
#   - ( Y(I-1) - Y(I) ) * ( X(I-2)**2 - X(I-1)**2 )
#   + ( Y(I-2) - Y(I-1) ) * ( Y(I-1)**2 - Y(I)**2 )
#   - ( Y(I-1) - Y(I) ) * ( Y(I-2)**2 - Y(I-1)**2 )
#   /(( X(I-2) - X(I-1) ) * ( Y(I-1) - Y(I) )
#   - ( X(I-1) - X(I) ) * ( Y(I-2) - Y(I-1) )) / 4.
B = (( X(I-1)**2 - X(I)**2 ) + ( Y(I-1)**2 - Y(I)**2 )
#   - 2. * A * ( X(I-1) - X(I) )) / 2 / ( Y(I-1) - Y(I) )
DX(I) = - ( Y(I) - B )
DY(I) = ( X(I) - A )
W(I) = SQRT ((X(I) - X(I-1))**2 + (Y(I) - Y(I-1))**2)/2.
```

```
CALL VELOCT      I The mid-course correction
```

```
DO 35 I = 1, NPANEL      I Average in the mid-course correction
U(I) = ( U0(I) + U(I) ) / 2.
```

```

35      V(I) = ( V0(I) + V(I) ) / 2.
        CONTINUE

        UC = ( UC0 + UC ) / 2.
        VC = ( VC0 + VC ) / 2.

        TSTEP = .025/TFAC

        DO 50 I = 1, NPANEL           I Final translation.
          X(I) = X0(I) + U(I) * TSTEP
          Y(I) = Y0(I) + V(I) * TSTEP
50      CONTINUE

        XC = XC0 + UC * TSTEP
        YC = YC0 + VC * TSTEP

I Stretching of tip core: conserve volume of the vortex ring.
      RC = RC * XC0/XC

      X(0) = 0
      Y(0) = Y(1)
      V(0) = V(1)

      TIME = TIME + TSTEP

      RETURN
      END

```

SUBROUTINE EULER

I This program is a Runge-Kutta integration scheme based on limiting
 I the largest convection of panels to some fraction of their widths.

```
COMMON /PANEL/ X(0:505), Y(0:505), DX(0:505), DY(0:505),
                W(0:505), DG(0:505)
```

```
COMMON /TIME/ NPANEL, NSTEP, NTIME, TIME, TSTEP
```

```
COMMON /CONV/ U(0:505), V(0:505)
```

```
COMMON /TFAC/ TFAC, GFAC
```

```
COMMON /CORE/ XC, YC, GC, RC, UC, VC
```

```
CALL VELOCT
```

```
TSTEP = .005 / TFAC
```

```
|----- Panel width based time step option -----|
I   TSTEP = .1
I   DO 10 I = 1, NPANEL
I   TPAN = W(I) / SQRT( U(I)**2 + V(I)**2 ) / TFAC
I 10  IF (TPAN .LT. TSTEP) TSTEP = TPAN
|-----|
```

```
DO 20 I = 0, NPANEL
X(I) = X(I) + U(I) * TSTEP
Y(I) = Y(I) + V(I) * TSTEP
20  CONTINUE
```

```
XC0 = XC
XC = XC + UC * TSTEP
YC = YC + VC * TSTEP
```

```
RC = RC * XC0 / XC
```

```
X(0) = 0
Y(0) = Y(1)
V(0) = V(1)
```

```
TIME = TIME + TSTEP
```

```
RETURN
END
```

SUBROUTINE VELOCT

I This program calculates the velocity field
I Induced by the panels for the program TOLLCALL.FOR

```
COMMON /PANEL/ X(0:505), Y(0:505), DX(0:505), DY(0:505),
W(0:505), DG(0:505)
COMMON /CONV/ U(0:505), V(0:505)
COMMON /TIME/ NPANEL, NSTEP, NTIME, TIME, TSTEP
COMMON /VELO/ R, XX, YY, DXT, DYT, WW, G
COMMON /ZOT/ ZOT
COMMON /CORE/ XC, YC, GC, RC, UC, VC
PI = ASIN(1.) * 2.
```

||||| Loop over the translated panels |||||

```
DO 10 J = 1, NPANEL
  UJ = 0.0
  VJ = 0.0
```

----- Loop over the inducing panels -----

```
DO 20 I = 1, NPANEL
  R = X(I)
  G = DG(I)
  WW = W(I)
  DXT = DX(I)
  DYT = DY(I)
  XX = X(J) - X(I)
  YY = Y(J) - Y(I)
```

I *** The Axisymmetric case ***
IF (ZOT.GE.1) THEN

I Interpolate the self-induced velocity

IF ((XX.EQ.0).AND.(YY.EQ.0)) THEN

```
  XX = -.1 * WW
  CALL VELIN ( UINA, VINA)
  CALL VELIO ( UIOA, VIOA)
  CALL VELOUT( UOUTA, VOUTA)
  XX = .1 * WW
  CALL VELIN ( UINB, VINB)
  CALL VELIO ( UIOB, VIOB)
  CALL VELOUT( UOUTB, VOUTB)
  UIN = (UINA + UINB) / 2.
  VIN = (VINA + VINB) / 2.
  UIO = (UIOA + UIOB) / 2.
  VIO = (VIOA + VIOB) / 2.
  UOUT = (UOUTA + UOUTB) / 2.
  VOUT = (VOUTA + VOUTB) / 2.
```

ELSE

```
  CALL VELIN ( UIN, VIN)
  CALL VELIO ( UIO, VIO)
  CALL VELOUT( UOUT, VOUT)
```

END IF

```
  UJ = UJ + UIN + UOUT - UIO
  VJ = VJ + VIN + VOUT - VIO
```

I *** 2D Case: Includes the mirror image component ***
ELSE

```
  CALL VEL2D (U1,V1)
  XX = X(J) + X(I)
  YY = Y(J) + Y(I)
  G = - DG(I)
  DYT = - DY(I)
  CALL VEL2D (U2,V2)
```

```

      UJ = UJ + U1 + U2
      VJ = VJ + V1 + V2
END IF

20      CONTINUE
|----- End of Loop -----|
      U(J) = UJ
      V(J) = VJ
10      CONTINUE
|==== End of Loop =====|

| Calculate the velocity induced by the tip-core

      U2 = 0
      V2 = 0
      R = XC

      DO 100 J = 1, NPANEL
      R = XC
      XX = X(J) - XC
      YY = Y(J) - YC
      G = GC

      IF (ZOT.GE.1) THEN
      WW = .5
      CALL VELOUT (J1, V1)
      GO TO 99
      END IF

      CALL VEL2DF (U1, V1)
      XX = X(J) + XC
      G = -GC
      CALL VEL2DF (U2, V2)
      | 2D case with mirror image

99      U(J) = U(J) + U1 + U2
      V(J) = V(J) + V1 + V2
100     CONTINUE

|-----|
| Calculate the velocity induced on the tip core by the panels

      UC = 0
      VC = 0

      DO 110 I = 1, NPANEL
      XX = XC - X(I)
      YY = YC - Y(I)
      DXT = DX(I)
      DYT = DY(I)
      WW = W(I)
      G = DG(I)
      R = X(I)

      IF (ZOT.GE.1) THEN
      CALL VELIN (UIN, VIN)
      CALL VELIO (UIO, VIO)
      CALL VELOUT(UOUT,VOUT)
      U1 = UIN + UOUT - UIO
      V1 = VIN + VOUT - VIO
      U2 = 0
      V2 = 0
      GO TO 105

```

```

      END IF
      CALL VEL2D (U1,V1)
      XX = XC + X(I)
      DYT = DY(I)
      WW = - W(I)
      G = -DG(I)
      CALL VEL2D (U2,V2)
      I 2D case with mirror image
105   UC = UC + U1 + U2
      VC = VC + V1 + V2
110   CONTINUE

I 2D Case Only: Velocity Induced by the mirror image of the tip core
  IF (ZOT.EQ.0) THEN
    XX = 2*XC
    YY = 0.0
    G = -GC
    CALL VEL2DF (U0,V0)
    UC = UC + U0
    VC = VC + V0
  END IF

I Axisymmetric Case Only: The Self-Induced Velocity of the Core
  IF (ZOT.GE.1) VC = VC - GC/4/PI/XC*( LOG(8*XC/RC) - .25)

  U(0) = 0.0

  RETURN
  END

```

SUBROUTINE REDISK(R,Z,G,NIN,NCUT,GMAX,SUML,DELTA)

C—THIS DOES CURVE FITTING USING BLENDED PARABOLAS ON R, Z, DGAM
I Modified from SPIRAL.FOR by John Kantella for use with panels

COMMON /TIME/ NP, NG, NT, T, TS
COMMON /CORE/ XC, YC, GC
COMMON /TFAC/ TFAC, GFAC
COMMON /ZOT/ ZOT

DIMENSION R(0:505),Z(0:505),G(0:505),S(0:505),QR(0:505),
\$ QZ(0:505),A0(0:505),A1(0:505),A2(0:505),A3(0:505),
\$ B0(0:505),B1(0:505),B2(0:505),B3(0:505),C0(0:505),
\$ C1(0:505),C2(0:505),C3(0:505),GMID(0:505),SMID(0:505),
\$ Q(0:505),RS(0:5050),ZS(0:5050),AL(0:5050),GS(0:5050)
DATA NSUB/5/

C—GET STRAIGHT LINE DISTANCES BETWEEN POINTS, S(I) IS THE TOTAL
C DISTANCE ALONG THE STRAIGHT LINES TO NODE I

S(0)=0.0
DO 20 I=1,NIN
20 S(I)=S(I-1)+SQRT((Z(I)-Z(I-1))**2+(R(I)-R(I-1))**2)

C—Get value of s for the trailing extended segment, this value
C of S is out at the presumed end of the sheet.

S(NIN+1)=S(NIN)+0.5*(S(NIN)-S(NIN-1))

C—GET SLOPES AT EACH INTERIOR NODE, QR(I)=D(R)/DS AT NODE I

DO 30 I=1,NIN-1
S1=(S(I+1)-S(I))/(S(I)-S(I-1))
S2=1.0/S1
S3=1.0/(S(I+1)-S(I-1))
QR(I)=(R(I)-R(I-1))*S1-(R(I+1)-R(I))*S2*S3
30 QZ(I)=(Z(I)-Z(I-1))*S1-(Z(I+1)-Z(I))*S2*S3

C—COEF'S FOR INTERIOR SEGMENTS

DO 40 I=1,NIN-2
S1=1.0/(S(I+1)-S(I))
A0(I)=R(I)
A1(I)=QR(I)
A2(I)=S1*(-QR(I+1)-2*QR(I)+3*S1*(R(I+1)-R(I)))
A3(I)=S1*S1*(QR(I+1)+QR(I)-2*S1*(R(I+1)-R(I)))
B0(I)=Z(I)
B1(I)=QZ(I)
B2(I)=S1*(-QZ(I+1)-2*QZ(I)+3*S1*(Z(I+1)-Z(I)))
40 B3(I)=S1*S1*(QZ(I+1)+QZ(I)-2*S1*(Z(I+1)-Z(I)))

C—COEF'S FOR FIRST SEGMENT

S1=S(1)-S(0)
S2=S(2)-S(0)
S3=1.0/(S(2)-S(1))
A0(0)=R(0)
A1(0)=(R(1)-R(0))*S2/S1-(R(2)-R(0))*S1/S2*S3
A2(0)=(R(2)-R(0))/S2-(R(1)-R(0))/S1*S3
A3(0)=0.0
B0(0)=Z(0)
B1(0)=(Z(1)-Z(0))*S2/S1-(Z(2)-Z(0))*S1/S2*S3

B2(0)=((Z(2)-Z(0))/S2-(Z(1)-Z(0))/S1)*S3
 B3(0)=0.0

C—COEF'S FOR LAST SEGMENT

N=NIN
 S1=S(N)-S(N-1)
 S2=S(N-2)-S(N-1)
 S3=1.0/(S(N-2)-S(N))
 A0(N-1)=R(N-1)
 A1(N-1)=((R(N)-R(N-1))*S2/S1-(R(N-2)-R(N-1))*S1/S2)*S3
 A2(N-1)=((R(N-2)-R(N-1))/S2-(R(N)-R(N-1))/S1)*S3
 A3(N-1)=0.0
 B0(N-1)=Z(N-1)
 B1(N-1)=((Z(N)-Z(N-1))*S2/S1-(Z(N-2)-Z(N-1))*S1/S2)*S3
 B2(N-1)=((Z(N-2)-Z(N-1))/S2-(Z(N)-Z(N-1))/S1)*S3
 B3(N-1)=0.0

C—Get the angle of the ring with index NSMALL wrt the tip core

CALL PULANG(NIN,THNIN)

C—Get the "A" coefficient for the Kadin spiral

RNU=XNU(THNIN)
 IF (ABS(SIN(THNIN)) .GE. 0.5) THEN
 A=(YC-Z(NIN))/(THNIN*(-RNU)*SIN(THNIN))
 ELSE
 A=(XC-R(NIN))/(THNIN*(-RNU)*COS(THNIN))
 ENDIF

C—GET ARRAY OF R AND Z AT THE SUBINTERVAL LOCATIONS, AND COMPUTE
 C THE TOTAL LENGTH OF THE CURVE

C—First do the blended parabolic segments

RS(0)=A0(0)
 ZS(0)=B0(0)
 AL(0)=0.0
 DO 50 I=0,NIN-1
 DO 50 KSUB=1,NSUB
 J=I+NSUB+KSUB
 T=(S(I+1)-S(I))*FLOAT(KSUB)/FLOAT(NSUB)
 RS(J)=A0(I)+T*(A1(I)+T*(A2(I)+T*A3(I)))
 ZS(J)=B0(I)+T*(B1(I)+T*(B2(I)+T*B3(I)))
 50 AL(J)=AL(J-1)+SQRT((RS(J)-RS(J-1))**2+(ZS(J)-ZS(J-1))**2)

C—The next few sections find the value of theta at the end of the
 C trailing extended segment, i.e., gets the theta corresponding
 C to arclength S(NIN+1)

C—First, before doing the numerical integration, need to get a
 C value to use for delta theta

ITERS=0
 DSGW=(S(NIN+1)-S(NIN))/20.0
 DTG=0.01
 62 TTEMP=THNIN+DTG/2.0
 RNU=XNU(TTEMP)
 ITERS=ITERS+1
 IF (ITERS .GT. 100) STOP 'ITERS .GT. 100 IN LOOP 61'
 DSG=A*TTEMP**2*(-RNU-1.0)*SQRT(RNU**2+TTEMP**2)*DTG

```

DTGN=(DSGW/DEG)*DTG
IF (ABS(DTGN-DTG) .LT. 0.001) GO TO 61
DTG=DTGN
GO TO 62
61 DTG=DTGN

```

C—Now have delta theta (i.e., $\Delta\theta$) which should yield approx. 20
C steps in the numerical integration from $S(NIN)$ to $S(NIN+1)$.

C—Now do the numerical integration and search for theta(NIN+1)

```

ITERS=0
SEND=S(NIN+1)-S(NIN)
STH=0.0
TH=THNIN
64 RNU=XNU(TH)
ITERS=ITERS+1
IF (ITERS .GT. 100) STOP 'ITERS .GT. 100 LOOP 63'
ARG1=A*TH*(-RNU-1.0)*SQRT(RNU**2+TH**2)
RNU=XNU(TH+DTG)
ARG2=A*(TH+DTG)*(-RNU-1.0)*SQRT(RNU**2+(TH+DTG)**2)
DS=(ARG1+ARG2)*DTG/2.0
IF (STH+DS .GE. SEND) GO TO 63
STH=STH+DS
TH=TH+DTG
GO TO 64
63 FRAC=(SEND-STH)/DS
THNIN1=TH+FRAC*DTG

```

C—Now can get the sub-interval locations over the extended spiral
C segment.

```

DTH=(THNIN1-THNIN)/NSUB
DO 65 KSUB=1,NSUB
THETA=THNIN+KSUB*DTH
J=NIN+NSUB+KSUB
RNU=XNU(THETA)
RS(J)=XC-A*THETA*(-RNU)*COS(THETA)
ZS(J)=YC-A*THETA*(-RNU)*SIN(THETA)
AL(J)=AL(J-1)+SQRT((RS(J)-RS(J-1))**2+(ZS(J)-ZS(J-1))**2)
65 CONTINUE

```

I Redistribute the Circulation over the Sub-Segments

```

DO 751 I = 0, NIN
DO 751 J = 1, NSUB
K = I * NSUB + J
IF (I.EQ.0) THEN
IF (ZOT.LE.1) THEN
GS(K) = FLOAT(J)/NSUB * (1+G(1))/2. - 1.
GS(0) = -1.
ELSE
GS(K) = FLOAT(J)/NSUB * G(1)/2.
GS(0) = 0
END IF
ELSE IF (I.EQ.NIN) THEN
DGN = (G(NIN) - G(NIN-1))/2
GS(K) = FLOAT(J)/NSUB * DGN + G(NIN-1) + DGN
ELSE
DGI = (G(I+1) - G(I-1))/2
DGIM1 = (G(I) - G(I-1))/2
GS(K) = (FLOAT(J)/NSUB * DGI) + G(I-1) + DGIM1

```

END IF
751 CONTINUE

C--TOTAL LENGTH OF CURVE IS SUM:

SUML=AL((NIN+1)*NSUB)

||||| Panel Discretization Criteria

IEND = (NIN+1) * NSUB | Limits Relative Distance End/Core
XLSEG = SQRT((XC-RS(IEND))**2+(YC-ZS(IEND))**2)/GFAC
IF (XLSEG.GT.DELTA)
XLSEG = DELTA | Always Shrinking Criteria
DELTA = XLSEG

C--GET NEW R AND Z POINTS

310 I=1

DO 60 J=1,NSUB*(NIN+1)

| Calculate the Distance to the positions of the sub-panels
80 WJM1 = SQRT((RS(J-1)-R(I-1))**2 + (ZS(J-1)-Z(I-1))**2)
WJM0 = SQRT((RS(J) - R(I-1))**2 + (ZS(J) - Z(I-1))**2)

| If not enough.
IF (XLSEG .LT. WJM1 .OR. XLSEG .GT. WJM0) GO TO 60
FRAC=(XLSEG - WJM1)/(WJM0 - WJM1) | Calculate where the new
R(I)=FRAC*(RS(J)-RS(J-1))+RS(J-1) | panel edge will be J up.
Z(I)=FRAC*(ZS(J)-ZS(J-1))+ZS(J-1)
G(I)=FRAC*(GS(J)-GS(J-1))+GS(J-1)
I=I+1

IF (I.GT.500) GO TO 300 | Too many panels

GO TO 80

60 CONTINUE

70 CONTINUE

R(I) = RS(NSUB*(NIN+1))

Z(I) = Z(NSUB*(NIN+1))

G(I) = GS(NSUB*(NIN+1))

NOU: = I

RETURN

| If the sheet is too stretched to the panelled by 500 panels, then
| stretch the panels by 10%.

300 XLSEG = XLSEG *1.1
WRITE(8,*) '***** OVER 500 PANELS ***** TSTEP, DLSEG:', NT, XLSEG
GOTO 310

END

SUBROUTINE PULANG(NIN,THNIN)

! Special Subroutine for routine REDISK which extrapolates
! the sheet edge using Kaden's exponential spiral model

```

COMMON /CORE/ XC, YC, GC
COMMON /PANEL/ R(0:505),Z(0:505),DX(0:505),DY(0:505),
$           W(0:505), GAMMA(0:505)
DIMENSION BETA(0:505)
REAL*4 MAG

C
RT=XC
ZT=YC

C
A=-1.0
B=0.0
C=R(0)-RT
D=Z(0)-ZT
DOT=A*C+B*D
CROSS=A*D-B*C
MAG=SQRT((A*A+B*B)*(C*C+D*D))
ARG=DOT/MAG
IF (ABS(ARG) .GT. 1.0) ARG=SIGN(1.0,ARG)
BETA(0)=SIGN(1.0,CROSS)*ACOS(ARG)

C
DO 100 I=1,NIN
A=R(I)-RT
B=Z(I)-ZT
C=R(I)-RT
D=Z(I)-ZT
DOT=A*C+B*D
CROSS=A*D-B*C
MAG=SQRT((A*A+B*B)*(C*C+D*D))
ARG=DOT/MAG
IF (ABS(ARG) .GT. 1.0) ARG=SIGN(1.0,ARG)
100 BETA(I)=BETA(I-1)+SIGN(1.0,CROSS)*ACOS(ARG)

THNIN=BETA(NIN)

RETURN
END
FUNCTION XNU(THETA)
DATA PI/3.141592654/
XNU=2.0/3.0
IF (THETA .LT. 2.0*PI) THEN
XNU=(1.0/(2.0*PI-1.0))-1.0/(THETA-1.0))+2.0/3.0
ENDIF
RETURN
END
```

SUBROUTINE PANELER (X,Y,DX,DY,W,DG,G,NPANEL)

! This program takes the results from routine REDISK and creates panels

```

      DIMENSION X(0:505), Y(0:505), DX(0:505), DY(0:505),
      #           W(0:505), DG(0:505),
      #           G(0:505), GS(0:505)

      DIMENSION R(0:505), Z(0:505)

      DO 10 I = 1, NPANEL
      R(I) = ( X(I) + X(I-1) ) / 2.
      Z(I) = ( Y(I) + Y(I-1) ) / 2.
      DX(I) = X(I) - X(I-1)
      DY(I) = Y(I) - Y(I-1)
      W(I) = SQRT( DX(I)**2 + DY(I)**2)/2.
      DG(I) = ( G(I) - G(I-1)) / W(I) / 2.
10    CONTINUE

      DO 20 I = 1, NPANEL
      X(I) = R(I)
20    Y(I) = Z(I)

      RETURN
      END

```

Appendix D

Inputs Used to Generate the Figures in the Text

Figure 5-7: Elliptically Loaded Wing Wake Case

NPANEL = 80
TFAC = 1
GFAC = 1
NCORE = 4
ZOT = 0

Figure 5-13: Formulation of Vortex Ring by a Disk

NPANEL = 80
TFAC = 1
GFAC = 1
NCORE = 1
ZOT = 1

Figure 5-21: Modelled Helicopter Rotor Wake Case

NPANEL = 80
TFAC = 1
GFAC = 1
NCORE = 1
ZOT = 2

Figure 5-28: Demonstration of Kelvin-Helmholtz-type Instability

This experiment was performed using an early version of the simulation program with different set of inputs.

Figure 5-29: Instability in the Roll-Up of Disk Wake

NPANEL = 80
TFAC = 1
GFAC = 2
NCORE = 1
ZOT = 1

1. Report No. NASA CR - 177365	2. Government Accession No.	3. Recipient's Catalog No.
4. Title and Subtitle A Panel Method Study of Vortex Sheets With Special Emphasis on Sheets of Axisymmetric Geometry		5. Report Date August 1985
7. Author(s) Ichiro Sugioka and Sheila E. Widnall		6. Performing Organization Code
9. Performing Organization Name and Address Fluid Dynamics Research Laboratory Department of Aeronautics and Astronautics Massachusetts Institute of Technology Cambridge, MA 02139		8. Performing Organization Report No. FDRL Report No. 85-3
12. Sponsoring Agency Name and Address National Aeronautics and Space Administration Washington, D. C. 20546		10. Work Unit No. T4523
		11. Contract or Grant No. NAG2-251
		13. Type of Report and Period Covered Contractor Report
		14. Sponsoring Agency Code 505-42-11
15. Supplementary Notes Point of Contact: Technical Monitor, Wayne Johnson, MS 247-1 Ames Research Center, Moffett Field, CA 94035 (415) 694-5043 or FTS 464-5043		
16. Abstract The self-induced evolution of a vortex sheet was simulated by modeling the sheet using an integration of discrete elements of vorticity. Replacing small sections of a vortex sheet by flat panels of constant vorticity is found to reproduce more accurately the initial conditions for the Lagrangian simulation technique than replacement by point vortices. The flat panel method for the vortex sheet was then extended to model axisymmetric vortex sheets. The local and far field velocities induced by the axisymmetric panels were obtained using matched asymptotic analysis, and some of the uncertainties involved in other models of the axisymmetric vortex sheet have been eliminated. One important result of this analysis is the determination of the proper choice of core size for a circular vortex filament which may replace a section of an axisymmetric vortex sheet. Roll-up of both two-dimensional and axisymmetric vortex sheets was computed using the panel methods developed in the report.		
17. Key Words (Suggested by Author(s)) Vortex Dynamics Rotor Wakes		18. Distribution Statement Unclassified --- Unlimited STAR Category 02
19. Security Classif. (of this report) Unclassified	20. Security Classif. (of this page) Unclassified	21. No. of Pages 107
		22. Price*